

Multigrid Method for the Coupled Free Fluid Flow and Porous Media System

Luo, Peiyao

DOI

[10.4233/uuid:fea96fa7-e720-443a-938a-c4a9c1483bd6](https://doi.org/10.4233/uuid:fea96fa7-e720-443a-938a-c4a9c1483bd6)

Publication date

2017

Document Version

Final published version

Citation (APA)

Luo, P. (2017). *Multigrid Method for the Coupled Free Fluid Flow and Porous Media System*. [Dissertation (TU Delft), Delft University of Technology]. <https://doi.org/10.4233/uuid:fea96fa7-e720-443a-938a-c4a9c1483bd6>

Important note

To cite this publication, please use the final published version (if applicable).
Please check the document version above.

Copyright

Other than for strictly personal use, it is not permitted to download, forward or distribute the text or part of it, without the consent of the author(s) and/or copyright holder(s), unless the work is under an open content license such as Creative Commons.

Takedown policy

Please contact us and provide details if you believe this document breaches copyrights.
We will remove access to the work immediately and investigate your claim.

Multigrid Method for the Coupled Free Fluid Flow and Porous Media System

Proefschrift

ter verkrijging van de graad van doctor
aan de Technische Universiteit Delft,
op gezag van de Rector Magnificus prof. ir. K. C. A. M. Luyben,
voorzitter van het College voor Promoties,
in het openbaar te verdedigen op
dinsdag 10 oktober 2017 om 12:30 uur

door

Peiyao Luo

Master of Science in Applied Mathematics,
Northwestern Polytechnical University, China,
geboren te Xi'an, Shaanxi Province, China.

This dissertation has been approved by the

Promotor: Prof. dr. ir. C.W. Oosterlee

Composition of the doctoral committee:

Rector Magnificus, voorzitter
Prof. dr. ir. C.W. Oosterlee, Technische Universiteit Delft, promotor

Independent members:

Prof. dr. L. Zikatanov, The Pennsylvania State University, United States
Prof. dr. S. Vandewalle, Katholieke Universiteit Leuven, Belgium
Prof. dr. ir. J. Frank, Utrecht University, The Netherlands
Prof. dr. ir. M. Verlaan, Technische Universiteit Delft, The Netherlands
Prof. dr. ir. C. Vuik, Technische Universiteit Delft, The Netherlands

Dependent member:

Prof. dr. F.J. Gaspar, Universidad de Zaragoza, Spain



Multigrid Method for the Coupled Free Fluid Flow and Porous Media System.

Dissertation at Delft University of Technology.

ISBN 978-94-6186-852-7

This research was supported by the China Scholarship Council (CSC).

Copyright © 2017 by Peiyao Luo

All rights reserved. No part of the material protected by this copyright notice may be reproduced or utilized in any form of by any means, electronic or mechanical, including photocopying, recording or by any information storage and retrieval system, without the prior permission of the author.

Printed in the Netherlands

Acknowledgements

This thesis concludes my PhD research in the Department of Applied Mathematics in Delft University of Technology, the Netherlands. I would like to attribute this success to a number of people, who have played important roles in various aspects of my research and personal life for past four years. Herewith I would like to express my gratitude for their kind help and support.

First of all, I would like to express my sincere gratitude to my supervisor Prof. Kees Oosterlee and my closely collaborators Prof. Francisco Gaspar and Dr. Carmen Rodrigo.

It is Kees who offered me such an amazing opportunity to work in TU Delft without any hesitation even I didn't hold a master degree at that moment. Thank Kees for his insights, long-term vision, professional experience, optimism and kindness, I benefit a lot during these four years not only for research but also for my personality and future development. For every small step I make in the research, Kees is even happier than myself. His encouragement and confidence on me are a great motivation for me to move forward. I have a strong sense of secure working with Kees, because he is always available to provide me immediate help although he has a very busy schedule. Moreover, He is concerned about every small issue arising in my work and always puts himself on my position. He created various opportunities for me, such as supporting me to attend international conferences, helping me apply the travel grant to work in Spain, building the bridge connecting me with Francisco and Carmen, encouraging me to join paper competitions, giving me freedom to explore the world and offering me possibilities when looking for jobs. I still remember clear that Kees once said he has two rules for himself: one is working hard, the other

is being good to students. I feel so lucky that I am being taken care of so well these four years. I could not have imagined having a better supervisor for my PhD life.

I would also like to thank Francisco who is from the University of Zaragoza, Spain. Without his continuous guidance and help, this work could not have been accomplished. There are countless times we work together in the same office, even on the same table, though most of the time he is in Spain while I am in the Netherlands. Thank him for teaching me so many things from zero. He is extremely patient with all of my “stupid” or repeated questions, and also he has the ability to explain me profound theories in an easy way. I appreciate his help and comments on every details of my research, even that he is willing to spend time checking my codes line by line. His endless enthusiasm, conscientious and hardworking attitude toward research motivate me and make working with him a real pleasure. In addition, I would also like to thank Francisco for taking care of me so well when I visited him in Zaragoza. We have a lot of beautiful memories together. Thank him for inviting me to his house in Acumur which is a small but pretty village far from Zaragoza. I will never forget the fantastic taste of the roasting lamb and the homemade mojito and sangria he made. I would like to say that it is really my great honour to know and work with Francisco.

I also want to thank Carmen for her contributions in this thesis. She is the most hardworking person I have ever met. I am grateful for her meticulous revision of our papers. Moreover, I would also like to say thanks to her for taking care of me in Zaragoza. Thank her for helping me with my accommodation, picking me up in the station, and accompanying with me almost every day there. She is the person who always thinks of others and tries to make everybody around feel comfort. With Carmen and Francisco, we experienced a lot of unforgettable moments, such as exploring the best tapas, hiking in the mountains, cooking meals together, and watching the World Cup in bars.

Many thanks to Kees, Francisco and Carmen again. Without their professional support and warm encouragement, I would never accomplish this work in such an enjoyable way. They are the most valuable gifts I obtain throughout my PhD life.

Next, I would like to thank committee members for sparing time to

read this thesis. Moreover, my appreciation goes to Prof. Kees Vuik for sharing me his experience of making presentations and introducing me to professionals at the conference. My appreciation also goes to Prof. Ludmil Zikatanov for coming to my talks at several conferences and those days we spent together in Zaragoza. Thanks to Prof. Stefan Vandewalle for talking with me on different occasions. Furthur more, I would like to thank my master supervisor, Prof. Yufeng Nie for supporting me to study abroad. Thanks to Dr. Xiaozhe Hu for inviting me to give a talk in Tufts University. Regarding official affairs, many thanks to Cees Timmers, Franca Post, Wim van Horsen, Deborah Dongor, Stefanie van Gentevooort and Cindy Bosman. I also want to thank Nada Mitrovic for her kindly help everytime when I work in CWI.

It is a pleasure to share the office with friendly mates Jing, Thea and Xiaozhou, then Zaza, Mohamed and Gabriela. Special thanks to Jing for treating me as her sister and willing to share everything without reservation. She gives me a lot of encouragement when I am either depressed or excited by my research outcome. She also gives me a strong support during the period of job hunting. Thanks to Thea for teaching me Dutch and talking about everything in life. Thea, Jing and I are good friends and we have a lot of happiness together. My appreciation also goes to Zaza for helping me translate the summary into Dutch and inviting me to her lovely house.

I would like to acknowledge all my other colleagues in TU Delft: Abdul, Anna, Baljinnyam, Berna, Behrouz, Daniel, Dennis, Domenico, Duncan, Edwin, Elwin, Fahim, Faraz, Fei, Fons, Fred, Guido, Guus, Jiao, Joanna, Johan, Jok, Joost, Lisa, Luis, Manuel, Martin, Martijn, Matthias, Menel, Mohamed, Neil, Reinaldo, Rohit, Shuaiqiang, Valia, Virginia, Xin and Yue. Thanks to Kees Lemmens for his technical support. Many thanks also go to the financial engineering research group formed by the students of Kees in CWI: Alvaro, Anton, Bowen, Fei, Kiwai, Lech, Prashant, Qian and Zaza. Special thanks to Prashant for his help and discussion of my research work.

My life has been enriched due to the big Chinese community in Delft. Many thanks go to my roommates, Long, Yixiao, Yu and Yueting. They are like my family in the Netherlands and always make me feel warm. I would also like to thank my closely friends Anqi, Daijie, Fei, Jiao, Jie, Jingtang, Mingjuan, Sixin, Shuaiqiang, Yexian and Zhijie for all of their

help and pleasant moment we shared.

I am lucky to have Qing as my best friend. We have known each other for more than fifteen years. After six years' high school, we are separate until now, from Xi'an to Beijing, then from the Netherlands to the United States. Our solid friendship is not affected by the long distance and time. The most relaxed time for me is to chat with her by phone at night. We share happiness and sorrow. We support and encourage each other to become a better person.

Finally, I would like to express my gratitude to my parents and grandparents for their unconditional love and endless support. They brought me up and taught me many things. Especially to my grandparents, I am glad and proud that I follow their path to research. Many appreciation also goes to my parents for always standing behind me, which makes me brave to face the coming tomorrow.

Peiyao Luo

Delft, September 2017

Summary

Multigrid Method for the Coupled Free Fluid Flow and Porous Media System

Peiyao Luo

Coupling of free fluid and flow in a porous medium is an attractive research area due to its many applications in different fields. For example, this coupling can be found in waste water treatment systems, when fluid flow passes through a filter. Another example in which this coupling is present is in the interaction between blood flow and the vessels during nutrients transport. Coupling is typically governed by the interaction between two different systems. This is challenging, since each system may be based on a specific physical model and appropriate internal interface conditions are needed to connect them.

In our case, the free fluid is governed by the incompressible Stokes equations, while the flow in the porous medium is described by either the Darcy flow equation or the poroelasticity equations, depending on the assumptions regarding the porous medium. When the porous medium is assumed to be rigid, the coupled system is the Darcy-Stokes problem, in our case, while the coupled Stokes-poroelasticity system is considered when the porous medium is deformable. By the poroelasticity system of equations, fluid motion and solid deformation are both taken into account, based on the well-developed Biot model. In Biot's model, the Darcy equation is used for the fluid motion, and linear elasticity equations are employed for the solid deformation. At the interface of the Stokes and porous medium equations, proper conditions such as conservation of mass and momentum,

a balance of normal stresses, no-slip conditions, need to be imposed.

The coupled system is discretized by the finite volume method, often on a staggered grid, which results in a discrete system of saddle point structure. Multigrid methods are efficient for solving the saddle point problem. We develop efficient and robust monolithic multigrid algorithms for the coupled system. Different from the classical domain decomposition (DD) method, the complete discrete system arising from the governing equations and the interface conditions is treated simultaneously during the solution process. In multigrid, the choice of each component affects the multigrid convergence performance. We pay special attention to the choice of each multigrid component, especially to the choice of the smoother.

To gain a deep insight in the equations, we start this PhD Thesis by focussing on the efficient iterative solution of the poroelasticity equations, in Chapters 2 and 3, as many studies have already been performed for the Stokes problem. We solve the linear as well as the nonlinear poroelasticity equations by means of the geometric multigrid method. Regarding the nonlinear system of partial differential equations, two nonlinear multigrid variants, i.e., Newton's multigrid and the Full Approximation Scheme (FAS) are employed in Chapter 2. Newton's multigrid is based on global linearization. The resulting linear problem after application of Newton's method, is then solved by linear multigrid. Different from the idea of Newton's multigrid, by FAS one solves the nonlinear problem on each fine and coarse grid level by employing nonlinear smoothers. We also solve a nonlinear problem with heterogeneous physical parameters, that are prescribed by random coefficients. In the test cases, we compare a point-wise Gauss-Seidel smoother with a coupled box smoother (also called "Vanka smoother").

In Chapter 3, we investigate the multigrid performance when employing a so-called decoupled Uzawa smoother for the linear poroelasticity equations. The Uzawa smoother is based on a symmetric Gauss-Seidel smoothing iteration for the displacements and a basic Richardson iteration for the updates of the pressure field. To choose optimal relaxation parameters within the Richardson iteration, Local Fourier Analysis (LFA) is applied. The asymptotic convergence factors of multigrid can be predicted quite well by means of two-grid LFA. To further accelerate the multigrid convergence for highly nontrivial heterogeneous problems, the iterant recombination

scheme is advocated in Chapter 3.

Based on the obtained knowledge of the poroelasticity (and Stokes) subsystems, we solve the coupled Darcy-Stokes system in Chapter 4, assuming that the porous medium is rigid. A special discretization scheme is developed for the unknowns at the interface. We propose a monolithic multigrid method with the decoupled Uzawa smoother, based on the grid partitioning strategy. Optimal relaxation parameters in the Uzawa smoother are again calculated by means of LFA for each subproblem. We have confirmed that the global convergence of multigrid matches the worst multigrid convergence factor of the individual subproblems. It is further worth noting that the multigrid convergence is independent of the physical parameter values. Moreover, we study the effect of heterogeneity on the multigrid convergence.

Finally, we develop a monolithic multigrid method for the coupled Stokes-poroelasticity system by taking into account the elastic deformation of the solid in Chapter 5. A novelty in our work is that at the interface between the two subsystems, two unknowns from the different subsystems are defined at the same grid point. We propose a special discretization for the unknowns at and close to the interface. In this chapter, we investigate the multigrid performance with both the coupled Vanka and decoupled Uzawa smoothers. In the Uzawa smoother, the results obtained in Chapter 3 provide us the necessary insight in the optimal relaxation parameter values for the poroelasticity equations. Within the grid partitioning scheme, the information is exchanged between neighboring subdomains on each grid level. This forms the basis to achieve a highly satisfactory multigrid convergence behavior in multi-block geometries.

So, this thesis reports on research about the monolithic multigrid method for the coupled free fluid flow and porous media systems. The theoretical quantitative analysis, numerical algorithms and results presented here provide insight and knowledge into multigrid methods for multi-physics systems. The combination of these two aspects, i.e., multigrid and coupled systems, is exciting and challenging.

Samenvatting

Multigrid Method for the Coupled Free Fluid Flow and Porous Media System

Peiyao Luo

Koppeling van vloeistofstroming en stroming in een poreus medium is een aantrekkelijk onderzoeksgebied vanwege de vele toepassingen. Een voorbeeld is te vinden in afvalwaterbehandelingssystemen, namelijk wanneer het afvalwater door een filter stroomt. Een ander voorbeeld is de interactie tussen de bloedstroom en de bloedvaten tijdens het transport van voedingsstoffen. De koppeling wordt doorgaans gemodelleerd door interactie tussen twee verschillende systemen. Dit is uitdagend, omdat elk systeem op een specifiek fysisch model is gebaseerd en bijbehorende interne koppelingsvoorwaarden zijn nodig om ze te verbinden.

In ons geval wordt de vloeistofstroming gegeven door de incompressibele Stokesvergelijkingen, terwijl de stroming in het poreuze medium wordt beschreven door ofwel de Darcy-stromingsvergelijking of de poroelasticiteitsvergelijkingen, afhankelijk van aannames betreffende het medium. Als we aannemen dat het poreuze medium stijf is, dan is het gekoppelde systeem een Darcy-Stokesprobleem. In ons geval is het poreuze systeem vervormbaar en daarom wordt het gekoppelde Stokes-poroelasticiteitssysteem beschouwd. In het systeem van poroelasticiteitsvergelijkingen worden vloeistofbeweging en vervorming van het poreuze medium beide meegenomen. Dit is gebaseerd op het Biotmodel, waarin de Darcy-vergelijking gebruikt wordt voor de vloeistofbeweging, terwijl lineaire elasticiteitsvergelijkingen de vervorming van het medium weergeven. Aan de koppeling van de Stokes- en

de poreuze mediumvergelijkingen moeten goede randvoorwaarden worden opgelegd, zoals behoud van massa en impuls, een evenwicht van spanning en geen wrijving.

Het gekoppelde systeem wordt gediscretiseerd met de eindige volumemethode, vaak op een gestaggered rooster, wat resulteert in een discreet systeem met een zadelpuntstructuur. Multiroostermethoden zijn efficiënt voor het oplossen van zadelpuntproblemen. Wij ontwikkelen efficiënte en robuuste monolithische multiroosteralgoritmen voor het gekoppelde systeem. Anders dan in een klassieke domeindecompositie methode (DD), wordt het volledige discrete systeem dat voortvloeit uit de overkoepelende vergelijkingen en de koppelingscondities gelijktijdig behandeld tijdens het oplosproces. In multigrid beïnvloedt de keuze van elke component de convergentie. Wij schenken speciale aandacht aan de keuze van elke component, en met name ook aan de keuze van de smoother.

Om een goed inzicht te krijgen in de vergelijkingen, beginnen we dit proefschrift met het focussen op de efficiënte iteratieve oplossing van de poroelasticiteitsvergelijkingen, in Hoofdstukken 2 en 3, omdat er reed vele studies zijn uitgevoerd naar het Stokesprobleem. We lossen zowel de lineaire als de niet-lineaire poroelasticiteitsvergelijkingen op met behulp van de geometrische multiroostermethode. Met betrekking tot het niet-lineaire systeem van partiële differentiaalvergelijkingen, worden twee niet-lineaire multiroostervarianten, d.w.z. Newtons multigrid en de Full Approximation Scheme (FAS), gebruikt in Hoofdstuk 2. Newtons multigrid is gebaseerd op globale linearisatie. Het verkregen lineaire probleem, na toepassing van Newtons methode, wordt opgelost met een lineaire multiroostermethode. Anders dan met Newtons multigrid, lost men met FAS het niet-lineaire probleem direct op. Dit gebeurt op zowel een fijn als een grof rooster door gebruik te maken van niet-lineaire smoothers. We lossen ook een niet-lineair probleem met heterogene fysische parameters op. Deze parameters worden gegeven door random coëfficiënten. In onze numerieke testen, vergelijken we een puntsgewijze Gauss-Seidelsmoother met een gekoppelde Vanka-smoother.

In Hoofdstuk 3 onderzoeken we de multiroosterprestatie met een zogenoemde ontkoppelde Uzawa-smoother voor de lineaire poroelasticiteitsvergelijkingen. De Uzawa-smoother is gebaseerd op een symmetrische Gauss-Seidel-iteratie voor de verplaatsingen en een Richardson-iteratie voor de

updates van het drukveld. Om optimale relaxatieparameters in de Richardson-iteratie te bepalen wordt Lokale Fourier Analyse (LFA) toegepast. De asymptotische convergentiefactoren van de multiroostermethode kunnen goed voorspeld worden door middel van twee-rooster LFA. Om de convergentie voor niet-triviale heterogene problemen verder te versnellen, wordt een recombinatieschema voorgesteld in Hoofdstuk 3.

Op basis van de verkregen kennis van de (Stokes- en) poroelasticiteitssystemen, lossen we het gekoppelde Darcy-Stokessysteem op in Hoofdstuk 4. Daarbij wordt aangenomen dat het poreuze medium stijf is. Een speciaal discretisatieschema is ontwikkeld voor de onbekenden op de koppeling van de beide subsystemen. Wij stellen een monolithische multiroostermethode in combinatie met de Uzawa-smoother voor, gebaseerd op de roosterpartitie parallelisatiestrategie. Optimale relaxatieparameters in de Uzawa-smoother worden opnieuw berekend door middel van LFA voor elk subprobleem. We hebben bevestigd dat de convergentie van multigrid overeen komt met de minste multiroosterconvergentiefactor van de individuele deelp Problemen. Het is verder goed om op te merken dat de multiroosterconvergentie onafhankelijk convergeert van de fysische parameterwaarden. Bovendien hebben we het effect van heterogeniteit op de multiroosterconvergentie bestudeerd.

Tenslotte ontwikkelen we een monolithische multiroostermethode voor het gekoppelde Stokes-poroelasticiteitssysteem door rekening te houden met de elastische vervorming van het poreuze medium in Hoofdstuk 5. Een vernieuwing in ons werk is dat bij de koppeling van de twee subsystemen, twee onbekenden uit de verschillende subsystemen worden gedefinieerd in hetzelfde roosterpunt. Wij stellen een speciale discretisatie voor de onbekenden op en nabij dit roosterpunt. In dit hoofdstuk onderzoeken we de multiroosterprestatie met de gekoppelde Vanka- en de ontkoppelde Uzawa-smoothers. Voor de Uzawa-smoother geven de resultaten uit Hoofdstuk 3 ons het nodige inzicht om de waarden van de relaxatieparameters voor de poroelasticiteitsvergelijkingen te optimaliseren. Binnen het roosterpartitieschema wordt de informatie uitgewisseld tussen naburige subdomeinen op elk roosterniveau. Dit vormt de basis om een zeer bevredigende multiroosterconvergentie te bereiken in multi-blok geometrieën. Dit proefschrift presenteert onderzoek naar de monolithische multiroostermethode voor systemen van gekoppelde vloeistofstromen en poreuze materialen. De

theoretische kwantitatieve analyse, numerieke algoritmen en resultaten die hier worden gepresenteerd geven inzicht en kennis in multiroostermethoden voor multi-fysische systemen. De combinatie van deze twee aspecten, d.w.z. multigrid en gekoppelde systemen, is spannend en uitdagend.

Contents

Acknowledgements	iii
Summary	vii
Samenvatting	x
1 Introduction	1
1.1 Background	1
1.2 Solution strategies	3
1.3 Multigrid method	4
1.4 Outline	7
2 Multigrid method for nonlinear poroelasticity equations	11
2.1 Introduction	11
2.2 Problem formulation	13
2.2.1 Unsteady case	13
2.2.2 Steady case	19
2.3 Numerical Method	20
2.3.1 Nonlinear multigrid method	20
2.3.2 Multigrid components	21
2.4 Numerical Results	24
2.4.1 Unsteady case	24
2.4.2 Steady case	26
2.5 Conclusions	33
3 On an Uzawa Smoother in Multigrid for Poroelasticity Equations	35

3.1	Introduction	35
3.2	Problem formulation	37
3.2.1	Poroelasticity equations	37
3.2.2	Discretization	38
3.3	The numerical method	40
3.3.1	Multigrid and acceleration	40
3.3.2	The Uzawa smoother	42
3.4	Local Fourier Analysis (LFA)	43
3.4.1	Basis of LFA	43
3.4.2	LFA for the Uzawa smoother	45
3.5	Uzawa based multigrid for poroelasticity equations	46
3.5.1	Staggered grid arrangement of unknowns	46
3.5.2	Collocated grid arrangement of unknowns	50
3.5.3	Heterogeneity case (collocated grids)	57
3.6	Conclusion	59
	Appendices	60
3.A	Non-square meshes: Staggered grid arrangement of unknowns	60
3.B	Non-square meshes: Collocated grid arrangement of unknowns	62
4	Uzawa smoother in multigrid for the coupled porous medium and Stokes flow system	65
4.1	Introduction	65
4.2	Problem formulation	68
4.2.1	Porous medium description	69
4.2.2	Free flow description	69
4.2.3	Interface conditions	70
4.3	Discretization	71
4.3.1	Discretization of Darcy equations	72
4.3.2	Discretization of Stokes equations	73
4.3.3	Discretization at the interface	74
4.4	Numerical method	76
4.4.1	Multigrid based on Uzawa smoother	77
4.4.2	Local Fourier analysis	80
4.4.3	Multigrid for the coupled Darcy-Stokes problem	83
4.5	Numerical experiments	89
4.5.1	No-slip interface condition	90

4.5.2	Beavers-Joseph-Saffman interface condition	94
4.5.3	Realistic test: cross-flow membrane filtration model	95
4.5.4	Heterogeneity test	99
4.6	Conclusions	102
5	Monolithic Multigrid Method for the Coupled Stokes Flow and Deformable Porous Medium System	103
5.1	Introduction	104
5.2	Problem formulation	106
5.2.1	Stokes flow description	106
5.2.2	Poroelastic flow description	107
5.2.3	Interface conditions	108
5.3	Discretization	109
5.3.1	Discretization for v^p and v^f at the interface	110
5.3.2	Discretization for u^p and u^f near the interface	112
5.3.3	Discretization for p^p and p^f near the interface	113
5.3.4	Saddle point structure	114
5.4	Fast solvers based on multigrid	115
5.4.1	Smoother	115
5.4.2	Coarse-grid correction	120
5.5	Numerical experiments	121
5.5.1	Analytic test	121
5.5.2	Two-block realistic test	126
5.5.3	Multi-block realistic test	127
5.6	Conclusions	132
	Appendices	134
5.A	Discretization of poroelastic equations at interior points	134
5.B	Discretization of Stokes equations at interior points	136
6	Conclusions and Outlook	137
6.1	Conclusions	137
6.2	Outlook	139
	Curriculum Vitae	151
	List of Publications	152

List of Presentations**154**

Introduction

1.1 Background

Fluid flow is everywhere in our natural and technical environment. The movement of a fluid is usually described by the dynamics of the flow and the interaction with its surrounding environment. Researchers are interested in applying fluid dynamics to various kinds of problems to better understand the flow patterns. In agriculture, people construct channels and water supply systems for the purpose of irrigation. In biology, essential nutrients and drugs are transported by flow in the blood vessels. In environmental sciences, people remove contaminants from sewage by filtration processes. In geosciences, hydraulic fracturing [53] is regarded as one of the methods for extracting oil or gas resources from the Earth surface.

Fluid dynamics [6] is an ancient science, which may date back to Ancient Greece, where Archimedes developed the fundamental principles of buoyancy. Ever since, outstanding scientists have devoted research efforts to fluid motion. In the 15th century, Leonardo da Vinci derived the conservation of mass equation for a one-dimensional steady-state flow. In the 17th century, Isaac Newton postulated the laws of motion and brought us the concept of Newtonian fluids. In the 18th century, the Bernoulli and Euler equations were stated respectively by Daniel Bernoulli and Leonhard Euler [34]. The Navier-Stokes equations [74, 89, 92] were stated in the 19th century when Newtonian viscous terms were added to the equations of motion. They are widely used to model water flow in a channel, ocean currents and air flow around aircraft. As a simplification of the full Navier-Stokes equations, the Stokes equations describe flow for which fluid

velocities are very slow and viscosities are large.

For long time, researchers have also been interested in the process of flow passing through a porous medium [25]. A porous medium consists of material containing voids, like rock and soil in natural, man-made cement and ceramics, sponges and also muscle or skin tissues. Often the solid skeleton and the pores network are tightly connected. Henry Darcy, in 1856, discovered the basic laws of flow [28] in porous media in one-dimension, based on experiments. Theoretically, Darcy's law can be derived from the Stokes equations via homogenization. In Darcy's law, the porous medium is assumed to be rigid and saturated. Moreover, for the movement of fluid in unsaturated porous media, the nonlinear Richards' equation [79] was derived by Lorenzo Richards in 1931. In unsaturated flow, hydraulic properties may change when fluids pass through the medium, filling some pores and draining others.

By taking also into account the deformation of the solid material, the theory of poroelasticity was proposed by Biot in 1941 [8]. Poroelasticity studies the interaction between the solid deformation and the fluid motion. In Biot's model, the fluid in saturated pores is modeled by the Darcy equation, and the deformation by means of linear elasticity equations. The poroelastic coupling implies that a change in the applied stresses of the solid skeleton will affect the pressure of the fluid, while a change in fluid pressure will lead to a change in the volume of the porous material.

Modeling the interaction of free flow and porous medium flow requires to consider coupled models with, in our case, the Stokes equations in the fluid domain and flow in the porous medium, like the Darcy equation or poroelasticity equations, resulting a coupled multi-physics system [85]. From this point of view, the application examples mentioned at the beginning of this introduction can be represented by a coupled model. In the filtration process, for example, the filter usually consists of a porous material. When fluid passes through a filter, properties of the material or fluid, such as pressure, permeability, stress and so on, may change. Simultaneously, these changes may affect the free fluid movement. Filtration processes have a wide range of application from engineering to biology, like waste water treatment, percolation of drugs into tissues, etc.

For the purpose of understanding and controlling the coupled process, it is desirable to simulate and investigate the interactions between fluid

flow and porous media. In the coupled system, except the separate models for each subdomain, the interface where the two domains meet plays an important role. In order to connect two subregions, appropriate boundary conditions need to be chosen at the interface [55, 82].

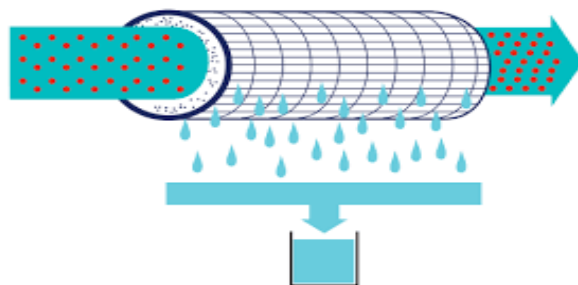


Figure 1.1: A filtration model (obtained from www.porexfiltration.com).

1.2 Solution strategies

The numerical solution of multi-physics problems is an active research area [30, 32, 51, 80, 81], since it is often impossible to solve the coupled problem analytically. Generally, there are two ways to solve a coupled multi-physics system numerically. The domain decomposition (DD) method is a popular approach, where the basic idea is to divide the problem geometry into subdomains, and the adjacent subdomains are related to each other by means of proper interface conditions. The subproblems are treated independently, which makes domain decomposition methods suitable for parallel computation. Regarding parallel computing, DD implies a distribution of the separate subdomain problems to different processors. An important aspect regarding the convergence of DD methods concerns the strength of the coupling of the different physical models in a multi-physics problem. We need to formulate accurate interface conditions to guarantee well-posedness of the problems and a meaningful information exchange across interfaces. DD methods can also be used as preconditioners for Krylov subspace iterative methods, such as the Generalized Minimal Residual (GMRES) method or the Conjugate Gradient (CG) method. More details and applications of DD methods can be found in [18, 23, 24].

There are several researchers applying DD methods for the coupled free fluid flow (Stokes equation) and the rigid porous media (Darcy equation)

model. In the coupled Darcy-Stokes model, the interaction between the fluid and the solid matrix in the porous media is neglected. In other words, the elastic properties of the solid matrix are not considered. Several advanced iterative solvers have been applied to the Darcy-Stokes system, as for example the Dirichlet-Neumann-type DD method [31], Robin-Robin DD method [22, 33], Lagrange multiplier-based DD method [61] and many others [19, 20, 69]. The main idea is to update the subdomain problems iteratively, until convergence.

The multi-physics problem becomes more involved by also considering the deformation of the porous medium. The coupling of free flow (Stokes equations) and deformable porous media (poroelasticity) has not yet been widely studied, probably due to the involved coupling at the interface. The DD method allows for each subdomain to employ different meshes, solvers and/or discretization schemes. The authors in [72] solve the coupled Stokes-poroelasticity system by means of a DD method, by using a separate multigrid method for the poroelastic equations and a SIMPLE-algorithm [76] for the Stokes equations. The essence of the DD method is modularity, where an important requirement is the data transfer at the interface between two existing fluid and poroelasticity software packages. The solvers are usually specifically designed for different subproblems. The issue is however the efficiency and convergence of the overall problem. In [17], the authors adopt a Lie operator splitting scheme for the fluid-poroelastic structure interaction (FPSI) problem, while in [71] partitioning strategies based on a Nitsche's coupling approach are proposed.

A second approach to deal with coupled multi-physics problems is to consider monolithic methods. In a monolithic approach, the complete discrete system arising from the coupled model of free flow and flow in the porous medium is treated at once. A single solution method is developed to simultaneously solve the governing equations together with the interface conditions. In this thesis, a monolithic multigrid method is developed as an efficient iterative solution method for the coupled multi-physics system.

1.3 Multigrid method

The multigrid method is an iterative solution method for solving linear as well as nonlinear discretized partial differential equations. The multigrid

technique was first proposed in 1964 by Fedorenko [35], who formulated a multigrid algorithm for the discrete Poisson equation obtained by the standard central finite difference method. In 1973 and 1977, Brandt reported practical results and showed the main insights in the multigrid method [11, 12]. The work by Brandt is regarded a landmark in the field of multigrid method development laying firm foundations for further development. Other pioneers include Hackbusch [42, 43, 44, 45], who developed the fundamental theory of multigrid. The multigrid method can be applied to various mathematical problems, such as elliptic and parabolic partial differential equations, integral equations and eigenvalue problems. There are many other applications of multigrid techniques and multilevel ideas in general, see [15, 46, 47, 73, 96].

Here, in this thesis, we restrict our attention to the application of multigrid methods in computational fluid dynamics which has a long tradition. At an early stage, multigrid methods were developed for the compressible potential equation [87]. Multigrid has been widely used for solving the incompressible Navier-Stokes problems, see [13, 99]. Highly efficient multigrid techniques have been developed for the Stokes and unsteady incompressible Navier-Stokes problems.

The main insight of multigrid methods is that they may improve the convergence properties of classical iterative methods, such as Gauss-Seidel and Jacobi methods, by additional corrections obtained from the solutions on coarser grids. Detailed information of multigrid, along with applications of practical problems can be found in the review article [90] by Trottenberg and Stüben, and the book [94].

It is well-known that the basic iterative relaxation methods are efficient for eliminating high frequency components of an error between exact solution and its numerical approximation. When the oscillatory components have been removed, the convergence of Jacobi or Gauss-Seidel methods slows down. When the resolution of the computational grid increases, the convergence of basic iterative methods gets much slower. These are the limitations of the classical iterative methods. The insight is that the smooth components of the error appear again oscillatory on a coarser grid forms the basis of the multigrid method. It becomes natural to transfer the smooth error components to coarse grids, where the basic iterative methods become effective again. Multigrid can be regarded as a technique in which basic

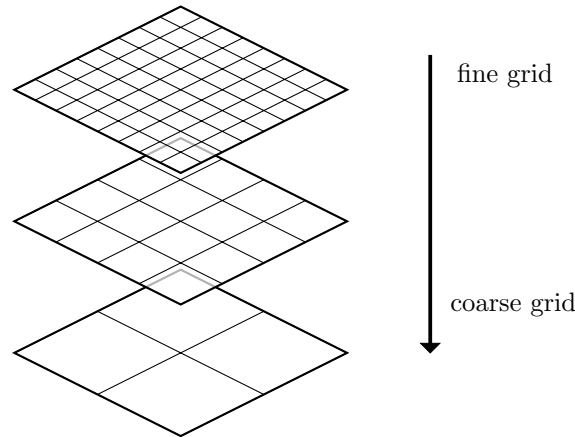


Figure 1.2: A sequence of coarse grids.

iterative methods are made efficient for all high and low frequency error components. The basic iterative methods are called relaxation methods or smoothers in the context of the multigrid method.

Just as its name implies, a multigrid method is based on a sequence of meshes obtained by successive coarsening, see Figure 1.2. The solution process may start with a basic iterative relaxation on the finest grid. Then, the residual belonging to the finest grid approximation of the solution is transferred by a restriction operator to a coarser grid. Since the problem on a coarser grid is similar to the fine grid problem, the same basic iterative relaxation method may be applied to eliminate the corresponding components of the error. This procedure is repeated until the coarsest grid is reached, where a direct solution of the problem is cheap. After that, the corrections to the solutions obtained on the coarsest grid are transferred back by a prolongation operator to finer grids. Additional relaxations by means of the basic iterative methods are needed on the finer grids for a rapid and reliable convergence. The multigrid method has a recursive structure. There are several possibilities when moving through the grid hierarchy, that are called the multigrid cycles. A typical property of multigrid is that the convergence rate is independent of the mesh size, which makes multigrid suitable for the efficient iterative solution of very large discretized systems of equations. It is challenging to define robust and efficient multigrid methods for all sorts of PDE problems. In order to determine suitable multigrid components, such as smoothers, transfer operators, coarse grid discretizations etc., a quantitative theoretical analysis

called Local Fourier Analysis (LFA) has been presented, see [94, 100]. The analysis was first proposed by Brandt [12] then developed and refined in various articles. The basic idea of LFA is that the errors can be expressed as a formal linear combination of certain functions, i.e., Fourier modes. A Fourier space is defined by these Fourier modes. We may analyze how the multigrid components act on the Fourier space, and aim to predict the performance of multigrid this way. LFA is based on the assumption that operators are defined on infinite grids and that boundary conditions are neglected.

An extension of the basic multigrid method for solving linear partial differential equations is the nonlinear multigrid method, which has been developed for solving nonlinear equations efficiently. To deal with nonlinearity, basically there are two multigrid approaches [94]. First of all, global linearization is naturally applied, like by Newton's method. After having linearized the PDE problem, in each linearization step, the basic multigrid method can be used for solving the resulting Jacobian system. Such a scheme is called the Newton multigrid method, i.e., Newton's method is used in an outer iteration and linear multigrid solves as an inner iteration.

A second approach is called the Full Approximation Scheme (FAS). Multigrid is then immediately employed for the nonlinear equations. It is worth noting that instead of solving an equation for corrections of the solution on a coarse grid, the original equation is prescribed and full solutions are also computed on coarse grids. The smoother on each grid level is a nonlinear basic iterative method, such as a nonlinear Gauss-Seidel or Jacobi iteration.

1.4 Outline

In this thesis, we develop efficient monolithic multigrid algorithms for multi-physics problems. First of all, we focus on the poroelastic equations. The multigrid method is applied to both linear and nonlinear poroelastic equations. An Uzawa smoother is used in this context, which is analyzed based on Local Fourier Analysis (LFA), providing information about suitable relaxation parameters. The convergence of multigrid is also examined for a heterogeneous poroelastic problem.

With a deeper understanding of the separate subproblems, we then pro-

pose a monolithic multigrid algorithm including the Uzawa smoother for the coupled Darcy-Stokes model. Based on the insights obtained in a previous chapter, we select optimal relaxation parameters for each subsystem. We investigate the robustness of the algorithm for small and realistic values of the physical parameters.

Moreover, the coupled Stokes-poroelasticity model is considered, in which the deformation of the porous media is taken into account. For the unknowns at, or close to, the Stokes-poroelasticity interface special discretization schemes have been developed. Monolithic multigrid methods with either a coupled Vanka-type smoother or a decoupled Uzawa smoother have been developed. The efficiency of multigrid is illustrated by several numerical experiments under different settings.

The organization of this thesis is as follows.

- In **Chapter 2**, we solve the system of unsteady incompressible poroelasticity equations by means of the two nonlinear multigrid methods, mentioned earlier, i.e., the Full Approximation Scheme (FAS) and Newton multigrid. Regarding the discretization of the equations, we focus on a vertex-centered collocated grid arrangement in this chapter. For accurate solutions, a stabilization term is added to one of the continuous equations, since oscillations may occur when the system is discretized on a vertex-centered grid by a finite volume method. Steady problems are considered for both homogeneous and heterogeneous permeability cases. For the FAS method, the multigrid convergence performance with two different smoothers is investigated. The contents of this chapter are published in [63].
- In **Chapter 3**, for the efficient multigrid solution of the poroelasticity system, a decoupled smoother called the Uzawa smoother is employed. The Uzawa smoother can be interpreted as a combination of a symmetric Gauss-Seidel (SGS) smoothing iteration for the displacement unknowns and a Richardson iteration for the pressure field. To select an optimal relaxation parameter for the Richardson iteration, the LFA is applied. The asymptotic convergence factors of multigrid can be accurately predicted with the help of LFA. For the poroelasticity system with heterogeneous coefficients, an acceleration scheme by means of an iterant recombination to improve the multigrid

convergence is applied. The contents of this chapter are published in [64].

- In **Chapter 4**, we solve the coupled porous media and Stokes flow problem by a monolithic multigrid method with the decoupled Uzawa smoother for the whole system. The porous media are assumed to be rigid. The coupled Darcy-Stokes system is discretized on a staggered grid by the finite volume method. Special care is taken regarding the non-trivial conditions at the interface between the two subproblems. LFA is again used to determine optimal Richardson relaxation parameters for each subproblem. The coupled model with a heterogeneous porous medium is also considered. The efficiency and robustness of the algorithm are examined in quite some detail. The contents of this chapter are published in [66].
- In **Chapter 5**, the staggered grid monolithic multigrid method is extended to the coupled unsteady fluid flow and deformable porous media system. At the interface between the Stokes and poroelastic subproblems, two unknowns belonging to different subsystems are defined at the same grid point. We present a special discretization scheme for the unknowns at or close to the interface. To solve the Stokes-poroelasticity system by multigrid, either a coupled Vanka or a decoupled Uzawa smoother is employed here. In the algorithm, the communication on each multigrid level between neighboring subdomains is based on the grid partitioning strategy. The contents of this chapter are presented in [65].
- In **Chapter 6**, conclusions are drawn and some possible topics for future research are given.

Multigrid method for nonlinear poroelasticity equations

In this chapter, a nonlinear multigrid method is applied for solving the system of incompressible poroelasticity equations considering nonlinear hydraulic conductivity. For the unsteady problem, an additional artificial term is utilized to stabilize the solutions when the equations are discretized on collocated grids. We employ two nonlinear multigrid methods, i.e. the “Full Approximation Scheme” (FAS) and “Newton multigrid” for solving the corresponding system of equations arising after discretization. For the steady case, both homogeneous and heterogeneous problems are solved and two different smoothers are examined to search for an efficient multigrid method. Numerical results show a good convergence performance for all the strategies. ¹

2.1 Introduction

Shale gas [27, 56] is natural gas which is formed by being trapped within shale layer formations. Shale layers have typically low hydraulic conductivity which dramatically reduces the mobility of this so-called unconventional gas. Hydraulic fracturing [53] has been regarded as one of the methods of extracting these gas resources. It is a process in which injection of a highly pressurized fluid creates fractures within rock layers.

¹The contents of this chapter have been published in paper [63]: P. Luo, C. Rodrigo, F.J. Gaspar and C.W. Oosterlee. Multigrid method for nonlinear poroelasticity equations. *Computing and Visualization in Science*, 17(5):255-265, 2015.

The concept of poroelasticity [25, 26, 29] can be used as a model describing the Earth. It is a well-developed theory that was originally studied by Terzaghi [93] who proposed a model for a one-dimensional consolidation problem. After that, in 1941, Biot [8, 9] extended the theory to a general three-dimensional model. The model has been widely used for problems in rock mechanics, and it describes the interaction between the solid (rock) deformation and the fluid motion. It is a coupled model considering the seepage and stress processes together. The 2D poroelasticity problem can be formulated as a system of partial differential equations for the unknowns displacements and pore pressure of the fluid. Existence and uniqueness of the solution of this problem have been studied for example by Showalter [84] and Barucq et al. [5].

Often porous material is assumed to be homogeneous in numerical experiments, however, in fact materials usually have complicated properties composed of different characteristics. Therefore, it is necessary to take heterogeneity into account which can influence the poroelastic behavior in many ways. Heterogeneity means that the coefficients in the equations are not constant and all (or several) characteristics of the main problem follow some distribution. Also the hydraulic conductivity of the material plays a role. There is a significant difference in conductivity once material deformations start to occur. The coefficient of conductivity depends on the stress and fluid pressure, resulting in a nonlinear set of equations. Both heterogeneity and nonlinear conductivity are included in the nonlinear poroelastic model studied here. As an analytic solution is usually not available, we solve the poroelasticity system by means of numerical techniques. We will employ the finite volume method for the nonlinear system of poroelasticity equations. Details about the convergence results of the multi-dimensional finite volume discretization for the nonlinear system of poroelasticity equations is, to our knowledge, not yet known or available in the literature. In one dimension, however, convergence of the discrete solution has been shown in [37] for a staggered arrangement of the poroelasticity unknowns in the nonlinear case. Convergence results of discrete schemes for the (multi-dimensional) linear system of poroelasticity equations, on a staggered and on a collocated grid, are available, see, for example, [38, 40].

We would like to employ the multigrid method [14, 16, 46, 94, 98] as

the iterative solution method for the discretized partial differential equations. It is known that many classical iterative methods, like Jacobi or Gauss-Seidel cannot efficiently eliminate low-frequency errors appearing in a numerical approximation. This may cause slow convergence, as low frequency error modes tend to disappear extremely slowly from a discrete approximation. Therefore, the multigrid method is chosen as a highly efficient solution method, improving the performance of the basic relaxation schemes. Regarding the nonlinear system, the multigrid iterative method can also be employed as a nonlinear solver. The “Full Approximation Scheme” (FAS) and “Newton Multigrid” are both considered for the time-dependent problem. With respect to the smoother in the multigrid algorithm, coupled smoothers called Vanka and point Gauss-Seidel (PGS) are chosen and compared.

The organization of this chapter is as follows: First of all, we present the governing equations of the unsteady and steady poroelastic model, together with the finite volume discretization scheme on a collocated grid in Section 2.2. In Section 2.3, the nonlinear multigrid methods are introduced. Each component of multigrid is clarified. After that, numerical experiments are presented in Section 2.4. All of the results show satisfactory convergence performance of the proposed methods. Finally, a conclusion is given in Section 2.5.

2.2 Problem formulation

2.2.1 Unsteady case

Governing equations

We deal with a deformable fluid-saturated porous medium, whose solid matrix is elastic and the fluid is viscous. Both solid matrix and pore network are considered to be continuous, and thus fully connected. Biot’s poroelastic theory [8, 9] is based on the coupling between the coherent solid skeleton and the pore fluid flow. A change in the applied stress of the skeleton will affect the pressure or mass of the fluid, and a change in fluid pressure will lead to a change in the volume of the porous material.

A poroelasticity system is constructed on the description of the fluid pressure, stress, displacement and strain in the medium, and mass and

momentum conservation principles. Supposing that the porous matrix is fluid-filled, the total Cauchy stress tensor σ_{ij} can be divided into two parts, pore pressure (fluid) p and effective stress of the soil skeleton (solid) σ_{ij}^e . The effective stress is defined as a subtraction of pore pressure from the total stress. Pore pressure only influences the normal stress. The total momentum balance reads:

$$\sigma_{ij,j} + F_i = 0 \quad (i, j = 1, 2, 3), \quad (2.1)$$

where F_i is the body force in the i -th direction. The summation convention is used when repeated subscripts occur. The strain quantity, ε_{ij} , is a measure of the solid deformation with respect to an initial state. Variables u_i and ε_{ij} are related according to the compatibility condition:

$$\varepsilon_{ij} = \frac{1}{2}(u_{i,j} + u_{j,i}). \quad (2.2)$$

Moreover, $\varepsilon_v = \varepsilon_{11} + \varepsilon_{22} + \varepsilon_{33}$, is the volume strain. The constitutive equation in Biot's model is based on the assumptions of linearity between stress and strain:

$$\sigma_{ij}^e = \sigma_{ij} - \alpha p \delta_{ij} = \lambda \delta_{ij} \varepsilon_v + 2G \varepsilon_{ij}, \quad (2.3)$$

where λ and G are the effective Lamé constants; δ_{ij} is the Kronecker delta; α denotes the coefficient of pore pressure, which is also called effective stress coefficient.

Darcy's law [52] describes the rate at which a fluid flows through a permeable medium. The seepage equation in the poroelasticity model is obtained when substituting Darcy's law into the continuity equation for the fluid, i.e.

$$\iota \frac{\partial p}{\partial t} - \nabla \cdot (K \nabla p) = -\alpha \frac{\partial \varepsilon_v}{\partial t}, \quad (2.4)$$

with K the hydraulic conductivity, and ι is the product of the porosity and the compressibility of the fluid.

When an element of rock undergoes elastic deformation, its hydraulic properties will change. Hydraulic conductivity regarding its transport property describes how easily fluid flows through the rock material which will be influenced by variation of stress. Supposing that the conductivity and stress follow a negative exponential function, the conductivity reads

$$K(\sigma_{ii}, p) = \xi K_0 e^{-\beta(\frac{\sigma_{ii}}{3} - \alpha p)}, \quad (2.5)$$

where K_0 is the initial conductivity of the rock element; β is a coupling coefficient which reflects the influence of stress on the coefficient of conductivity; $\sigma_{ii}/3$ is the average stress; and ξ is a mutation coefficient to account for the increase in conductivity of the material during fracture formation. When $\xi > 1$, the above expression gives a higher conductivity caused by damage. In other words, the conductivity in equation (2.5) will dramatically increase when there is a “failure” in the element.

For the unsteady-state case in 2D, the governing equations have a time dependent term and a Navier-type equation for displacement vector \mathbf{u} resulting by applying the constitutive equation (2.3) and the geometric relation (2.2), where ε_{ij} is expressed in terms of the displacement gradient to the balance equation (2.1), with $F_i = 0$, i.e.,

$$\begin{cases} -G \Delta \mathbf{u} - (\lambda + G) \text{grad div } \mathbf{u} + \alpha \text{grad } p = \mathbf{g}, \\ -\nabla \cdot (K \nabla p) + \alpha \frac{\partial}{\partial t} (\text{div } \mathbf{u}) = f, \\ K(\sigma, p) = \xi K_0 e^{-\beta((\lambda+G) \cdot \text{div } \mathbf{u} - \alpha p)}. \end{cases} \quad (2.6)$$

The source terms $\mathbf{g} = (g_1, g_2)$ and f are supposed to be in $(L^2(\Omega))^2$ and $L^2(\Omega)$, respectively. They are used to represent a density of applied body forces and a forced fluid extraction or injection process for each case [38]. The term $(\alpha \text{grad } p)$ presents the stress due to fluid pressure within the medium, and $\text{div } \mathbf{u}$ is the volume change rate.

Coefficients λ and G are related to Young’s modulus and Poisson’s ratio by

$$\lambda = \frac{\nu E}{(1 + \nu)(1 - 2\nu)}, \quad G = \frac{E}{2(1 + \nu)}. \quad (2.7)$$

Discretization

When discretizing the poroelasticity equations (2.6), we employ a collocated grid [38, 75, 94] on which all variables - displacements vector $\mathbf{u} = (u, v)$ and fluid pressure p , are placed at the vertex-centered grid points. Collocated grid arrangements are convenient for numerical iteration methods like multigrid. Whereas for unsteady poroelasticity simulations an artificial stabilization has to be used, this is not the case for the steady poroelasticity case, as oscillations of pressure do not occur in that case.

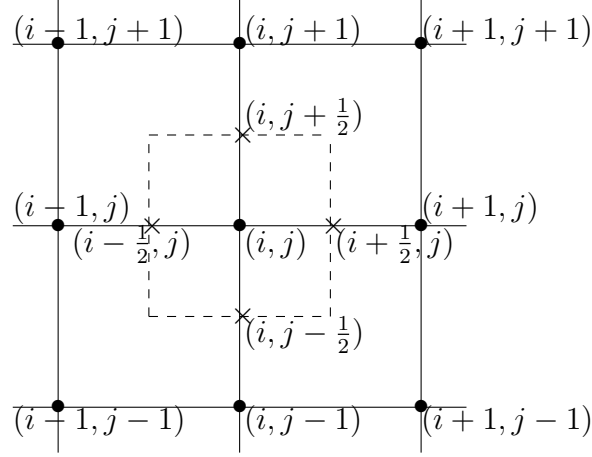


Figure 2.1: Control volume for an arbitrary node (i, j) and corresponding numbering of the neighboring grid points.

The finite volume method is employed as the discretization scheme. We take the first equation in (2.6) as an example. It can be written as

$$-\operatorname{div} \sigma + \alpha \nabla p = \mathbf{g}, \quad (2.8)$$

where σ denotes the two-dimensional stress matrix $\begin{pmatrix} \sigma_{xx} & \sigma_{xy} \\ \sigma_{yx} & \sigma_{yy} \end{pmatrix}$. In Figure 2.1, the square with dotted lines represents a control volume $V_{i,j}$ used for the vertex-centered grid, and $\Omega_{i,j}$ denotes the boundary of $V_{i,j}$.

Now, we consider the first equation in (2.8) for example, which can be expressed as,

$$-\nabla \cdot (\sigma_{xx}, \sigma_{xy}) + \alpha p_x = g_1. \quad (2.9)$$

By integration of (2.9) over the control volume $V_{i,j}$, one obtains,

$$-\int_{V_{i,j}} \nabla \cdot (\sigma_{xx}, \sigma_{xy}) \, dV_{i,j} + \alpha \int_{V_{i,j}} p_x \, dV_{i,j} = \int_{V_{i,j}} g_1 \, dV_{i,j}. \quad (2.10)$$

The Gauss divergence theorem converts volume integrals to surface integrals, resulting here in

$$-\int_{\Omega_{i,j}} (\sigma_{xx}, \sigma_{xy}) \cdot \mathbf{n} \, ds + \alpha \int_{V_{i,j}} p_x \, dV_{i,j} = \int_{V_{i,j}} g_1 \, dV_{i,j}, \quad (2.11)$$

or

$$\begin{aligned} & - \int_{\tau_1} \sigma_{xx} \, ds - \int_{\tau_2} \sigma_{xy} \, ds + \int_{\tau_3} \sigma_{xx} \, ds + \int_{\tau_4} \sigma_{xy} \, ds \\ & + \alpha \int_{V_{i,j}} p_x \, dV_{i,j} = \int_{V_{i,j}} g_1 \, dV_{i,j}, \end{aligned} \quad (2.12)$$

where \mathbf{n} is the unit normal vector to the volume, and τ_i ($i = 1, 2, 3, 4$) is the right, top, left and bottom boundary of control volume $V_{i,j}$, respectively. By applying to (2.12) the following relations,

$$\begin{cases} \sigma_{xy} = G(u_y + v_x), \\ \sigma_{yy} = \lambda u_x + (\lambda + 2G)v_y, \\ \sigma_{xx} = (\lambda + 2G)u_x + \lambda v_y, \end{cases} \quad (2.13)$$

the resulting discrete equation is given by

$$\begin{aligned} & -h[(\lambda + 2G)u_x + \lambda v_y]_{i+\frac{1}{2},j} - h[G(u_y + v_x)]_{i,j+\frac{1}{2}} \\ & + h[(\lambda + 2G)u_x + \lambda v_y]_{i-\frac{1}{2},j} + h[G(u_y + v_x)]_{i,j-\frac{1}{2}} \\ & + \alpha h(p_{i+\frac{1}{2},j} - p_{i-\frac{1}{2},j}) = h^2 g_1, \end{aligned} \quad (2.14)$$

where h is the grid size of a uniform grid used for the space discretization. Central differences are applied to the first-order derivatives u_x , u_y , v_x , and v_y . Similarly, the discrete equation for the second equation in (2.8) can also be obtained.

It is convenient to apply stress boundary conditions to equation (2.12), by substituting the given stress at boundaries, of course, adapting the control volume.

Regarding the seepage equation, we discretize it on a collocated grid as well. However, such discretization for unsteady problems will be unstable, because oscillations may appear in the first time steps of a numerical solution. After this phase, the solution becomes smoother and these oscillations tend to disappear. Some special care is needed to construct a stable discretization for the whole process. A stabilized discretization can be achieved by adding an artificial elliptic pressure term [38, 75] to the seepage equation in (2.6), as follows

$$-\nabla \cdot (K \nabla p) + \alpha \frac{\partial}{\partial t} (\text{div } \mathbf{u}) - \frac{\partial}{\partial t} (\nabla \cdot (\varepsilon \nabla p)) = f, \quad (2.15)$$

where the artificial term is $\frac{\partial}{\partial t}(\nabla \cdot (\varepsilon \nabla p))$, with $\varepsilon = \frac{h^2}{4(\lambda+2G)}$, see [38]. When the mesh size $h \rightarrow 0$, the artificial term tends to 0. Now the system of equations with a stabilization term added, can be discretized on a collocated grid by the finite volume method. Since this term is proportional to h^2 , second-order accuracy can be maintained.

Since equation (2.15) represents a time-dependent problem, a time discretization is required. The discrete problem has to be solved each time step. In each of the finite volumes $V_{i,j}$, the integral formulation of (2.15) has the form,

$$\begin{aligned} & - \int_{V_{i,j}} \nabla \cdot (K \nabla p) \, dV_{i,j} + \int_{V_{i,j}} \frac{\partial}{\partial t} (u_x + v_y) \, dV_{i,j} \\ & - \int_{V_{i,j}} \frac{\partial}{\partial t} (\nabla \cdot (\varepsilon \nabla p)) \, dV_{i,j} = \int_{V_{i,j}} f \, dV_{i,j}. \end{aligned} \quad (2.16)$$

Using the Gauss theorem, we have

$$\begin{aligned} & -(\varepsilon + K_{i+\frac{1}{2},j} \theta \tau) p_{i+1,j}^{\bar{m}+1} - (\varepsilon + K_{i,j+\frac{1}{2}} \theta \tau) p_{i,j+1}^{\bar{m}+1} \\ & -(\varepsilon + K_{i-\frac{1}{2},j} \theta \tau) p_{i-1,j}^{\bar{m}+1} - (\varepsilon + K_{i,j-\frac{1}{2}} \theta \tau) p_{i,j-1}^{\bar{m}+1} \\ & + (4\varepsilon + (K_{i+\frac{1}{2},j} + K_{i,j+\frac{1}{2}} + K_{i-\frac{1}{2},j} + K_{i,j-\frac{1}{2}}) \theta \tau) p_{i,j}^{\bar{m}+1} \\ & + \frac{\alpha h}{2} (u_{i+1,j}^{\bar{m}+1} - u_{i-1,j}^{\bar{m}+1} + v_{i,j+1}^{\bar{m}+1} - v_{i,j-1}^{\bar{m}+1}) = \\ & -(\varepsilon - K_{i+\frac{1}{2},j} (1-\theta) \tau) p_{i+1,j}^{\bar{m}} - (\varepsilon - K_{i,j+\frac{1}{2}} (1-\theta) \tau) p_{i,j+1}^{\bar{m}} \\ & -(\varepsilon - K_{i-\frac{1}{2},j} (1-\theta) \tau) p_{i-1,j}^{\bar{m}} - (\varepsilon - K_{i,j-\frac{1}{2}} (1-\theta) \tau) p_{i,j-1}^{\bar{m}} \\ & + (4\varepsilon - (K_{i+\frac{1}{2},j} + K_{i,j+\frac{1}{2}} + K_{i-\frac{1}{2},j} + K_{i,j-\frac{1}{2}}) (1-\theta) \tau) p_{i,j}^{\bar{m}} \\ & + \frac{\alpha h}{2} (u_{i+1,j}^{\bar{m}} - u_{i-1,j}^{\bar{m}} + v_{i,j+1}^{\bar{m}} - v_{i,j-1}^{\bar{m}}) \\ & + \tau \theta f_{i,j}^{\bar{m}+1} h^2 + \tau (1-\theta) f_{i,j}^{\bar{m}} h^2, \end{aligned} \quad (2.17)$$

where τ is the step-size in time direction and the approximation of conductivity $K_{i+\frac{1}{2},j}$ can be expressed as

$$\begin{aligned} K_{i+\frac{1}{2},j} &= \xi K_0 \exp(-\beta[(\lambda + G) [\frac{u_{i+1,j} - u_{i,j}}{h} \\ & + \frac{1}{2} (\frac{v_{i+1,j+1} - v_{i+1,j-1}}{2h} + \frac{v_{i,j+1} - v_{i,j-1}}{2h})] \\ & - \alpha \frac{p_{i+1,j} + p_{i,j}}{2}]). \end{aligned} \quad (2.18)$$

For other values of permeabilities, a similar formulation can be obtained without any difficulties. Obviously, the values of unknowns $\{\mathbf{u}^{\bar{m}+1}, p^{\bar{m}+1}\}$ at a new time $t + \tau$ can be calculated immediately from the values of the previous time. From discrete formula (2.17), the backward Euler and Crank-Nicolson schemes can both be used by choosing with $\theta = 1$ and $\theta = 0.5$, respectively. We prefer to use the Crank-Nicolson scheme here, so that second-order accuracy in time can be obtained.

2.2.2 Steady case

Governing equations

Under steady-state conditions, (2.4) becomes a Poisson-like equation,

$$-\nabla \cdot (K \nabla p) = 0. \quad (2.19)$$

From equations (2.6) and (2.19), the governing equations for the 2D steady poroelasticity model can be obtained as

$$\begin{cases} -G \Delta \mathbf{u} - (\lambda + G) \text{grad div } \mathbf{u} + \alpha \text{grad } p = 0, \\ -\nabla \cdot (K \nabla p) = 0, \\ K(\sigma, p) = \xi K_0 e^{-\beta((\lambda+G)\text{div } \mathbf{u} - \alpha p)}. \end{cases} \quad (2.20)$$

Here we simply consider the case that the source terms are all zeros.

Discretization

Since the seepage equation in (2.20) is a Poisson-type equation, second-order accuracy can be achieved again by applying finite volumes on a uniform rectangular grid. Note that the artificial stabilization term is not needed for the steady case. The discrete form of the seepage equation reads

$$-\int_{V_{i,j}} \nabla \cdot (K \nabla p) \, dV_{i,j} = 0. \quad (2.21)$$

The left-hand side of (2.21) can be reformulated as an integral over the boundary of the volume $V_{i,j}$,

$$-\int_{\tau_1} K \frac{\partial p}{\partial x} \, ds - \int_{\tau_2} K \frac{\partial p}{\partial y} \, ds + \int_{\tau_3} K \frac{\partial p}{\partial x} \, ds + \int_{\tau_4} K \frac{\partial p}{\partial y} \, ds = 0. \quad (2.22)$$

Replacing p_x and p_y by a centered approximation, one obtains

$$\begin{aligned} & -K_{i+\frac{1}{2},j}(p_{i+1,j} - p_{i,j}) - K_{i,j+\frac{1}{2}}(p_{i,j+1} - p_{i,j}) \\ & + K_{i-\frac{1}{2},j}(p_{i,j} - p_{i-1,j}) + K_{i,j-\frac{1}{2}}(p_{i,j} - p_{i,j-1}) = 0. \end{aligned} \quad (2.23)$$

It can be seen that Lamé coefficients and permeabilities are required at the four mid-points $(i + \frac{1}{2}, j)$, $(i - \frac{1}{2}, j)$, $(i, j + \frac{1}{2})$ and $(i, j - \frac{1}{2})$ that are at the control volume boundaries. If the material is heterogeneous, these parameters are determined from a stochastic distribution, which means they are different at each vertex of the collocated grid. Due to this, the averaged values of two adjacent vertices are used for those middle points in the discrete formulas. Boundary conditions will be specified in Section 2.4.

2.3 Numerical Method

The multigrid method - an efficient numerical technique for solving systems of linear and nonlinear equations - is employed for the solution of the discretized poroelastic partial differential equations, based on earlier multigrid work on poroelasticity model problems [38, 75].

2.3.1 Nonlinear multigrid method

To deal with the nonlinearity, there are basically two approaches.

Newton multigrid. There is no doubt that Newton's method is the most important method for solving nonlinear equations. Newton multigrid is based on global linearization. Newton's method is applied to linearize the equations, and multigrid solves the resulting linear Jacobian system.

Full Approximation Scheme. The other multigrid technique suitable for nonlinear problems is the Full Approximation Scheme (FAS) [14, 94] which treats directly the nonlinear equations on fine and coarse grids. In FAS, a nonlinear iteration, such as the nonlinear Gauss-Seidel method is applied to smooth the error. Differently from linear multigrid, the full-scale equation is solved on the coarse grid instead of the residual equation, because of the nonlinearity.

2.3.2 Multigrid components

For efficient multigrid methods, each component of multigrid needs to be selected with special attention. Those components are related to the collocated grid arrangement of the poroelasticity discretization chosen here. The multigrid transfer operators, restrictions and prolongations, are then well-known in geometric multigrid. Regarding the most important component in this setting, i.e., the smoothing scheme, we consider two methods for the time-dependent system of equations - Gauss-Seidel relaxation and box-relaxation [38, 75].

Smoothers. The choice of smoother is the most significant part which can crucially affect the performance of multigrid. Several branches of robust smoothers have been developed for the poroelasticity equations. They all fall into two major categories: decoupled and coupled smoothers. With respect to the decoupled smoothers, that are also denoted as equation-wise relaxation, DGS (distributive Gauss-Seidel) is the original method, introduced in [13]. Here we focus on the other type of smoothers - coupled relaxation. A coupled smoother is a state-of-the-art relaxation scheme for saddle point problems. The technique is based on processing the grid cells in some order and to relax all unknowns associated with that cell simultaneously.

A point-wise collective Gauss-Seidel (PGS) relaxation is chosen, which processes three unknowns $u_{i,j}$, $v_{i,j}$ and $p_{i,j}$ at grid point (i, j) simultaneously. A small 3×3 system is solved for each grid point. We consider the correction equation during smoothing for convenience, i.e.,

$$\begin{pmatrix} a_{1,1} & a_{1,2} & a_{1,3} \\ a_{2,1} & a_{2,2} & a_{2,3} \\ a_{3,1} & a_{3,2} & a_{3,3} \end{pmatrix} \begin{pmatrix} eu_{i,j} \\ ev_{i,j} \\ ep_{i,j} \end{pmatrix}^{\hat{m}+1} = \begin{pmatrix} ru_{i,j} \\ rv_{i,j} \\ rp_{i,j} \end{pmatrix}^{\hat{m}}, \quad (2.24)$$

where $eu_{i,j}^{\hat{m}+1} = u_{i,j}^{\hat{m}+1} - u_{i,j}^{\hat{m}}$ is an increment to the solution u corresponding to node (i, j) . It is the same for v and p . $ru_{i,j}$, $rv_{i,j}$ and $rp_{i,j}$ represent the corresponding residuals. After solving the residual equations, the computed increments will be added to the current solution (take u for example),

$$u_{i,j}^{\hat{m}+1} = u_{i,j}^{\hat{m}} + \omega eu_{i,j}^{\hat{m}+1}, \quad (2.25)$$

with an underrelaxation parameter $\omega \in [0, 1]$.

The use of a collective smoother in the case of nonlinear systems of equations requires some more explanation. In principle, we have a variety of choices of local linearization and grid point processing at our disposal, like Newton-Gauss-Seidel, Newton-Jacobi, Picard-Gauss-Seidel, Picard-Jacobi relaxation, and many others, see, for example [46, 94].

We here employ a “straightforward” basic linearization variant to deal with the nonlinearity locally.

When we process the unknowns at a certain grid point, in the collocated grid, we assume that we work in a lexicographical Gauss-Seidel fashion, and that we have already updated the poroelasticity unknowns on previous grid points. Because of the form of the nonlinearity in (2.20), we will use the most recent updated unknowns when we set up the matrix element related to the nonlinearity, in the system (2.24).

In the nonlinear term,

$$K(\sigma, p) = \xi K_0 e^{-\beta((\lambda+G)\operatorname{div} \mathbf{u} - \alpha p)}$$

we need to define $\operatorname{div} \mathbf{u}$ at a certain grid point (i, j) , and we will always take the latest updates of the displacement unknowns to define this matrix element. This means, the just updated neighbouring \mathbf{u} -values are combined with the “old” displacement values for the points that have not yet been processed. For the pressure in the nonlinear term, we always take the “old” value, in the linearization process.

This is a pragmatic way of linearization, related to Gauss-Seidel-Picard linearization. We will perform the same local linearization when dealing with the Vanka smoother in (2.26), and carefully consider each equation, take the latest values for all unknowns. These are sometimes recently updated values, and sometimes the values from a previous iteration.

The second smoothing scheme considered is the Vanka smoother which is also called box relaxation. It was originally proposed by Vanka [95] for solving the Navier-Stokes equations discretized by the finite difference method on a staggered grid. This approach can be applied to a wide range of problems, which we extend to the poroelasticity equations, see also [38]. Instead of the three unknowns at each grid point as in PGS, five unknowns (pressure $p_{i,j}$ and displacements $u_{i+1,j}$, $u_{i-1,j}$, $v_{i,j+1}$, $v_{i,j-1}$) are relaxed at the same time (see Figure 2.2). At each grid-point, a (5×5) -system is

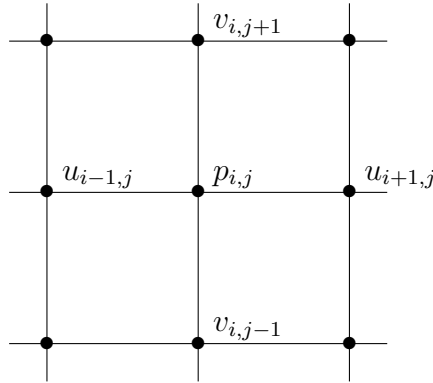


Figure 2.2: Five unknowns updated simultaneously in the Vanka-type smoother.

solved. Similarly as for PGS, we solve the so-called correction equations which play a vital role during relaxations,

$$\begin{pmatrix} a_{1,1} & a_{1,2} & a_{1,3} & a_{1,4} & a_{1,5} \\ a_{2,1} & a_{2,2} & a_{2,3} & a_{2,4} & a_{2,5} \\ a_{3,1} & a_{3,2} & a_{3,3} & a_{3,4} & a_{3,5} \\ a_{4,1} & a_{4,2} & a_{4,3} & a_{4,4} & a_{4,5} \\ a_{5,1} & a_{5,2} & a_{5,3} & a_{5,4} & a_{5,5} \end{pmatrix} \begin{pmatrix} eu_{i+1,j} \\ eu_{i-1,j} \\ ev_{i,j+1} \\ ev_{i,j-1} \\ ep_{i,j} \end{pmatrix}^{\hat{m}+1} = \begin{pmatrix} ru_{i+1,j} \\ ru_{i-1,j} \\ rv_{i,j+1} \\ rv_{i,j-1} \\ rp_{i,j} \end{pmatrix}^{\hat{m}}. \quad (2.26)$$

Obviously, in one iteration for the whole domain, all displacement unknowns are updated twice, whereas pressure unknowns are updated once. The updated solution has the same expression as (2.25).

Coarse grid correction. With respect to the coarse grid correction, we choose geometric grid coarsening as we will deal with regular Cartesian grids in these experiments. The sequence of coarse grids is obtained by doubling the mesh size in each spatial direction and we use a (2×2) -grid as the coarsest grid. As in the scalar case, any suitable solver can be applied on the coarsest level.

Transfer operators. Supposing we have performed several smoothing steps to obtain an updated solution and a sequence of coarse grids is ready, the next step is to restrict the approximation to the next coarser grid. Since we are trying to solve a system of equations, there is more than one equation at each grid point. The restriction is done separately for each of these

equations in the system. As a standard choice for the scalar problem, the Full Weighting (FW) operator [94] is chosen for the restriction in our case.

With respect to the prolongation, a typical choice is bilinear interpolation for each unknown grid function from coarse grid to the next finer grid.

Grid	Smoother	Conv.	Time(s)	$\frac{\ p_h - p\ _\infty}{\ p\ _\infty}$	$\frac{\ u_h - u\ _\infty}{\ u\ _\infty}$
$16 \times 16 \times 2$	PGS	0.20	0.06	6.89×10^{-3}	1.96×10^{-3}
	Vanka	0.19	0.08		
$32 \times 32 \times 4$	PGS	0.20	0.24	9.83×10^{-4}	5.69×10^{-4}
	Vanka	0.18	0.46		
$64 \times 64 \times 8$	PGS	0.20	1.56	1.81×10^{-4}	1.39×10^{-4}
	Vanka	0.17	3.30		
$128 \times 128 \times 16$	PGS	0.20	11.48	5.69×10^{-5}	3.50×10^{-5}
	Vanka	0.17	25.58		

Table 2.1: Convergence performance by FAS.

2.4 Numerical Results

2.4.1 Unsteady case

We present some comparison results for the unsteady case for a model problem.

Initial settings. For the unsteady problem, we first consider the case of a homogeneous, isotropic and incompressible medium. The computational domain is $(0, 1) \times (0, 1)$. We numerically solve the poroelasticity problem with a simple analytic solution given by

$$\begin{aligned}
 u &= \cos(\pi x) \sin(\pi y) \sin(\pi t), \\
 v &= \sin(\pi x) \cos(\pi y) \sin(\pi t), \\
 p &= -2(\lambda + 2G)\pi \sin(\pi x) \sin(\pi y) \sin(\pi t).
 \end{aligned} \tag{2.27}$$

Source terms \mathbf{g} and f are consequently determined from (2.6). Dirichlet boundary conditions are considered. Before fluid starts to flow, the

following initial condition is considered,

$$\operatorname{div} \mathbf{u}(x, y, 0) = 0, \quad (x, y) \in (0, 1) \times (0, 1). \quad (2.28)$$

The nonlinear conductivity $K(\sigma, p) = e^{(\lambda+G) \cdot \operatorname{div} \mathbf{u} - p}$ is used in the computations.

We discretize the incompressible and time-dependent poroelasticity equations with an artificial pressure term by finite volume methods and Crank-Nicolson scheme in time. The PGS smoother and box-relaxation, i.e. Vanka smoother, are both taken into consideration. The Lamé coefficients are taken as $\lambda = G = 0.1$ and the final time is set as $t = 0.5$.

FAS. First of all, FAS is employed to solve the time-dependent problem. It is known that in FAS the full equation is solved on the coarse grids. It is required to transfer the current approximation from the fine grid to the coarse grid. After this process, the coarse grid error is subtracted from the solution. The correction is then interpolated and added to the fine grid approximation [50].

The underrelaxation parameters for the two smoothers, i.e. PGS and Vanka, are $\omega = 1.0$ and $\omega = 0.7$, respectively. The results are generated by an F -cycle with two pre- and two post-smoothing steps. The stopping criterion is that the maximum norm of the residual $\|r_u\|_\infty + \|r_v\|_\infty + \|r_p\|_\infty$ should be less than 10^{-7} . Table 2.1 presents the relative errors between analytic and numerical (with subscript h) solutions in the maximum norm at final time $t = 0.5$ with the artificial pressure term for different target grids. With the decrease of the mesh size, the relative error is one quarter of the previous one. The CPU time and multigrid convergence factors are also shown in Table 2.1. The convergence factor represents an average residual reduction factor over previous iterations. From Table 2.1, we can conclude that second-order accuracy is maintained and FAS performs very well.

When the nonlinear conductivity is an extremely small value, i.e. $K(\sigma, p) = 10^{-13} \cdot e^{(\lambda+G) \cdot \operatorname{div} \mathbf{u} - p}$, the convergence performance of Vanka is much better than PGS, see Table 2.2. With very fine grids and a small time step, we will have a saddle point problem. PGS doesn't work, which results in multigrid divergence. Vanka is still efficient for this kind of problem.

Grid	Smoother	Conv.	Time(s)
$16 \times 16 \times 2$	PGS	0.52	0.09
	Vanka	0.33	0.12
$32 \times 32 \times 4$	PGS	0.67	0.90
	Vanka	0.44	0.89
$64 \times 64 \times 8$	PGS	0.79	12.60
	Vanka	0.52	8.83
$128 \times 128 \times 16$	PGS	0.88	161.67
	Vanka	0.60	89.44
$256 \times 256 \times 32$	PGS	/	/
	Vanka	0.68	1001.82

Table 2.2: Convergence performance by FAS with an extremely small conductivity. (“/” denotes divergence)

Newton multigrid. Different from the idea of FAS, Newton multigrid is employed too. A standard Newton method is applied to linearize the equations, then multigrid follows for the solution of the (linear) Jacobian system in each iteration. It is a combination of Newton’s method for the outer iteration and multigrid for the inner iteration.

In this test, only one F -cycle is used to solve the Jacobian system. The convergence factors in Table 2.3 are corresponding to the Newton multigrid method. A comparison between Table 2.1 and Table 2.3 indicates that convergence of FAS is a bit faster than that of Newton multigrid. In general, the convergence performance of both methods is very satisfactory.

Regarding the small value of the nonlinear conductivity, we reach the same conclusion. Vanka relaxation still works fine even with fine grids and a small time step. However, PGS fails to get a convergent solution, see Table 2.4. Here we still applied one multigrid cycle for the Jacobian system.

2.4.2 Steady case

Now we only consider FAS as the solver for the steady numerical tests. In this section, we will also consider poroelasticity systems with heterogeneous

Grid	Smoother	Conv.	Time(s)
$16 \times 16 \times 2$	PGS	0.42	0.07
	Vanka	0.35	0.11
$32 \times 32 \times 4$	PGS	0.45	0.39
	Vanka	0.34	0.61
$64 \times 64 \times 8$	PGS	0.45	2.88
	Vanka	0.32	4.45
$128 \times 128 \times 16$	PGS	0.45	22.91
	Vanka	0.30	34.74

Table 2.3: Convergence performance by Newton multigrid.

Grid	Smoother	Conv.	Time(s)
$16 \times 16 \times 2$	PGS	/	/
	Vanka	0.81	0.47
$32 \times 32 \times 4$	PGS	/	/
	Vanka	0.76	2.82
$64 \times 64 \times 8$	PGS	/	/
	Vanka	0.79	25.42
$128 \times 128 \times 16$	PGS	/	/
	Vanka	0.80	215.44
$256 \times 256 \times 32$	PGS	/	/
	Vanka	0.78	1736.54

Table 2.4: Convergence performance by Newton multigrid with an extremely small conductivity.

coefficients, which is closer to the real engineering applications.

The simulation domain is again a $(0, 1) \times (0, 1)$ block of porous material. The average Young's modulus \bar{E}_0 , Poisson ratio ν , conductivity K_0 , coefficient of pore pressure α and coupling coefficient β are taken as 50GPa, 0.25, 0.01m², 1 and 0.01, respectively. A compressive stress $\sigma = 5$ MPa is applied on both top and bottom boundaries. There is also an injection water pressure $p = 2$ MPa on the bottom. The lateral boundaries are assumed to be impermeable and the rigid condition is applied, see Figure 2.3.

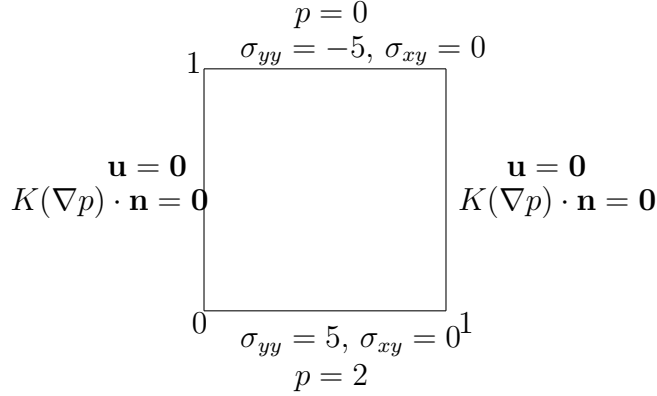


Figure 2.3: Boundary conditions.

Homogeneous test

First, a numerical test with homogeneous material is chosen for the steady problem (2.20). The mechanical parameters are constant at each grid point.

System (2.20) is solved iteratively by multigrid with both the PGS smoother and the Vanka smoother on different grid sizes. Table 2.5 shows the multigrid convergence results by using an F -cycle. $F(3, 3)$ means three pre- and three post-smoothing steps. The numbers in the table denote multigrid convergence factors, and the corresponding CPU time in seconds is presented in brackets. In general, the performance of both smoothing schemes is satisfactory, resulting in h -independent convergence of the multigrid method. PGS takes less CPU time than the box relaxation method, as expected.

Heterogeneous test

Weibull distribution. Usually, a material has complicated properties and boundaries. Rock mass is assumed to be a heterogeneous deformable body

Smoother	F -cycle	32×32	64×64	128×128
PGS	$F(2, 2)$	0.22 (0.13)	0.21 (0.44)	0.21 (1.64)
	$F(3, 3)$	0.19 (0.15)	0.19 (0.49)	0.18 (2.00)
Vanka	$F(2, 2)$	0.23 (0.25)	0.23 (0.88)	0.23 (3.58)
	$F(3, 3)$	0.18 (0.28)	0.18 (1.05)	0.18 (3.98)

Table 2.5: Multigrid convergence results for the homogeneous test.

composed of different material properties. Heterogeneity is a concept relating to nonuniformity (composition or character) in a substance. Rock specimen in numerical tests is subdivided into square elements with randomly distributed mechanical properties in each element. Due to the size and shape consistency, there is no geometric preference orientation in the specimen. In order to simulate random heterogeneity in a rock, a statistical approach is used. In [91] the material heterogeneity is defined by a Weibull distribution, with the probability density function given by

$$f(s, m) = \frac{m}{\bar{s}} \left(\frac{s}{\bar{s}} \right)^{m-1} \exp \left(- \left(\frac{s}{\bar{s}} \right)^m \right), \quad (2.29)$$

where s denotes a given mechanical property, such as Young's modulus, the coefficient of conductivity or the strength; \bar{s} is the mean value; and m represents the homogeneity index which defines the shape of the distribution function. The corresponding Weibull distribution function is given by

$$F(s; m, \bar{s}) = \begin{cases} 1 - \exp \left(- \left(\frac{s}{\bar{s}} \right)^m \right) & \text{if } s \geq 0, \\ 0 & \text{if } s < 0. \end{cases} \quad (2.30)$$

Figure 2.4 displays, for different values of the homogeneity index m , the probability density function in terms of the ratio between s and \bar{s} . It is obvious that a higher value of m represents a more homogeneous material and vice versa, as for higher m , the values of s are concentrated around \bar{s} . As an example, we consider initial Young's modulus E_0 with a mean value \bar{E}_0 of 50GPa and homogeneity index $m = 3$. In this case, Figure 2.5 shows a possible randomly distributed Young's modulus E_0 in each element.

In our model, the Young's modulus and initial conductivity are modeled in this way. So, these parameters differ for each element.

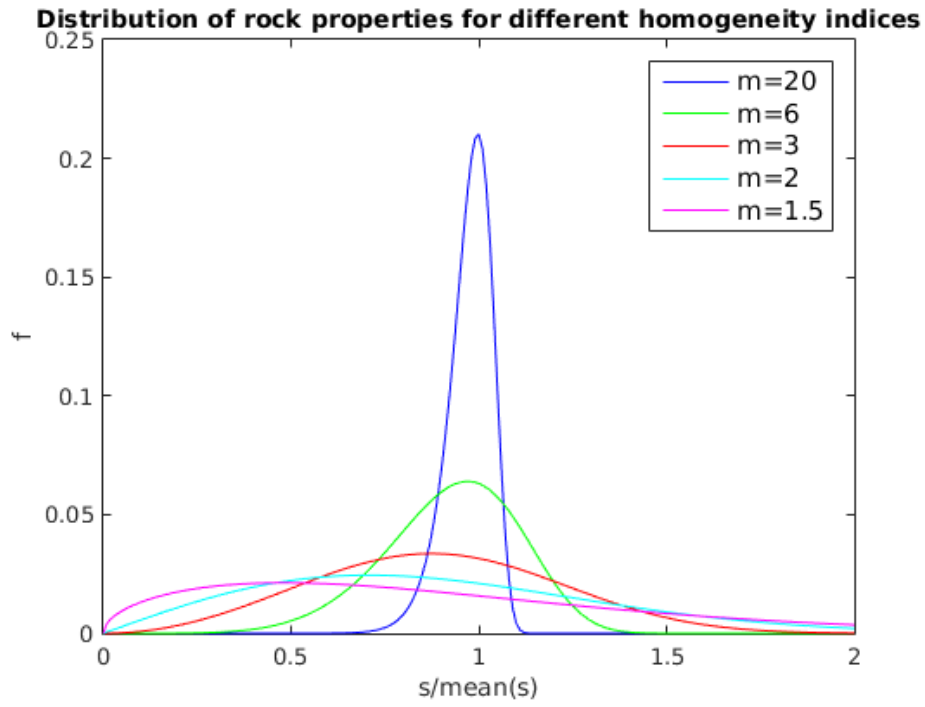


Figure 2.4: Probability density function for different values of the homogeneity index $m = 1.5, 2, 3, 6, 20$.

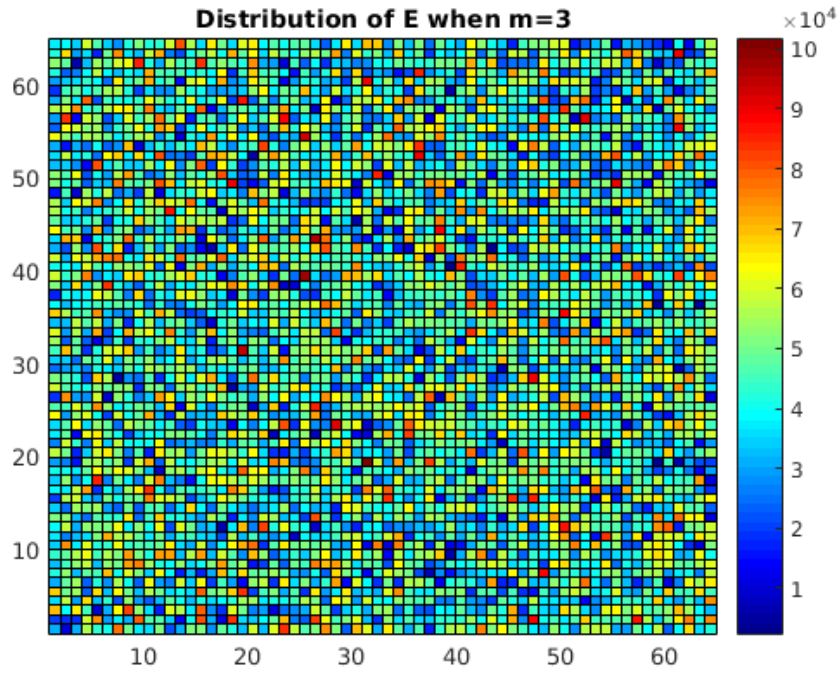


Figure 2.5: Distribution function of E_0 in each element of the grid.

Figure 2.6 presents histograms of the observed Young's modulus in three simulations with different homogeneity indices, $m = 1, 3, 5$. The chosen average is the same as in Figure 2.5.

Notice that the randomly distributed parameters on coarser grids are generated from finer grids. In this way, the coarse system is related to the fine system, thus the same characteristics of the material are presented. The standard restriction operator "Full Weighting" is used to transfer these parameters to each grid level of the grids. Then we perform a regular finite volume method discretization with these averaged coefficients on the coarse grids.

Some results. In this test we solve the steady equations for a heterogeneous material. Two different homogeneity indices m are chosen to investigate the convergence results of multigrid. Figure 2.7 shows the randomly distributed Young's modulus $\bar{E}_0 = 50\text{GPa}$ with different homogeneity indices $m = 1$ and $m = 5$. Obviously, $m = 5$ denotes a more homogeneous material compared to $m = 1$. Conductivity also follows the stochastic distribution and the average value of K_0 is taken as 0.01m^2 . All the other parameters, i.e. Poisson ratio ν and coupling coefficient β , are the same as for the homogeneous test.

We consider it a challenge to deal with these heterogeneous cases using the standard multigrid components described above. So, we do not use the Galerkin coarse matrices or operator-dependent prolongation and restriction here. We merely wish to study the impact of the heterogeneity on the FAS multigrid convergence using the standard geometric multigrid components, like the direct discretization of the operator on the coarse grids, and the two described smoothers.

Tables 2.6 and 2.7 show the multigrid convergence results for the heterogeneous tests with $m = 1$ and $m = 5$, respectively. It can be seen that the convergence factors are larger than the results from the homogeneous test case, as expected. Comparing the results in Table 2.6 with those in Table 2.7, the multigrid convergence is better when the distributions of the mechanical parameters are more homogeneous. PGS is still faster than the Vanka method for this steady problem in CPU time. Overall, the multigrid convergence is still highly satisfactory for the heterogeneous test cases used here with the standard multigrid components. Convergence can be

further improved in this framework by using multigrid as a preconditioner for a Krylov subspace iteration, like in the setting of the recombination technique in [88, 97].

Smoother	F -cycle	32×32	64×64	128×128
PGS	$F(2, 2)$	0.43 (0.22)	0.44 (0.82)	0.54 (4.04)
	$F(3, 3)$	0.38 (0.25)	0.40 (0.97)	0.48 (4.60)
Vanka	$F(2, 2)$	0.47 (0.50)	0.44 (1.78)	0.65 (13.47)
	$F(3, 3)$	0.38 (0.54)	0.40 (2.45)	0.56 (14.17)

Table 2.6: Multigrid convergence results for homogeneity index $m = 1$.

Smoother	F -cycle	32×32	64×64	128×128
PGS	$F(2, 2)$	0.22 (0.17)	0.22 (0.49)	0.21 (1.82)
	$F(3, 3)$	0.18 (0.19)	0.19 (0.55)	0.18 (2.30)
Vanka	$F(2, 2)$	0.27 (0.30)	0.24 (1.00)	0.26 (4.35)
	$F(3, 3)$	0.17 (0.45)	0.18 (1.18)	0.17 (4.60)

Table 2.7: Multigrid convergence results for homogeneity index $m = 5$.

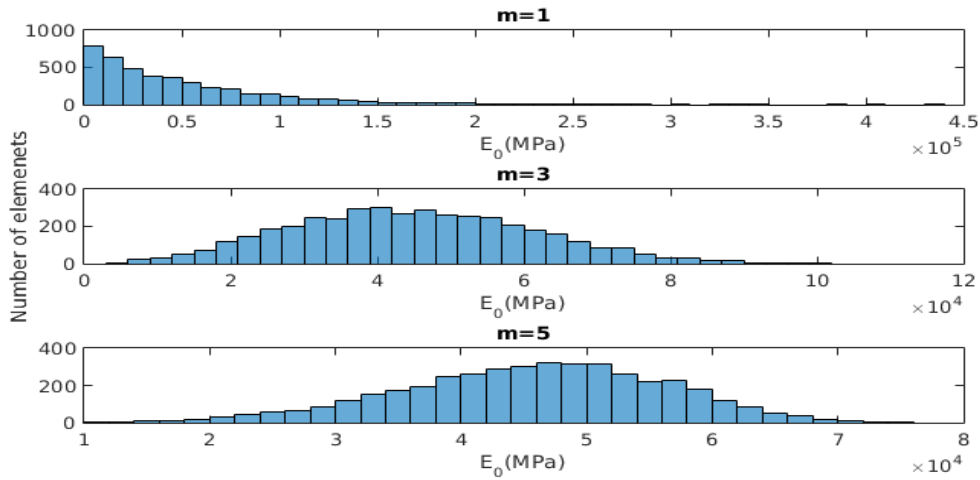


Figure 2.6: Histograms of the heterogeneity distribution in numerical examples.

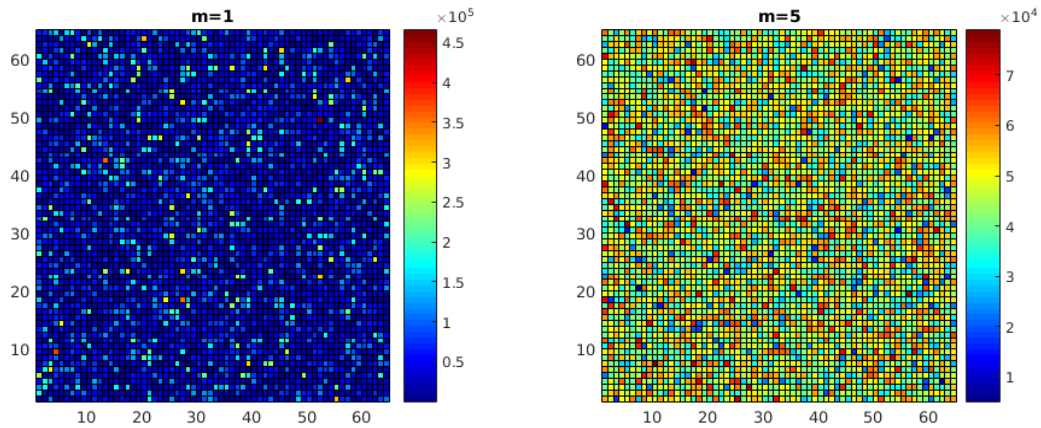


Figure 2.7: Heterogeneity of E_0 for different homogeneity values m .

2.5 Conclusions

In this chapter, we have used the nonlinear multigrid method to solve the poroelasticity system considering material heterogeneity and a nonlinear conductivity.

First, we have solved an unsteady problem. Since oscillations may occur in the first time steps of the solution when the equations are discretized on a collocated grid by the finite volume method, some special care is needed. The stabilization can be achieved by adding an artificial term in one of the continuous equations. A simple analytic test is employed to verify our method. This is done by FAS and Newton multigrid with a coupled smoother “Vanka” which solves the discrete equations locally cell by cell, and the point Gauss-Seidel (PGS) method. Numerical results show that both nonlinear strategies are stable and second-order accurate. Vanka is more efficient and robust for some difficult problems where the values of the coefficient are extremely small or the system is discretized on a very fine grid.

Next to these tests, we consider steady problems for homogeneous and heterogeneous cases. Heterogeneity means that some characteristics of the main problem follow a random distribution. The Full Approximation Scheme with collective point-wise Gauss-Seidel smoother, that is, updating all unknowns at each grid point together, shows highly satisfactory multigrid convergence. For the heterogeneity tests performed, we do not need the commonly used box relaxation scheme as smoother.

On an Uzawa Smoother in Multigrid for Poroelasticity Equations

In this chapter, for the efficient solution of the poroelastic equations, a multigrid method is employed with an Uzawa-type iteration as the smoother. The Uzawa smoother is an equation-wise procedure. It shall be interpreted as a combination of the symmetric Gauss-Seidel smoothing for displacements, together with a Richardson iteration for the Schur complement in the pressure field. The Richardson iteration involves a relaxation parameter which affects the convergence speed, and has to be carefully determined. The analysis of the smoother is based on the framework of local Fourier analysis (LFA) and it allows us to provide an analytic bound of the smoothing factor of the Uzawa smoother as well as an optimal value of the relaxation parameter. Numerical experiments show that our upper bound provides a satisfactory estimate of the exact smoothing factor, and the selected relaxation parameter is optimal. In order to improve the convergence performance, the acceleration of multigrid by iterant recombination is taken into account. Numerical results confirm the efficiency and robustness of the acceleration scheme. ¹

3.1 Introduction

The concept of poroelasticity describes the behavior of a deformable fluid-saturated porous medium. Usually, there are two basic phenomena regard-

¹The contents of this chapter have been published in paper [64]: P. Luo, C. Rodrigo, F.J. Gaspar and C.W. Oosterlee. On an Uzawa Smoother in Multigrid for Poroelasticity Equations. *Numerical Linear Algebra with Applications*, 24, e2074. doi:10.1002/nla.2074, 2016.

ing poroelastic behavior. One is the “solid to fluid coupling” which means that a change in the applied stresses of the skeleton will affect the pressure or mass of the fluid. The other is the “fluid to solid coupling” when a change in the fluid will lead to a change in the volume of the material.

The multigrid method is employed for solving the discretized poroelastic partial differential equations. An important multigrid component is the smoother, and the performance of multigrid crucially depends on it. There are several branches of robust smoothers developed for the poroelasticity equations. They all fall into two major categories: coupled and decoupled smoothers, see [38, 39, 75]. Here we focus on a specific type of decoupled smoothers called Uzawa smoothers, for different discretizations of the poroelasticity problem.

A first study of the Uzawa smoother was done in the PhD thesis, as well as in a conference proceedings paper, by P. Nigon [68]. A symmetric Gauss-Seidel (SGS) smoother will be employed here for the displacement variables. In [68], two forward Gauss-Seidel sweeps were used instead, but numerical results in [41] revealed that, everything else being equal, the SGS choice is indeed more effective. In addition, for the pressure unknowns, the Uzawa method shall be interpreted as a Richardson iteration for solving the Schur complement equation in which a relaxation parameter is involved. Optimization of this parameter is necessary for fast multigrid convergence. Detailed research of this method for a family of Stokes problems has already been done in [41].

A suitable relaxation parameter is chosen by means of local Fourier analysis (LFA) [94]. In this chapter, we are concerned with the convergence behavior of multigrid with the Uzawa smoother with respect to relaxation parameters and the poroelastic model’s coefficients. We get an upper bound for the smoothing factor and a concrete formulation of the relaxation parameter which is governed by the main problem coefficients. We consider both staggered and collocated finite volume discretizations of poroelasticity equations in our analysis for which we find different relaxation parameters. In order to confirm our study, several numerical tests are performed.

We are also interested in heterogeneous poroelasticity problems. For the heterogeneous case, the same multigrid method with Uzawa smoother is applied, however the convergence performance will be influenced by the

anisotropy. To improve the convergence, the so-called acceleration of multigrid by an iterant recombination scheme [94] is taken into account. In practice, this leads to a similar algorithm as a multigrid preconditioning method. Different numerical experiments validate the efficiency and robustness of the acceleration scheme.

The organization of the chapter is as follows. We present the incompressible poroelasticity equations in Section 3.2. The numerical method is introduced in Section 3.3. In Section 3.4, we analyze the proposed smoother in the framework of local Fourier analysis. We obtain an analytic bound of the smoothing factor. After that, the multigrid method is applied to both staggered and collocated grids. Numerical experiments illustrate the efficiency of the method and confirm our analysis in Section 3.5. Acceleration of multigrid by the iterant recombination scheme is employed for the heterogeneous poroelasticity system. Finally, conclusions are drawn in Section 3.6.

3.2 Problem formulation

3.2.1 Poroelasticity equations

We consider the quasi-static Biot model for soil consolidation. The porous medium is assumed to be linearly elastic, homogeneous and isotropic, and the porous matrix is supposed to be saturated by an incompressible Newtonian fluid. The continuous medium is characterized by the knowledge of elastic displacements $\mathbf{u} = (u, v)$, and fluid pressure p at each point, and in terms of these unknowns the governing equations of the consolidation problem are given by

$$-\nabla \cdot G \nabla \mathbf{u} - \nabla(\lambda + G)(\nabla \cdot \mathbf{u}) + \nabla p = \mathbf{g}(\mathbf{x}, t), \quad (3.1)$$

$$\frac{\partial}{\partial t}(\nabla \cdot \mathbf{u}) - \nabla \cdot \left(\frac{k}{\eta} \nabla p \right) = f(\mathbf{x}, t), \quad \mathbf{x} \in \Omega, \quad 0 < t \leq T, \quad (3.2)$$

where λ and G are the Lamé coefficients, which can be computed from the values of the Young modulus E and the Poisson ratio ν in the following way,

$$\lambda = \frac{\nu E}{(1 + \nu)(1 - 2\nu)}, \quad G = \frac{E}{2(1 + \nu)}, \quad (3.3)$$

k is the permeability of the porous medium and η is the viscosity of the fluid. The source terms $\mathbf{g}(\mathbf{x}, t)$ and $f(\mathbf{x}, t)$ represent a density of applied body forces and a forced fluid extraction or injection process, respectively. The following initial condition is assumed,

$$\nabla \cdot \mathbf{u}(\mathbf{x}, 0) = 0, \quad \mathbf{x} \in \Omega.$$

For simplicity, we will consider homogeneous Dirichlet boundary conditions for both displacements and pressure, $\mathbf{u} = \mathbf{0}$ and $p = 0$ on $\partial\Omega$.

Whatever the chosen space discretization scheme and an implicit scheme in time, the discretization of (3.1)-(3.2) leads at each time step to a linear system of the form

$$\begin{pmatrix} A & B^T \\ B & -C \end{pmatrix} \begin{pmatrix} \mathbf{u} \\ p \end{pmatrix} = \begin{pmatrix} \mathbf{g} \\ f \end{pmatrix}, \quad (3.4)$$

where A is the discrete representation of the elasticity operator $-\nabla \cdot G \nabla \mathbf{u} - \nabla(\lambda + G)(\nabla \cdot \mathbf{u})$. It follows that A is symmetric positive definite (SPD). The matrix block B^T is the discrete gradient and B the negative discrete divergence; C contains the term $-\nabla \cdot (\frac{k}{\eta} \nabla p)$ and also it can contain a stabilization term that is needed for some discretization schemes to avoid spurious oscillations. Notice that in practice operator C is an almost zero block since the permeability k is very small and also this block contains the time-discretization parameter as a multiplicative factor, which can also be arbitrarily small.

3.2.2 Discretization

Discretization on staggered grids In a staggered arrangement of the poroelasticity equations, the discrete values of u_h and v_h , the components of the displacement vector, are located at the grid cell faces in the \bullet - and \circ -points, respectively, and the discrete pressure unknowns p_h are defined at the grid points (the \times -points), as in poroelasticity applications pressure values are often prescribed at the boundary, see Figure 3.1 (left side).

For each equation, the discretization is centered around the equation's primary unknown. On a staggered grid, the stencil form in the case of constant coefficients and the finite volume scheme typically results in the

following:

$$\begin{bmatrix} & -G & \\ -(\lambda + 2G) & 2(\lambda + 3G) & -(\lambda + 2G) \\ & -G & \end{bmatrix} u_h - (\lambda + G) \begin{bmatrix} -1 & 1 \\ & \star \\ 1 & -1 \end{bmatrix} v_h + h \begin{bmatrix} -1 & \star & 1 \end{bmatrix} p_h = g_h^1 h^2, \quad (3.5)$$

$$-(\lambda + G) \begin{bmatrix} -1 & 1 \\ & \star \\ 1 & -1 \end{bmatrix} u_h + \begin{bmatrix} -G & -(\lambda + 2G) \\ -G & 2(\lambda + 3G) \\ -(\lambda + 2G) & -G \end{bmatrix} v_h + h \begin{bmatrix} 1 \\ \star \\ -1 \end{bmatrix} p_h = g_h^2 h^2, \quad (3.6)$$

$$h \begin{bmatrix} -1 & \star & 1 \end{bmatrix} u_h + h \begin{bmatrix} 1 \\ \star \\ -1 \end{bmatrix} v_h + \kappa \begin{bmatrix} -1 & -1 & -1 \\ & 4 & \\ -1 & -1 & -1 \end{bmatrix} p_h = f_h h^2, \quad (3.7)$$

where $\kappa = \frac{k\tau}{\eta}$, with τ the time step. The \star denotes the position on the grid at which the discrete operator is applied, i.e., \bullet , \circ or \times -points, respectively.

Discretization on collocated grids We also consider the vertex-centered finite volume discretization of the poroelastic system on a collocated grid. We assume a uniform grid of cells of size h . In a collocated grid all variables are placed at the grid points, see Figure 3.1 (right side). Collocated

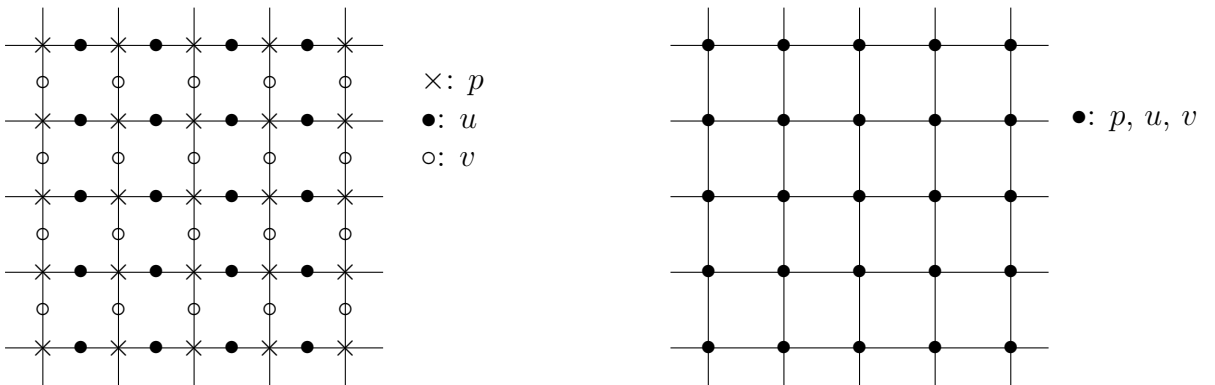


Figure 3.1: Staggered (left) and collocated (right) grid location of unknowns for poroelasticity equations.

grid arrangements are convenient for grid generation and also for numerical methods like multigrid. However, as mentioned in Chapter 2, when a standard collocated discretization is used for the poroelasticity problem, non-physical oscillations can appear in the pressure field approximation of the numerical solution [38, 75]. To avoid this, a stabilization term has to be added to the flow equation (3.2). A stable discretization was proposed in [38]. In this way, matrix C in (3.4) contains an artificial term, i.e.

$$-C = \nabla \cdot (\kappa \nabla) + \nabla \cdot \left(\frac{h^2}{4(\lambda + 2G)} \nabla \right). \quad (3.8)$$

Since the stabilization term is proportional to h^2 , second-order accuracy is maintained if all terms in the system are discretized with second-order accuracy.

3.3 The numerical method

3.3.1 Multigrid and acceleration

With respect to the numerical solution method, multigrid is considered for the discrete poroelasticity problems due to its efficiency and robustness. The multigrid method is based on two crucial components. One is the relaxation method (the smoother), the other is the coarse grid correction. Regarding the coarse grid correction, geometric grid coarsening is chosen as we will deal with regular Cartesian grids here. The sequence of coarse grids is obtained by doubling the mesh size in each spatial direction.

For the staggered case, the inter-grid transfer operators that act on the different unknowns are defined as follows: At u - and v -grid points one considers 6-point restrictions and at p -grid points a 9-point vertex-centered full weighting restriction is applied. In stencil notation the restriction operators are given by

$$R_{h,2h}^u = \frac{1}{8} \begin{pmatrix} 1 & & 1 \\ 2 & * & 2 \\ 1 & & 1 \end{pmatrix}_h, \quad R_{h,2h}^v = \frac{1}{8} \begin{pmatrix} 1 & 2 & 1 \\ & * & \\ 1 & 2 & 1 \end{pmatrix}_h, \quad R_{h,2h}^p = \frac{1}{16} \begin{pmatrix} 1 & 2 & 1 \\ 2 & 4 & 2 \\ 1 & 2 & 1 \end{pmatrix}_h,$$

respectively. As the prolongation operators $P_{2h,h}^{u/v/p}$, one applies the usual interpolation operators based on bilinear interpolation of neighboring coarse grid unknowns on the staggered grid.

For the collocated case, the multigrid transfer operators, restriction $R_{h,2h}$ and prolongation $P_{2h,h}$, are well-known in geometric multigrid. In a standard way, the full-weighting restriction and the bilinear interpolation are applied as the inter-grid transfer operators, see ([94], Chapter 2).

The choice of smoother, which has a great impact on the behavior of a multigrid method, needs to be done with special attention. The Uzawa smoother which is discussed in detail in the next section, is chosen here since it is a simple algorithm with low computational cost.

To improve the multigrid performance, we also consider an acceleration scheme. The acceleration of multigrid means that multigrid is applied as a preconditioner in connection with a Krylov subspace method. As is known, a Krylov acceleration technique helps to capture eigenvectors connected to the isolated large eigenvalues of the iteration matrix. These eigenvectors are the main reason for limited multigrid convergence in some specific situations. For detailed information, see [97].

From the multigrid point of view, multigrid as a preconditioner is identical to multigrid acceleration by iterant recombination [94, Section 7.8]. The technique of iterant recombination is easily implemented on both staggered and collocated grids, and can also be used in the nonlinear case. This algorithm will be described shortly.

Supposing we already had successive approximations of the solution $\mathbf{w}_h^1, \mathbf{w}_h^2, \dots, \mathbf{w}_h^q$ with $\mathbf{w}_h^i = (\mathbf{u}_h^i, p_h^i)$, $i = 1, \dots, q$, and corresponding residuals $\mathbf{r}_h^1, \mathbf{r}_h^2, \dots, \mathbf{r}_h^q$ from previous multigrid cycles. For the sake of a more optimal approximation of the solution $\mathbf{w}_{h,new}$, a linear combination of the $\tilde{q} + 1$ ($\tilde{q} < q$), recent intermediate approximations $\mathbf{w}_h^{q-i}, i = 0, \dots, \tilde{q}$, is considered,

$$\mathbf{w}_{h,new} = \mathbf{w}_h^q + \sum_{i=1}^{\tilde{q}} \alpha_i (\mathbf{w}_h^{q-i} - \mathbf{w}_h^q). \quad (3.9)$$

For linear problems, the improved residual will have the same form as (3.9),

$$\mathbf{r}_{h,new} = \mathbf{r}_h^q + \sum_{i=1}^{\tilde{q}} \alpha_i (\mathbf{r}_h^{q-i} - \mathbf{r}_h^q). \quad (3.10)$$

In order to select an optimal candidate $\mathbf{w}_{h,new}$ for the solution, the parameters α_i are required to minimize the residual (3.10), for example, with respect to the L_2 -norm $\|\cdot\|_2$.

The acceleration of multigrid is thus transferred to a classical minimization problem. Usually, we search for the desired coefficients α_i through a (Gram-Schmidt) orthonormalization process. The structure of a multigrid V -cycle with the acceleration by iterant recombination is presented in Figure 3.2. We will particularly employ the acceleration for the heterogeneous poroelastic cases, for which it may be nontrivial to define an optimal multigrid solver.

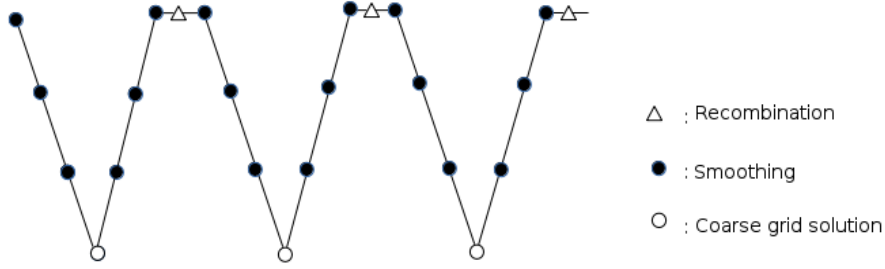


Figure 3.2: Recombination of multigrid iterants.

3.3.2 The Uzawa smoother

Here, we are interested in a decoupled Uzawa smoother which was analyzed for Stokes problems in fluid dynamics in [41].

The smoother is obtained by splitting the discrete operator as follows

$$\begin{pmatrix} A & B^T \\ B & -C \end{pmatrix} = \begin{pmatrix} M_A & \\ B & -\omega^{-1} I \end{pmatrix} - \begin{pmatrix} M_A - A & -B^T \\ C - \omega^{-1} I & \end{pmatrix}, \quad (3.11)$$

where M_A is a typical smoother for A and ω is some positive parameter. M_A helps to make the approach less costly because of the inexact solve for displacements at each iteration.

Supposing we already got an approximation of the solution $(\mathbf{u}, p)^T$ to the system, the relaxed approximation $(\hat{\mathbf{u}}, \hat{p})^T$ is computed according to the decoupled Uzawa smoother as

$$\begin{pmatrix} M_A & \\ B & -\omega^{-1} I \end{pmatrix} \begin{pmatrix} \hat{\mathbf{u}} \\ \hat{p} \end{pmatrix} = \begin{pmatrix} M_A - A & -B^T \\ C - \omega^{-1} I & \end{pmatrix} \begin{pmatrix} \mathbf{u} \\ p \end{pmatrix} + \begin{pmatrix} \mathbf{g} \\ f \end{pmatrix}. \quad (3.12)$$

A single step of the iteration is described as

- Relax the displacements by applying M_A : $\hat{\mathbf{u}} = \mathbf{u} + M_A^{-1}(\mathbf{g} - A\mathbf{u} - B^T p)$;
- Update the pressure: $\hat{p} = p + \omega(B\hat{\mathbf{u}} - Cp - f)$.

Here, the symmetric Gauss-Seidel method is considered as M_A , which consists of one forward and one backward sweep for all displacements in the computational domain. M_A has two important properties used in our theoretical analysis. One is that M_A is SPD if A is SPD. The other is that the associated largest eigenvalue satisfies (see, e.g., [3, Theorem 7.17])

$$\lambda_{\max}(M_A^{-1}A) \leq 1. \quad (3.13)$$

3.4 Local Fourier Analysis (LFA)

The Uzawa smoother is analyzed by means of Local Fourier Analysis (LFA). In particular, we aim to define an optimal ω in (3.12). We assume the parameters λ , G and κ are constants here.

3.4.1 Basis of LFA

In LFA, it is assumed that the discrete operator is defined on an infinite grid \mathcal{G}_h , and boundary conditions are neglected. For example, an infinite collocated grid in 2D can be defined as

$$\mathcal{G}_h = \{\mathbf{x} = \mathbf{k}\mathbf{h} := (k_1h_1, k_2h_2), \mathbf{k} \in \mathbb{Z}^2\}, \quad (3.14)$$

where we denote $\mathbf{x} = (x_1, x_2) \in \mathcal{G}_h$ and $\mathbf{h} = (h_1, h_2)$. The basic idea of LFA is that all occurring multigrid components, the discrete approximation and its corresponding error or residual can be represented by linear combinations of Fourier modes, defined in the case of a collocated grid as

$$\varphi_h(\boldsymbol{\theta}, \mathbf{x}) = e^{i\boldsymbol{\theta} \cdot \mathbf{x}/\mathbf{h}} := e^{i\theta_1 x_1/h_1} e^{i\theta_2 x_2/h_2}, \quad (3.15)$$

where $\boldsymbol{\theta} \in \boldsymbol{\Theta} := (-\pi, \pi]^2$, which form a unitary basis of the space of infinite grid functions. The Fourier space generated by Fourier modes is given by

$$\mathcal{F}(\mathcal{G}_h) := \text{span}\{\varphi_h(\boldsymbol{\theta}, \cdot) | \boldsymbol{\theta} \in \boldsymbol{\Theta}\}. \quad (3.16)$$

For the analysis, we distinguish high and low frequency components on \mathcal{G}_h ,

$$\boldsymbol{\Theta}_{low}^{2h} := (-\frac{\pi}{2}, \frac{\pi}{2}]^2, \quad \boldsymbol{\Theta}_{high}^{2h} := \boldsymbol{\Theta} \setminus \boldsymbol{\Theta}_{low}^{2h}. \quad (3.17)$$

In multigrid, the purpose of the smoother is to eliminate the high frequency components of an error, whereas the low frequency ones are typically reduced by coarse grid correction. In our case, the Uzawa smoothing iteration can be written as $Q_h = I - M_h^{-1}K_h$, where K_h and M_h are the matrices of systems (3.4) and (3.12), respectively. To study how the high frequency components are eliminated, we define the smoothing factor μ as:

$$\mu = \sup_{\boldsymbol{\theta} \in \boldsymbol{\Theta}_{high}^{2h}} \rho(Q_h(\boldsymbol{\theta})). \quad (3.18)$$

In the transition from \mathcal{G}_h to \mathcal{G}_{2h} , each low-frequency $\boldsymbol{\theta} = \boldsymbol{\theta}^{00} \in \boldsymbol{\Theta}_{low}^{2h}$ is coupled with three high-frequencies $\boldsymbol{\theta}^{11}$, $\boldsymbol{\theta}^{10}$, $\boldsymbol{\theta}^{01}$, given by

$$\boldsymbol{\theta}^{ij} = \boldsymbol{\theta}^{00} - (i \operatorname{sign}(\theta_1), j \operatorname{sign}(\theta_2))\pi, \quad i, j = 0, 1. \quad (3.19)$$

Only low frequency components are distinguishable on the coarse grid \mathcal{G}_{2h} . In other words, for each $\boldsymbol{\theta}^{00}$, three other Fourier modes $\varphi_{2h}(\boldsymbol{\theta}^{11}, \cdot)$, $\varphi_{2h}(\boldsymbol{\theta}^{10}, \cdot)$ and $\varphi_{2h}(\boldsymbol{\theta}^{01}, \cdot)$ are identical to $\varphi_{2h}(\boldsymbol{\theta}^{00}, \cdot)$ on \mathcal{G}_{2h} . This means that they are invisible on the coarse grid. As a result, the Fourier space is subdivided into corresponding four-dimensional subspaces, known as $2h$ -harmonics,

$$\mathcal{F}^{2h}(\boldsymbol{\theta}) := \operatorname{span}\{\varphi_h(\boldsymbol{\theta}^{00}, \cdot), \varphi_h(\boldsymbol{\theta}^{11}, \cdot), \varphi_h(\boldsymbol{\theta}^{10}, \cdot), \varphi_h(\boldsymbol{\theta}^{01}, \cdot)\}, \quad \text{with } \boldsymbol{\theta} = \boldsymbol{\theta}^{00} \in \boldsymbol{\Theta}_{low}^{2h}. \quad (3.20)$$

By the definitions above, we can analyze the behavior of multigrid by investigating the effect of the multigrid components acting on the Fourier space.

In a two-grid analysis, it is assumed that the coarse grid solution is exact on the first coarser grid level. The iteration operator of the two-grid method is given by

$$M_{h,2h} = Q_h^{\nu_2}(I_h - P_{2h,h}(K_{2h})^{-1}R_{h,2h}K_h)Q_h^{\nu_1}, \quad (3.21)$$

where ν_1 , ν_2 are, respectively, the number of pre- and post-smoothing steps. Since the representation of $M_{h,2h}$ on the Fourier space has a block-diagonal structure regarding the partitioning in $2h$ -harmonics, it is possible to efficiently calculate the LFA two-grid convergence factor,

$$\rho = \rho(M_{h,2h}). \quad (3.22)$$

For the staggered case, the definition of the infinite grid and as a consequence the definition of the Fourier modes are different, what makes the

analysis more involved, see [67, 100] and Section 4.4.2 for details. (Please note that the staggered grid in Section 4.4.2 is a little different from the staggered grid in Figure 3.1 (left).)

3.4.2 LFA for the Uzawa smoother

A local Fourier analysis for the considered Uzawa smoother was already developed in [41]. In particular, the authors provided an upper bound on the smoothing factor associated with the proposed Uzawa smoother which gave an excellent estimate of the exact smoothing factor. More concretely, this bound was given by

$$\mu \leq \bar{\mu} = \max \left((\mu_A)^{1/2}, \mu_S \right), \quad (3.23)$$

where μ_A is the smoothing factor corresponding to the relaxation scheme M_A , and μ_S can be interpreted as the smoothing factor associated with the Richardson iteration for the Schur complement,

$$\mu_S := \sup_{\Theta_{high}^{2h}} \rho \left(I - \omega \left(C + BA^{-1}B^T \right) \right).$$

In order to bound μ_A , available results in the literature were used from scalar elliptic PDEs. Notice that in our case also the smoothing factors of several smoothers for the elasticity operator are well-known. However, bounding μ_S is more involved since the eigenvalues of the Schur complement contribute to the analysis of this smoothing factor. In addition to that, the information of these eigenvalues plays an important role in selecting the relaxation parameter for the Richardson iteration. In [41], a detailed study of the maximum and minimum eigenvalues of the Schur complement gave rise to the following bound of μ_S :

$$\mu_S \leq \max \left(\zeta - 1, 1 - \frac{\zeta}{\kappa_\beta} \right), \quad (3.24)$$

where

$$\kappa_\beta = \frac{\beta_{\max}}{\beta_{\min}}, \quad (3.25)$$

with β_{\max} and β_{\min} the following eigenvalue bounds,

$$\max_{\boldsymbol{\theta} \in \Theta_{high}^{2h}} \left(\tilde{C}(\boldsymbol{\theta}) + \tilde{B}(\boldsymbol{\theta}) \widetilde{A^{-1}}(\boldsymbol{\theta}) \widetilde{B^T}(\boldsymbol{\theta}) \right) = \beta_{\max}, \quad (3.26)$$

$$\min_{\boldsymbol{\theta} \in \Theta_{high}^{2h}} \left(\tilde{C}(\boldsymbol{\theta}) + \tilde{B}(\boldsymbol{\theta}) \widetilde{A^{-1}}(\boldsymbol{\theta}) \widetilde{B^T}(\boldsymbol{\theta}) \right) = \beta_{\min}, \quad (3.27)$$

with $\widetilde{C}(\boldsymbol{\theta})$, $\widetilde{B}(\boldsymbol{\theta})$, $\widetilde{A^{-1}}(\boldsymbol{\theta})$ and $\widetilde{B^T}(\boldsymbol{\theta})$ the symbols or Fourier representations of operators C , B , A^{-1} and B^T for a fixed frequency $\boldsymbol{\theta}$, and where ζ is a positive real number such as $\zeta < 2$ (to ensure that $\mu_S < 1$). This analysis resulted in a formula to determine the appropriate relaxation parameter as (see [41], Theorem 3.2)

$$\omega = \frac{\zeta}{\beta_{\max}} = \frac{2}{\beta_{\max} + \beta_{\min}}, \quad (3.28)$$

where ζ was chosen to minimize the value of the maximum in (3.24). All these results can be extrapolated to the analysis of the Uzawa smoother for the poroelasticity equations that we consider here, and in the next section we will provide exact values for the bounds of the eigenvalues which will give us optimal relaxation parameters for different discretizations of our problem.

3.5 Uzawa based multigrid for poroelasticity equations

We will work out the smoothing analysis from the previous section for staggered and collocated poroelasticity discretizations.

3.5.1 Staggered grid arrangement of unknowns

Theoretical analysis. For the staggered discretization of the poroelastic equations, a geometric multigrid is adopted. The Uzawa smoother can be applied, and we can perform the theoretical analysis explained in Section 3.4.2 in order to obtain a suitable parameter ω for the part corresponding to the Richardson iteration for the pressure.

To obtain $\beta_{\max}(h)$ and $\beta_{\min}(h)$, in (3.26) and (3.27), we will take into account the following equalities which are valid only for the staggered arrangement

$$\widetilde{B}(\boldsymbol{\theta})\widetilde{A}(\boldsymbol{\theta}) = -(\lambda + 2G)\widetilde{\Delta}(\boldsymbol{\theta})\widetilde{B}(\boldsymbol{\theta}), \quad (3.29)$$

$$\widetilde{B}(\boldsymbol{\theta})\widetilde{B^T}(\boldsymbol{\theta}) = -\widetilde{\Delta}(\boldsymbol{\theta}), \quad (3.30)$$

so that

$$\widetilde{B}(\boldsymbol{\theta})\widetilde{A^{-1}}(\boldsymbol{\theta})\widetilde{B^T}(\boldsymbol{\theta}) = -\frac{1}{\lambda + 2G}\widetilde{\Delta^{-1}}(\boldsymbol{\theta})\widetilde{B}(\boldsymbol{\theta})\widetilde{B^T}(\boldsymbol{\theta}) = \frac{1}{\lambda + 2G}. \quad (3.31)$$

Denoting $s_1 = \sin^2(\frac{\theta_1}{2})$ and $s_2 = \sin^2(\frac{\theta_2}{2})$, the symbol of $-\Delta$ for a frequency $\boldsymbol{\theta} = (\theta_1, \theta_2)$ is given by $-\tilde{\Delta}(\boldsymbol{\theta}) = \frac{4}{h^2}(s_1 + s_2)$. Therefore, the symbol of the Schur complement is written as

$$\tilde{C}(\boldsymbol{\theta}) + \tilde{B}(\boldsymbol{\theta})\tilde{A}^{-1}(\boldsymbol{\theta})\tilde{B}^T(\boldsymbol{\theta}) = \frac{4\kappa}{h^2}(s_1 + s_2) + \frac{1}{\lambda + 2G}. \quad (3.32)$$

Then, we obtain

$$\beta_{\max}(h) = \frac{8\kappa}{h^2} + \frac{1}{\lambda + 2G} \quad (\text{achieved for } \theta_1 = \theta_2 = \pi), \quad (3.33)$$

$$\beta_{\min}(h) = \frac{2\kappa}{h^2} + \frac{1}{\lambda + 2G} \quad (\text{achieved for } \theta_1 = 0, \theta_2 = \frac{\pi}{2}). \quad (3.34)$$

With these values, we can write

$$\kappa_\beta = \frac{\beta_{\max}}{\beta_{\min}} = \frac{8\kappa(\lambda + 2G) + h^2}{2\kappa(\lambda + 2G) + h^2}, \quad (3.35)$$

and when $\kappa = 0$ the simplified expression reads $\kappa_\beta = 1$. We find the value of ζ which gives the lowest value of the maximum in (3.24), resulting in (taking into account that $\zeta \leq 2$)

$$\zeta = \frac{2\kappa_\beta}{1 + \kappa_\beta} = \frac{8\kappa(\lambda + 2G) + h^2}{5\kappa(\lambda + 2G) + h^2}, \quad (3.36)$$

and with this value, the smoothing factor is bounded by 0.6, independently of the values of κ and Lamé coefficients λ, G ,

$$\mu_S = \frac{3\kappa(\lambda + 2G)}{5\kappa(\lambda + 2G) + h^2} \leq 0.6. \quad (3.37)$$

Moreover, following (3.28) the relaxation parameter is given by the expression

$$\omega = \frac{h^2(\lambda + 2G)}{5\kappa(\lambda + 2G) + h^2}. \quad (3.38)$$

Some results. We would like to quantitatively determine μ_S based on the previous theory. A suitable relaxation parameter ω needs to be selected for the Richardson iteration. To define this ω with the rule (3.38), we need first to compute $\beta_{\max}(h)$ and $\beta_{\min}(h)$ from (3.33) and (3.34). After that, κ_β and ζ are obtained via (3.35), (3.36).

Table 3.1 shows the values of the parameters necessary to compute the relaxation parameter and smoothing factor μ_S for different coefficients of κ on the staggered grid. We consider the following values of the Lamé coefficients: $\lambda = 12500$ and $G = 8333$.

Parameters	$\kappa = 1$	$\kappa = 10^{-3}$	$\kappa = 10^{-6}$	$\kappa = 10^{-10}$	$\kappa = 0$
β_{\max}	5.24×10^5	524.29	0.52	8.67×10^{-5}	3.43×10^{-5}
β_{\min}	1.31×10^5	131.07	0.13	4.74×10^{-5}	3.43×10^{-5}
κ_β	4	4	4	1.83	1
ζ	1.6	1.6	1.6	1.29	1
ω	3.05×10^{-6}	3.10×10^{-3}	3.05	14913	29166
μ_S	0.6	0.6	0.6	0.29	0

Table 3.1: Values of the parameters computed by the theory, together with the resulting relaxation parameters ω and smoothing factors μ_S when $h = \frac{1}{256}$ on a staggered grid.

The smoothing factor corresponding to the symmetric Gauss-Seidel smoother is $\mu_A = 0.4927$ for only one smoothing step. Therefore, $(\mu_A)^{1/2} = 0.70$, which results in a bound of the smoothing factor for the whole system based on inequality (3.23).

In Table 3.2, we present the smoothing and two-grid convergence factors for the proposed multigrid method with Uzawa smoother for different values of κ and considering only one smoothing step. Also, the asymptotic convergence factor ρ_h , experimentally obtained, is shown in the table. Homogeneous Dirichlet boundary conditions are applied and the right-hand sides of the poroelasticity equations are all set to zero, so that we can iterate until the asymptotic convergence factor is reached. All results are based on the relaxation parameter ω given in Table 3.1.

κ	1	10^{-3}	10^{-6}	10^{-10}	0
μ	0.60	0.61	0.60	0.52	0.50
ρ (ρ_h)	0.60 (0.59)	0.61 (0.60)	0.60 (0.59)	0.48 (0.54)	0.61 (0.57)

Table 3.2: Smoothing and two-grid convergence factors predicted by LFA for different values of κ by using one smoothing step, together with the asymptotic convergence factors experimentally computed.

Numerical computation shows that the asymptotic multigrid convergence factor is accurately predicted by the LFA two-grid convergence factor. Regarding the smoothing factor, we obtained an upper bound for all cases.

Remark 3.1. *A well-known challenge for poroelasticity equations is to consider incompressible materials, when the Poisson ratio is close to 0.5. As can be seen from formula (3.37), the smoothing factor μ_S is bounded by 0.6, independently of all physical parameters. However, it is known that standard smoothers, like the one considered here, for the elasticity operator do not give satisfactory results in the incompressible case, since it is a grad-div dominating problem. For this case, more suitable smoothers, as for example the distributive relaxation proposed in [36], should be used.*

The presented analysis can be adapted to the case of non-square meshes, and the corresponding results are shown in Appendix 3.A.

Comparison with Vanka smoother In order to support the choice of the proposed Uzawa smoother, in Table 3.3 for a finest grid with $h = \frac{1}{256}$, we observe that its convergence rate is comparable to that of the Vanka smoother, which has been widely used for saddle point problems and for poroelasticity equations, see also Chapter 2. A relaxation parameter $\omega = 0.7$ is used for the Vanka smoother to perform a fair comparison, since this parameter provides the best multigrid convergence with this smoother. In Table 3.3, for different values of permeability and numbers of smoothing steps, the number of multigrid iterations to reduce the maximum norm of the residual by 10^{-10} are presented. Whereas the number of iterations is comparable, the Uzawa smoother has a lower computational cost.

Three-dimensional case The analysis performed in the two-dimensional case can be straightforwardly extended to the three-dimensional case. In particular, it is easy to derive $\beta_{\max}(h) = \frac{12\kappa}{h^2} + \frac{1}{\lambda + 2G}$ and $\beta_{\min}(h) = \frac{2\kappa}{h^2} + \frac{1}{\lambda + 2G}$. As a consequence, the bound for the smoothing factor is $\mu_S \leq \frac{5}{7}$, if the optimal value $\omega = \frac{2}{\beta_{\max} + \beta_{\min}}$ is chosen. The LFA smoothing and two-grid convergence factors are displayed in Table 3.4 for different

smoothing steps	smoother	$\kappa = 10^{-2}$	$\kappa = 10^{-6}$	$\kappa = 10^{-10}$	$\kappa = 0$
1	Vanka	30	30	31	31
	Uzawa	32	32	28	35
2	Vanka	16	16	16	17
	Uzawa	17	17	15	18
3	Vanka	11	11	12	14
	Uzawa	12	12	11	13
4	Vanka	9	9	11	12
	Uzawa	10	10	9	10

Table 3.3: Number of multigrid iterations necessary to reduce the initial residual by a factor of 10^{-10} .

values of the permeability and different smoothing steps. The numerically obtained asymptotic convergence factors are also included to validate the LFA results.

	(1,0)			(1,1)			(2,1)			(2,2)		
κ	$\mu^{\nu_1+\nu_2}$	ρ	ρ_h	$\mu^{\nu_1+\nu_2}$	ρ	ρ_h	$\mu^{\nu_1+\nu_2}$	ρ	ρ_h	$\mu^{\nu_1+\nu_2}$	ρ	ρ_h
1	0.71	0.71	0.70	0.51	0.51	0.49	0.36	0.36	0.35	0.26	0.26	0.24
10^{-3}	0.71	0.71	0.70	0.51	0.51	0.49	0.36	0.36	0.35	0.26	0.26	0.24
10^{-6}	0.70	0.70	0.68	0.49	0.49	0.47	0.34	0.34	0.33	0.24	0.24	0.22
10^{-10}	0.55	0.55	0.54	0.30	0.30	0.29	0.16	0.17	0.17	0.09	0.12	0.11
0	0.55	0.55	0.54	0.30	0.30	0.29	0.17	0.17	0.17	0.09	0.12	0.11

Table 3.4: Three-dimensional results - factors predicted by LFA and the asymptotic convergence factors with different number of pre- and post-smoothing steps (ν_1 and ν_2 , respectively) and for different values of κ .

3.5.2 Collocated grid arrangement of unknowns

Theoretical analysis. Next, we consider the multigrid method with Uzawa smoother for the poroelastic system of equations discretized on a collocated grid. In this case, we also determine the optimal ω -value by the theoretical results in Section 3.4.2. For this purpose, we first need to get bounds of

the eigenvalues of the Schur complement.

The theoretical analysis for the collocated grid is more involved than the staggered case, since equalities (3.29) and (3.30) do not hold in the collocated case and therefore we need to follow a different strategy. We rewrite the symbol of the elasticity operator as follows,

$$\begin{aligned}\tilde{A}(\boldsymbol{\theta}) &= (\lambda + G)\tilde{Y}(\boldsymbol{\theta}) = (\lambda + G)(\tilde{N}(\boldsymbol{\theta}) + \tilde{B}^T(\boldsymbol{\theta})\tilde{B}(\boldsymbol{\theta})) \\ &= (\lambda + G) \left(\left(-\frac{G}{\lambda + G}\tilde{\Delta}_v(\boldsymbol{\theta}) + \frac{h^2}{4}\tilde{J}(\boldsymbol{\theta}) \right) + \tilde{B}^T(\boldsymbol{\theta})\tilde{B}(\boldsymbol{\theta}) \right),\end{aligned}\quad (3.39)$$

where $\tilde{\Delta}_v(\boldsymbol{\theta}) = \begin{pmatrix} -\frac{4}{h^2}(s_1 + s_2) & \\ & -\frac{4}{h^2}(s_1 + s_2) \end{pmatrix}$ and $\tilde{J}(\boldsymbol{\theta}) = \begin{pmatrix} \frac{16s_1^2}{h^4} & \\ & \frac{16s_2^2}{h^4} \end{pmatrix}$ are the Fourier symbols of operators $\Delta_v = \begin{pmatrix} \Delta & \\ & \Delta \end{pmatrix}$ and $J = \begin{pmatrix} \partial_{xxxx} & \\ & \partial_{yyyy} \end{pmatrix}$, with ∂_{xxxx} and ∂_{yyyy} the standard discretization of the fourth-order derivative with respect to x and y , respectively.

Instead of computing the symbol of A^{-1} , we first consider the symbol of Y^{-1} . $\tilde{Y}^{-1}(\boldsymbol{\theta})$ can be calculated by applying the Sherman-Morrison-Woodbury formula,

$$\begin{aligned}\tilde{Y}^{-1}(\boldsymbol{\theta}) &= (\tilde{N}(\boldsymbol{\theta}) + \tilde{B}^T(\boldsymbol{\theta})\tilde{B}(\boldsymbol{\theta}))^{-1} \\ &= \tilde{N}^{-1}(\boldsymbol{\theta}) - \tilde{N}^{-1}(\boldsymbol{\theta})\tilde{B}^T(\boldsymbol{\theta})(I + \tilde{B}(\boldsymbol{\theta})\tilde{N}^{-1}(\boldsymbol{\theta})\tilde{B}^T(\boldsymbol{\theta}))^{-1}\tilde{B}(\boldsymbol{\theta})\tilde{N}^{-1}(\boldsymbol{\theta}),\end{aligned}\quad (3.40)$$

and therefore

$$\begin{aligned}\tilde{B}(\boldsymbol{\theta})\tilde{Y}^{-1}(\boldsymbol{\theta})\tilde{B}^T(\boldsymbol{\theta}) &= \tilde{B}(\boldsymbol{\theta})\tilde{N}^{-1}(\boldsymbol{\theta})\tilde{B}^T(\boldsymbol{\theta}) \\ &\quad - \tilde{B}(\boldsymbol{\theta})\tilde{N}^{-1}(\boldsymbol{\theta})\tilde{B}^T(\boldsymbol{\theta})(I + \tilde{B}(\boldsymbol{\theta})\tilde{N}^{-1}(\boldsymbol{\theta})\tilde{B}^T(\boldsymbol{\theta}))^{-1}\tilde{B}(\boldsymbol{\theta})\tilde{N}^{-1}(\boldsymbol{\theta})\tilde{B}^T(\boldsymbol{\theta}).\end{aligned}\quad (3.41)$$

Denoting $X = \tilde{B}(\boldsymbol{\theta})\tilde{N}^{-1}(\boldsymbol{\theta})\tilde{B}^T(\boldsymbol{\theta})$, then

$$\tilde{B}(\boldsymbol{\theta})\tilde{Y}^{-1}(\boldsymbol{\theta})\tilde{B}^T(\boldsymbol{\theta}) = X - X(1 + X)^{-1}X = \frac{X}{1 + X}.\quad (3.42)$$

We would like to compute X , based on the symbol of N , i.e.,

$$\begin{aligned}\tilde{N}(\boldsymbol{\theta}) &= \frac{G}{\lambda + G} \begin{pmatrix} \frac{4}{h^2}(s_1 + s_2) & \\ & \frac{4}{h^2}(s_1 + s_2) \end{pmatrix} + \frac{h^2}{4} \begin{pmatrix} \frac{16}{h^4}s_1^2 & \\ & \frac{16}{h^4}s_2^2 \end{pmatrix} \\ &= \frac{4}{h^2} \begin{pmatrix} \frac{G}{\lambda + G}(s_1 + s_2) + s_1^2 & \\ & \frac{G}{\lambda + G}(s_1 + s_2) + s_2^2 \end{pmatrix},\end{aligned}\tag{3.43}$$

and subsequently

$$\widetilde{N^{-1}}(\boldsymbol{\theta}) = \frac{h^2}{4} \begin{pmatrix} \frac{\lambda + G}{G(s_1 + s_2) + (\lambda + G)s_1^2} & \\ & \frac{\lambda + G}{G(s_1 + s_2) + (\lambda + G)s_2^2} \end{pmatrix}.\tag{3.44}$$

By computing the symbol of B and B^T , we can write

$$\begin{aligned}X &= \begin{pmatrix} \frac{-i \sin \theta_1}{h}, \frac{-i \sin \theta_2}{h} \end{pmatrix} \widetilde{N^{-1}}(\boldsymbol{\theta}) \begin{pmatrix} \frac{i \sin \theta_1}{h} \\ \frac{i \sin \theta_2}{h} \end{pmatrix} \\ &= (\lambda + G) \left(\frac{s_1(1 - s_1)}{G(s_1 + s_2) + (\lambda + G)s_1^2} + \frac{s_2(1 - s_2)}{G(s_1 + s_2) + (\lambda + G)s_2^2} \right).\end{aligned}\tag{3.45}$$

With the relations above, we get

$$\tilde{B}(\boldsymbol{\theta}) \widetilde{A^{-1}}(\boldsymbol{\theta}) \tilde{B}^T(\boldsymbol{\theta}) = \frac{1}{\lambda + G} \tilde{B}(\boldsymbol{\theta}) \widetilde{Y^{-1}}(\boldsymbol{\theta}) \tilde{B}^T(\boldsymbol{\theta}) = \frac{1}{\lambda + G} \frac{X}{1 + X}.\tag{3.46}$$

With the symbol of C given by $\tilde{C}(\boldsymbol{\theta}) = \frac{s_1 + s_2}{\lambda + 2G} + \frac{4\kappa}{h^2}(s_1 + s_2)$, the following symbol of the Schur complement is obtained,

$$\tilde{S}(\boldsymbol{\theta}) = \tilde{C}(\boldsymbol{\theta}) + \tilde{B}(\boldsymbol{\theta}) \widetilde{A^{-1}}(\boldsymbol{\theta}) \tilde{B}^T(\boldsymbol{\theta}) = \frac{4\kappa(s_1 + s_2)}{h^2} + \frac{s_1 + s_2}{\lambda + 2G} + \frac{1}{\lambda + G} \frac{X}{1 + X},\tag{3.47}$$

with X from (3.45). We obtain β_{\max} and β_{\min} as the maximum and minimum of $\tilde{S}(\boldsymbol{\theta})$ in the high frequencies. Based on (3.24), an optimal ζ -value minimizing the smoothing factor, is given by $\zeta = \frac{2\kappa_\beta}{1 + \kappa_\beta}$. Relaxation parameter ω has the same expression as in (3.28).

Approximation. From (3.47), it is nontrivial to obtain a closed formula for the maximum and minimum eigenvalues of the Schur complement. However, we find by using a sufficiently fine computational grid in the frequency space that these values for the high frequencies can be accurately expressed as,

$$\beta_{\max}(h) \approx \frac{8\kappa}{h^2} + \frac{2}{\lambda + 2G} \quad (\text{achieved for } \theta_1 = \theta_2 = \pi), \quad (3.48)$$

$$\beta_{\min}(h) \approx \frac{2\kappa}{h^2} + \frac{1}{\lambda + 2G} \quad (\text{achieved for } \theta_1 = 0, \theta_2 = \pi/2). \quad (3.49)$$

The eigenvalues of $\frac{1}{\lambda + G} \frac{X}{1 + X}$ are small compared to the eigenvalues of C . We have checked the eigenvalues numerically and the maximum and minimum values are identical to the expressions (3.48) and (3.49). Taking into account these approximations, we can write

$$\kappa_\beta = \frac{\beta_{\max}(h)}{\beta_{\min}(h)} \approx \frac{8\kappa(\lambda + 2G) + 2h^2}{2\kappa(\lambda + 2G) + h^2}, \quad (3.50)$$

and in the limit case, when $\kappa = 0$, the simplified expression reads $\kappa_\beta = 2$. With an optimal ζ -value,

$$\zeta = \frac{2\kappa_\beta}{1 + \kappa_\beta} \approx \frac{16\kappa(\lambda + 2G) + 4h^2}{10\kappa(\lambda + 2G) + 3h^2}, \quad (3.51)$$

the smoothing factor is found to be

$$\mu_S(h) = \zeta - 1 \approx \frac{6\kappa(\lambda + 2G) + h^2}{10\kappa(\lambda + 2G) + 3h^2}.$$

If $\kappa = 0$, then $\mu_S = 1/3$, independently of h , whereas if $\kappa \neq 0$, then $\mu_S = 0.6$, for h sufficiently small. Therefore, we can write

$$\mu_S = \sup_{h \leq h_0} \mu_S(h) = 0.6,$$

independently of the values of κ and the Lamé coefficients λ and G . From (3.28), (3.48) and (3.49), the expression for ω approximately reads

$$\omega = \frac{2h^2(\lambda + 2G)}{10\kappa(\lambda + 2G) + 3h^2}. \quad (3.52)$$

Obviously, ω is dependent on the mesh size, and the relaxation parameter needs to be determined on each grid level. The limit case $\kappa = 0$ yields $\zeta = 4/3$, $\mu_S = 1/3$ and $\omega = 2/3(\lambda + 2G)$.

Numerical results. Table 3.5 shows the values of the parameters for the computation of the smoothing factors μ_S and relaxation parameters $\omega > 0$ for different values of the parameter κ , when $h = \frac{1}{256}$ (fixed).

Parameters	$\kappa = 1$	$\kappa = 10^{-3}$	$\kappa = 10^{-6}$	$\kappa = 10^{-10}$	$\kappa = 0$
β_{\max}	5.24×10^5	524.28	0.52	1.21×10^{-4}	6.86×10^{-5}
β_{\min}	1.31×10^5	131.07	0.13	4.74×10^{-5}	3.43×10^{-5}
κ_β	4	4	4	2.55	2
ζ	1.6	1.6	1.6	1.44	1.33
ω	3.05×10^{-6}	3.05×10^{-3}	3.05	11877	19444
μ_S	0.6	0.6	0.6	0.44	0.33

Table 3.5: Values of the parameters computed by the theory, together with the resulting smoothing factors μ_S when $h = \frac{1}{256}$ on a collocated grid.

We are also interested in the smoothing factor of the symmetric Gauss-Seidel method μ_A of the elasticity operator on the collocated grid. This value can be computed by LFA, giving $\mu_A = 0.47$ and therefore $(\mu_A)^{1/2} = 0.68$. Since μ_S is smaller, we get a bound $\bar{\mu}$ for the smoothing factor of the whole system from (3.24), as $\bar{\mu} = \max(0.68, \mu_S) = 0.68$. The upper bound on the smoothing factor is determined by the smoother considered for the displacements in this case.

As commented before, the relaxation parameter ω has to be determined on each grid of the hierarchy. Table 3.6 shows the values of ω from (3.52) for different values of the mesh size h and permeability κ . In this table, only results for three grid sizes are presented for simplicity.

mesh size	$\kappa = 10^{-3}$	$\kappa = 10^{-6}$	$\kappa = 10^{-7}$	$\kappa = 10^{-8}$
$h = \frac{1}{512}$	7.63×10^{-4}	7.60×10^{-1}	7.63×10^0	7.60×10^1
$h = \frac{1}{256}$	3.05×10^{-3}	3.05×10^0	3.05×10^1	3.00×10^2
$h = \frac{1}{128}$	1.22×10^{-2}	1.22×10^1	1.21×10^2	1.20×10^3

Table 3.6: Relaxation parameters ω on different levels of the grid hierarchy.

Next, with a fixed value of $\kappa = 10^{-6}$, we analyze the performance of the Uzawa smoother for the collocated discretization of the poroelasticity

system. For different sizes of the finest grid, the LFA smoothing factor μ for the whole system together with the two-grid convergence factor ρ predicted by LFA with only one smoothing step are given by $\mu = \rho = 0.60$ in all cases, using ω as in Table 3.6.

We also consider the numerical multigrid convergence. The performance of the multigrid algorithm and the results predicted by LFA are compared in Table 3.7. The actual multigrid convergence factors ρ_h are obtained when the residual is reduced to 10^{-20} in maximum norm. The results are shown for different numbers of smoothing steps ((1,0) and (1,1)) and using the relaxation parameters ω as in Table 3.6. The numerical multigrid results are computed for F -cycles on a grid with $h = \frac{1}{256}$. The numerical experiments show that the asymptotic multigrid convergence factors ρ_h accurately resemble the LFA two-grid convergence factors ρ .

	(1,0)			(1,1)		
κ	$\mu^{\nu_1+\nu_2}$	ρ	ρ_h	$\mu^{\nu_1+\nu_2}$	ρ	ρ_h
10^{-3}	0.60	0.60	0.60	0.36	0.36	0.36
10^{-6}	0.60	0.60	0.60	0.36	0.36	0.36
10^{-8}	0.60	0.60	0.59	0.35	0.35	0.38

Table 3.7: Comparison results - factors predicted by LFA and the asymptotic convergence factors with different number of pre- and post-smoothing steps (ν_1 and ν_2 , respectively) and for different values of κ .

We also confirm the h -independent convergence behavior of the multigrid method. For $\kappa = 10^{-3}$ and a multigrid $F(1,1)$ -cycle, computing on different meshes with $h = 1/2^{k_l}$, $k_l = 6, 7, 8, 9$, the multigrid convergence factor is around 0.22 for all cases, and the multigrid method exhibits a highly satisfactory behavior.

We wish to check the sensitivity of the multigrid convergence with respect to the exact choice of the relaxation parameter ω . Supposing ω has already been obtained from (3.52) on each level ($h = \frac{1}{128}$ being the finest grid here), the convergence behavior of the multigrid is plotted in Figure 3.3 (dashed line). However, we can also simply round the significant digits of ω to the nearest integer number, while leaving the exponent part unchanged. For example, instead of $\omega = 7.63 \cdot 10^{-4}$ in Table 3.6, we use “the inexact value” $\omega = 8 \cdot 10^{-4}$. The convergence with the inexact param-

eter is denoted by asterisks in Figure 3.3. There is no significant difference between the multigrid convergence results with exact parameters and those with these inexact parameters. To improve the convergence performance, the iterant recombination scheme as presented in Section 3.3.1, can be employed. The acceleration scheme with either exact or inexact ω are denoted by crosses and circles, respectively. The results show a highly satisfactory convergence performance in Figure 3.3.

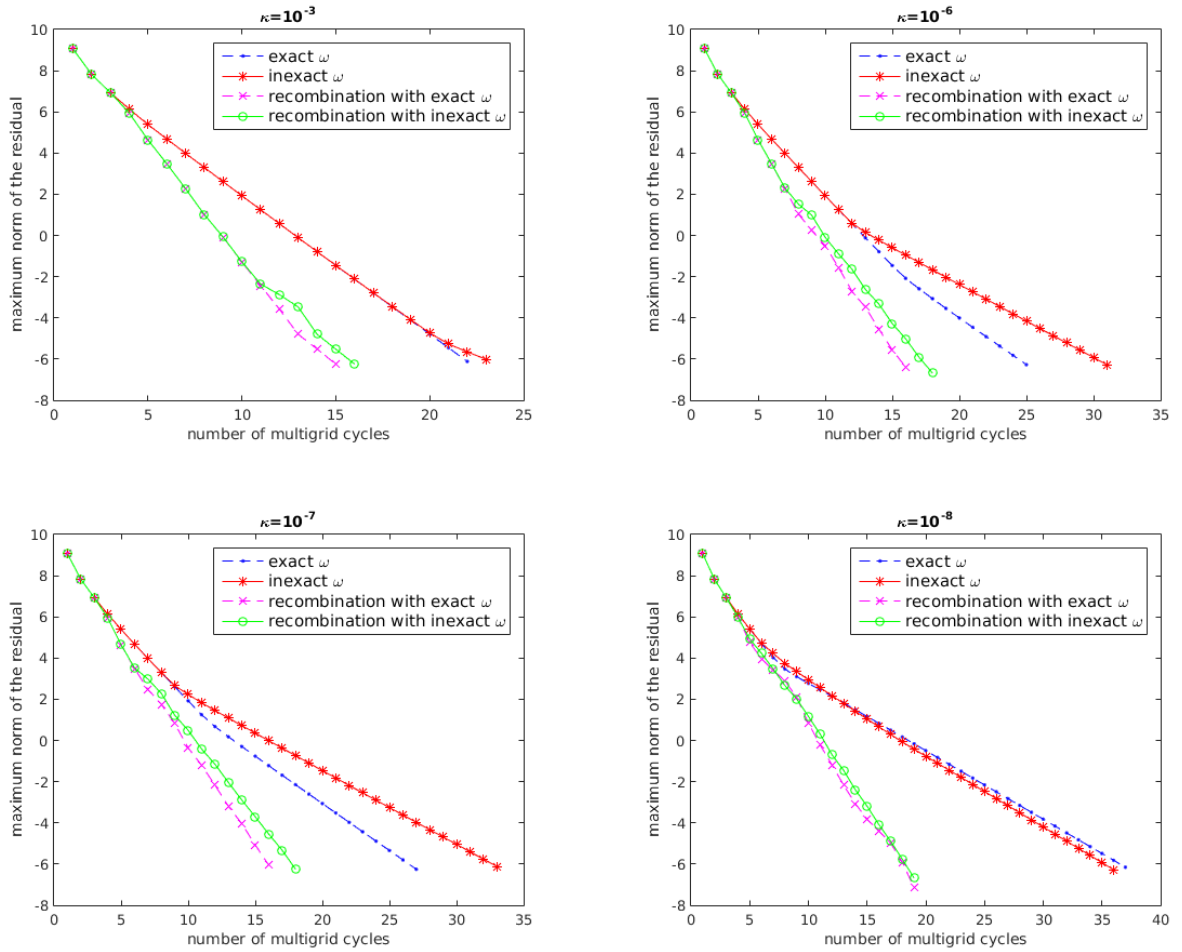


Figure 3.3: Sensitivity regarding the choice of ω when $h = \frac{1}{128}$ for different values of the permeability.

The deviation from the “exact” value of ω can be assessed by LFA too. In Figure 3.4, we show the two-grid convergence factors predicted by LFA with respect to the ratio between the “inexact” value of ω and “exact” optimal ω , for the case $\kappa = 10^{-6}$. Similar pictures are obtained for other values of the permeability.

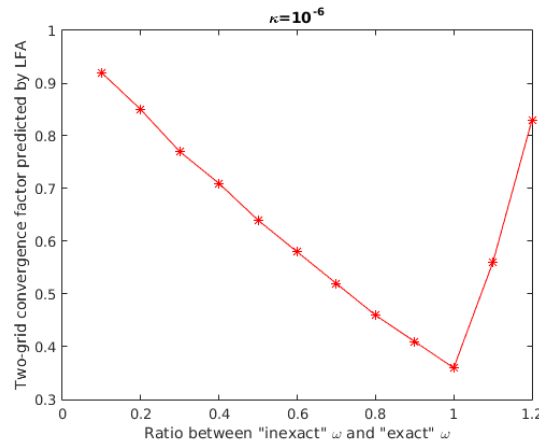


Figure 3.4: Two-grid convergence factors predicted by LFA for different choices of “inexact” ω and $\kappa = 10^{-6}$.

Some more numerical tests in which we consider Uzawa parameters for non-square meshes are discussed in Appendix 3.B.

3.5.3 Heterogeneity case (collocated grids)

In this section, we consider the poroelasticity system with heterogeneous coefficients. The heterogeneity can influence the poroelastic behavior in many ways. We wish to consider the effect of heterogeneity on the multigrid convergence. To simulate heterogeneity in the porous medium, the Weibull distribution is considered as in Section 2.4.2.

It is known that heterogeneity is one of the complicating factors which can influence the multigrid convergence behavior. To improve the convergence performance, we consider the acceleration scheme for multigrid as in Section 3.3.1.

In a multigrid algorithm, the material properties need to be transferred to coarse grids. In this way, the coarse system is related to the fine system, so that the same characteristics of the material are present. Lamé coefficients and the permeability are restricted to each grid level by full weighting operators. Then we perform a regular finite volume discretization with these averaged coefficients on the coarse grids. The highly varying properties cannot represent the original material on coarse grids accurately. We wish to study the impact of the heterogeneity on the multigrid convergence using the standard multigrid components described above on a collocated grid.

Comparison test. In Table 3.8, for different homogeneity indices m and permeabilities κ , the numerical multigrid convergence factors for an F -cycle with one pre- and one post-smoothing step are presented. The values

index	scheme	$\kappa = 10^{-3}$	$\kappa = 10^{-6}$	$\kappa = 10^{-7}$	$\kappa = 10^{-8}$
$m = 10$	Multigrid	0.24 (23)	0.28 (25)	0.30 (27)	0.43 (38)
	Acc Multigrid	0.12 (15)	0.13 (16)	0.14 (17)	0.17 (19)
$m = 5$	Multigrid	0.25 (24)	0.28 (26)	0.31 (27)	0.43 (38)
	Acc Multigrid	0.12 (16)	0.14 (17)	0.15 (17)	0.19 (19)
$m = 3$	Multigrid	0.28 (26)	0.29 (26)	0.31 (28)	0.42 (37)
	Acc Multigrid	0.13 (16)	0.16 (18)	0.19 (20)	0.24 (23)
$m = 2$	Multigrid	0.31 (28)	0.31 (28)	0.38 (34)	/
	Acc Multigrid	0.15 (18)	0.24 (23)	0.28 (26)	0.69 (93)

Table 3.8: Convergence factors (and number of iterations between brackets) of multigrid method and multigrid with iterant recombination for a heterogeneous test. (“/” denotes divergence)

in parentheses are the numbers of multigrid iterations needed to reduce the residual to 10^{-6} in maximum norm. All results are obtained on a grid with $h = \frac{1}{128}$. Notice that the relaxation parameters ω are varied in the computational domain for the heterogeneity case, since ω is related to the stochastically distributed Lamé coefficients and permeability. Multigrid does not converge for very small homogeneity index, such as $m = 1$. This is due to the heterogeneity properties of the material and the choice of multigrid components here. For the problems with strongly “varying” coefficients, Galerkin coarse matrices, operator-dependent prolongation and restriction should be considered, (see [94], Chapter 7).

To illustrate the efficiency of the acceleration method proposed in Section 3.3.1, Table 3.8 also shows the convergence results with multigrid acceleration by iterant recombination denoted as “Acc Multigrid”. All the initial settings in this numerical test are the same as in “Multigrid” without acceleration. When the acceleration scheme is applied, \tilde{q} is set equal to 5. Obviously, the convergence behavior corresponding to “Multigrid” is nicely improved by the iterant recombination for each heterogeneity case. The additional work required for “Acc Multigrid” is negligible.

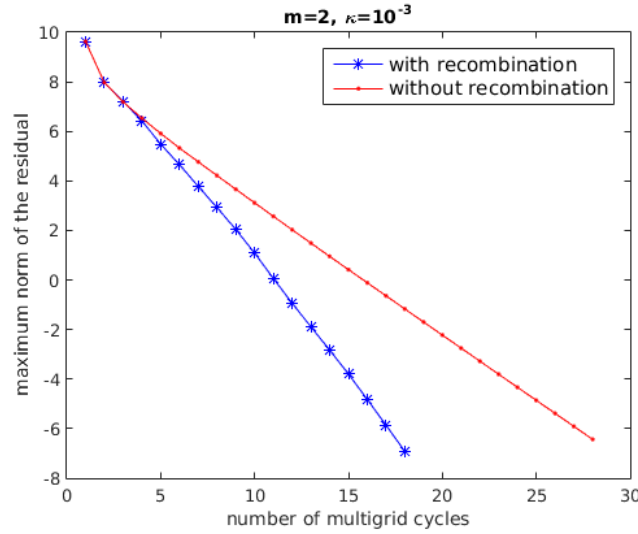


Figure 3.5: Comparison results between the history of the convergence for multigrid method and iterant recombination scheme.

We consider an extreme case where the homogeneity index is two and the coefficient of permeability is 10^{-3} . Figure 3.5 plots the decreasing residuals with respect to multigrid iterations. The errors are plotted in logarithmic scale. It can be seen that it takes fewer multigrid cycles for the acceleration scheme to reach a same residual tolerance. The CPU time is also compared. The cost of iterant recombination is much less than the cost of standard multigrid to solve the problem. Based on the discussions above, the robustness of the iterant recombination is confirmed. For complicated problems, the recombination technique may give a more prominent acceleration performance.

3.6 Conclusion

In this chapter, we focused on an efficient multigrid method for the poroelasticity equations based on Biot's model of consolidation. A decoupled smoother called Uzawa smoother is chosen in the multigrid algorithm. It involves a symmetric Gauss-Seidel smoothing for displacements and a simple Richardson iteration for the Schur complement regarding the pressure field. In order to select an optimal relaxation parameter in the Richardson iteration, local Fourier analysis is applied. The convergence performance can also be predicted in the framework of LFA. Numerical tests confirm

our theoretical analysis. At the same time, some test problems towards engineering applications are considered. We use the iterant recombination scheme for the heterogeneous poroelasticity equations. It is demonstrated that the convergence factors are nicely improved by this scheme in many cases.

Appendix

In this appendix we detail the extension of the proposed analysis for the Uzawa-based multigrid method to the case in which the grid has different horizontal and vertical mesh sizes h_x and h_y . We describe the analysis for both staggered and collocated meshes.

3.A Non-square meshes: Staggered grid arrangement of unknowns

When the mesh size in x -direction h_x is not equal to the size in y -direction h_y , it is not immediately clear which parameter ω should be used. The symbol of $-\Delta$ is in this case,

$$-\tilde{\Delta}(\boldsymbol{\theta}) = 4 \left(\frac{s_1}{h_x^2} + \frac{s_2}{h_y^2} \right). \quad (3.53)$$

From (4.41) and (3.53), the symbol of the Schur complement S equals

$$\tilde{S}(\boldsymbol{\theta}) = 4\kappa \left(\frac{s_1}{h_x^2} + \frac{s_2}{h_y^2} \right) + \frac{1}{\lambda + 2G}. \quad (3.54)$$

The maximum eigenvalue of $-\Delta$ is achieved when $s_1 = s_2 = 1$, then

$$\beta_{\max}(h) = 4\kappa \left(\frac{1}{h_x^2} + \frac{1}{h_y^2} \right) + \frac{1}{\lambda + 2G}. \quad (3.55)$$

The minimum value of $-\Delta$ results to be $\frac{2\kappa}{h_y^2}$ if $h_y > h_x$ (for $s_1 = 0, s_2 = \frac{1}{2}$) or $\frac{2\kappa}{h_x^2}$ otherwise (for $s_1 = \frac{1}{2}$ and $s_2 = 0$). Therefore $\beta_{\min}(h)$ becomes

$$\beta_{\min}(h) = 2\kappa \min \left\{ \frac{1}{h_x^2}, \frac{1}{h_y^2} \right\} + \frac{1}{\lambda + 2G} = \frac{2\kappa}{\max\{h_x^2, h_y^2\}} + \frac{1}{\lambda + 2G}. \quad (3.56)$$

To compute $\kappa_\beta = \frac{\beta_{\max}}{\beta_{\min}}$ using (3.55) and (3.56), we have that

$$\kappa_\beta = \begin{cases} \frac{h_x^2 h_y^2 + 4\kappa(h_x^2 + h_y^2)(\lambda + 2G)}{h_x^2 h_y^2 + 2\kappa(\lambda + 2G)h_y^2}, & \text{when } h_x > h_y, \\ \frac{h_x^2 h_y^2 + 4\kappa(h_x^2 + h_y^2)(\lambda + 2G)}{h_x^2 h_y^2 + 2\kappa(\lambda + 2G)h_x^2}, & \text{when } h_x < h_y. \end{cases}$$

Therefore,

$$\kappa_\beta = \frac{h_x^2 h_y^2 + 4\kappa(h_x^2 + h_y^2)(\lambda + 2G)}{h_x^2 h_y^2 + 2\kappa(\lambda + 2G) \min\{h_x^2, h_y^2\}}. \quad (3.57)$$

Assuming $h_x > h_y$ for the following analysis, we choose the optimal ζ giving the lowest value of the maximum from (3.24),

$$\zeta = \frac{2\kappa_\beta}{1 + \kappa_\beta} = \frac{h_x^2 h_y^2 + 4\kappa(\lambda + 2G)(h_x^2 + h_y^2)}{h_x^2 h_y^2 + 3\kappa(\lambda + 2G)h_y^2 + 2\kappa(\lambda + 2G)h_x^2}. \quad (3.58)$$

In this way, the relaxation parameter can be obtained by substituting (3.55) and (3.56) in the expression of ω in (3.38),

$$\omega = \frac{2}{\beta_{\max} + \beta_{\min}} = \frac{1}{\frac{1}{\lambda + 2G} + \frac{3\kappa}{h_x^2} + \frac{2\kappa}{h_y^2}}. \quad (3.59)$$

By using these relaxation parameters, the smoothing factor can be computed as

$$\mu_S = \zeta - 1 = \frac{\kappa(\lambda + 2G)(2h_x^2 + h_y^2)}{h_x^2 h_y^2 + 3\kappa(\lambda + 2G)h_y^2 + 2\kappa(\lambda + 2G)h_x^2}. \quad (3.60)$$

If the grid size is extremely small, the term $h_x^2 h_y^2$ can be neglected. The smoothing factor is dominated by the value $\frac{2h_1^2 + h_2^2}{3h_2^2 + 2h_1^2}$. However, for the case $h_x \gg h_y$, the smoothing factor tends to 1. It indicates that when the grid becomes anisotropic, we obtain worse convergence results and appropriate block-wise smoothers or semi-coarsening may be required.

In Table 3.9, we fix h_x to $\frac{1}{128}$ and gradually change h_y . We have chosen $\kappa = 10^{-6}$ and two smoothing steps. The optimal parameter ω on the finest grid and the two-grid convergence factor ρ predicted from LFA are displayed.

		$h_x = \frac{1}{128}$		
mesh		$h_y = \frac{1}{64}$	$h_y = \frac{1}{128}$	$h_y = \frac{1}{256}$
LFA	ω	22.17	12.20	5.55
	ρ	0.67	0.38	0.69

Table 3.9: Values of ω , ρ predicted by LFA when $h_x \neq h_y$ on a staggered grid.

3.B Non-square meshes: Collocated grid arrangement of unknowns

Here, we will analyze the case where the collocated grid has different horizontal and vertical mesh sizes h_x and h_y . We have

$$C = -\kappa\Delta - \frac{h_x^2}{4(\lambda + 2G)}\partial_{xx} - \frac{h_y^2}{4(\lambda + 2G)}\partial_{yy}$$

with the stabilization term. The symbols of ∂_{xx} and ∂_{yy} are $-\frac{4s_1}{h_x^2}$, $-\frac{4s_2}{h_y^2}$, and

$$\tilde{C}(\boldsymbol{\theta}) = 4\kappa \left(\frac{s_1}{h_x^2} + \frac{s_2}{h_y^2} \right) + \frac{s_1 + s_2}{\lambda + 2G}.$$

Subsequently, the symbol of the Schur complement is given by

$$\tilde{S}(\boldsymbol{\theta}) = \tilde{C}(\boldsymbol{\theta}) + \tilde{B}(\boldsymbol{\theta})\widetilde{A^{-1}}(\boldsymbol{\theta})\tilde{B}^T(\boldsymbol{\theta}) = 4\kappa \left(\frac{s_1}{h_x^2} + \frac{s_2}{h_y^2} \right) + \frac{s_1 + s_2}{\lambda + 2G} + \frac{1}{\lambda + G} \frac{X}{1 + X},$$

where $X = \tilde{B}(\boldsymbol{\theta})\widetilde{N^{-1}}(\boldsymbol{\theta})\tilde{B}^T(\boldsymbol{\theta})$ and $\tilde{N}(\boldsymbol{\theta}) = -\frac{G}{\lambda + G}\widetilde{\Delta_v}(\boldsymbol{\theta}) + \tilde{J}_1(\boldsymbol{\theta})$.

Note that

$$\widetilde{\Delta_v}(\boldsymbol{\theta}) = \begin{pmatrix} -4 \left(\frac{s_1}{h_x^2} + \frac{s_2}{h_y^2} \right) & \\ & -4 \left(\frac{s_1}{h_x^2} + \frac{s_2}{h_y^2} \right) \end{pmatrix},$$

$\tilde{J}_1(\boldsymbol{\theta}) = \begin{pmatrix} \frac{4s_1^2}{h_x^2} & \\ & \frac{4s_2^2}{h_y^2} \end{pmatrix}$ and $\tilde{B}(\boldsymbol{\theta}) = \begin{pmatrix} \frac{-i \sin \theta_1}{h_x} & \frac{-i \sin \theta_2}{h_y} \end{pmatrix}$ are the necessary

symbols for computing X . The exact expression of the relaxation parameter ω is not obtained due to the involved expression for the collocated case. So, we compute the parameter numerically for non-square meshes.

In the following test, h_x is fixed to $\frac{1}{128}$ and h_y is gradually changed. LFA is applied to compute the optimal parameter ω on the finest grid and predict the two-grid convergence factor ρ . With the obtained ω -values, we employ both the pure multigrid cycles and the iterant recombination scheme mentioned earlier for a homogeneous problem. When the residual is reduced to 10^{-20} in maximum norm, the asymptotic convergence factor ρ_h is well predicted by the two-grid convergence factor ρ . However, in real applications, such a small residual is not necessary. In Table 3.10, we display the convergence factors and the number of multigrid cycles (in parentheses) needed to reduce the initial residual to 10^{-6} in maximum norm, together with the values of ω and ρ obtained by LFA. The efficiency of the recombination scheme is demonstrated since the observed convergence factors reduce by a factor two compared to those obtained with the multigrid cycle. Obviously, the convergence factor $\rho_{h,acc}$ is much smaller than ρ_h for all cases.

		$h_x = \frac{1}{128}$		
mesh		$h_y = \frac{1}{64}$	$h_y = \frac{1}{128}$	$h_y = \frac{1}{256}$
LFA	ω	22.17	12.20	5.55
	ρ	0.67	0.36	0.67
	ρ_h	0.58 (58)	0.27 (25)	0.60 (62)
	$\rho_{h,acc}$	0.28 (25)	0.13 (16)	0.28 (26)

Table 3.10: Convergence factors (and number of iterations between brackets) corresponding to multigrid (ρ_h) and to the iterant recombination technique ($\rho_{h,acc}$) necessary to reduce the initial residual to 10^{-6} together with values of ω , ρ predicted by LFA when $h_x \neq h_y$.

In Table 3.11, the same test as in Table 3.10 is performed, with the only difference that we use non-optimal parameters associated with $h_x = h_y = \frac{1}{256}$ for all the cases in Table 3.11. We observe that the convergence factors become much worse compared to the values in Table 3.10. This points out the need for a good choice of relaxation parameters.

In addition, we find that if the relaxation parameters corresponding to $h_x = h_y = \frac{1}{128}$ are used for the case $h_x = \frac{1}{256}$, $h_y = \frac{1}{128}$, the algorithm does not converge. The value of ω depends on the minimum size of the grid. Therefore, for the test $\frac{1}{256} = h_x < h_y = \frac{1}{128}$, the parameter with respect

		$h_x = \frac{1}{256}$		
mesh		$h_y = \frac{1}{128}$	$h_y = \frac{1}{192}$	$h_y = \frac{1}{256}$
LFA	ρ	0.81	0.60	0.36
	ρ_h	0.72 (99)	0.47 (44)	0.26 (25)
	$\rho_{h,acc}$	0.36 (32)	0.21 (22)	0.12 (16)

Table 3.11: Convergence factors (and number of iterations between brackets) corresponding to the multigrid ρ_h and to the iterant recombination technique ($\rho_{h,acc}$) necessary to reduce the initial residual to 10^{-6} together with values of ρ predicted by LFA with ω corresponding to $h_x = h_y = \frac{1}{256}$.

to the smaller size h_x should be considered. The convergence performance is described in Table 3.11. Again, LFA can predict the asymptotic convergence factor (not shown in the table) accurately and the recombination scheme indeed improves the efficiency. When $h_x \neq h_y$ and even the optimal parameters are not available, we can use the parameters that correspond to the minimum of h_x and h_y .

Uzawa smoother in multigrid for the coupled porous medium and Stokes flow system

In this chapter, the multigrid solution of coupled porous media and Stokes flow problems is considered. The Darcy equation as the saturated porous medium model is coupled to the Stokes equations by means of appropriate interface conditions. We focus on an efficient multigrid solution technique for the coupled problem, which is discretized by finite volumes on staggered grids, giving rise to a saddle point linear system. Special treatment is required regarding the discretization at the interface. An Uzawa smoother is employed in multigrid, which is a decoupled procedure based on symmetric Gauss-Seidel smoothing for velocity components and a simple Richardson iteration for the pressure field. Since a relaxation parameter is part of a Richardson iteration, Local Fourier Analysis (LFA) is applied to determine the optimal parameters. Highly satisfactory multigrid convergence is reported, and, moreover, the algorithm performs very well for small values of the hydraulic conductivity and fluid viscosity, that are relevant for applications.¹

4.1 Introduction

Coupling of free flow and a saturated porous medium has received considerable attention due to applications in environmental and industrial context, such as in flood simulation, filtration and contamination. It is challeng-

¹The contents of this chapter have been published in paper [66]: P. Luo, C. Rodrigo, F.J. Gaspar and C.W. Oosterlee. Uzawa smoother in multigrid for the coupled porous medium and Stokes flow system, *SIAM journal on Scientific Computing*, in press, 2017.

ing to deal with a coupled multi-physics system, since each part of the system is based on a different model and an appropriate coupling at the interface is required. Flow in the saturated porous medium is modeled by the conventional Darcy equation here (the solid framework is assumed to be rigid and there is no interaction between the fluid and solid matrix in the porous medium), while the Newtonian flow through a channel is modeled by the incompressible Stokes equations. Appropriate interface conditions are based on the principles of mass conservation, equilibrium of normal stresses across the interface and a special condition called the Beavers-Joseph-Saffman condition [55, 82] describing the relation between the shear stress and the tangential velocity. Many researchers have studied multi-physics problems theoretically, see, for example, [2, 21, 62, 70].

The numerical solution of these multi-physics problems is also an active research area [30, 32, 51, 80, 81]. We discretize the Darcy-Stokes problem by the finite volume method on a staggered grid, which results in a symmetric system. The mixed formulation of the Darcy problem is used, so that the discretized equations on the staggered grid result in a matrix of saddle point form [7], where a zero block appears on the diagonal of the system matrix. The zero block thus appears in the matrix of the complete problem, because a stable staggered discretization is used for the Darcy-Stokes equations.

There are basically two ways to solve a coupled multi-physics system. A popular approach is based on the domain decomposition (DD) method [78, 86]. DD exploits the principle of divide-and-conquer and is based on decoupling the global problem so that mainly independent subproblems are to be solved. Several advanced iterative solvers of this type have been applied to the Darcy-Stokes system, as for example the Dirichlet-Neumann-type DD [31], Robin-Robin DD [22, 33], Lagrange multiplier-based DD [61] and many others [19, 20, 69]. DD is often used as a preconditioner for a Krylov subspace method for such coupled multi-physics problems. On the other hand, the so-called *monolithic solution approach* focusses on the simultaneous solution of the multi-physics system. Methods in this class typically exhibit robust convergence when there is a strong coupling between the two subsystems. Based on this insight, different monolithic methods have been proposed in the literature, such as preconditioned GMRES methods [18, 23, 24], where it was demonstrated that block-triangular

and constraint preconditioners yield mesh-independent convergence.

We solve the coupled system by developing an efficient *monolithic multigrid algorithm*. Often, multigrid methods have been applied for the efficient solution of saddle point systems, even dating back to the early days of multigrid for systems of incompressible Navier-Stokes equations [13, 14]. Other efficient multigrid methods for Stokes and incompressible Navier-Stokes problems have been developed, for example, in [10, 41, 54, 60, 95]. In [1] an efficient monolithic method was proposed for the magneto-hydrodynamics system.

Basically, there are two major categories of multigrid smoothers for saddle point problems, classified as coupled and decoupled smoothers, see [38, 39, 75]. In this paper, we consider the equation-wise decoupled Uzawa smoother within monolithic multigrid for the Darcy-Stokes system. The Uzawa smoother [68] will be applied for this discrete coupled system. This smoother has been enhanced for the Stokes equations in [41]. For the problem considered here, the velocities in the Darcy and Stokes equations are updated first, after which the pressures for both subsystems are relaxed. The Uzawa smoother is based on a Richardson iteration in which a relaxation parameter is present. As the optimal relaxation parameter for the Stokes problem has already been determined in [41], we are concerned with the selection of an optimal parameter for the Darcy problem through LFA in the present chapter. LFA is applied to the Darcy and Stokes subproblems separately, and it is shown that the worst of these factors results to be the global multigrid convergence for the coupled problem. By using the monolithic multigrid approach, we are able to achieve a *textbook multigrid convergence rate*, even when the values of the physical parameters are realistically small.

We deal with the so-called multiblock multigrid method which is based on the grid partitioning technique [94]. Boundary updates are communicated between neighboring blocks within the algorithm on each multigrid level. In [94] (Chapter 6), a detailed introduction of the grid partitioning technique is given. The convergence of the multiblock multigrid algorithm is identical to its single block equivalent in our case.

The chapter is organized as follows. The equations in free flow and porous media, together with the interface conditions are introduced in Section 4.2. Section 4.3 deals with the discretization of the coupled Darcy-

Stokes system. We give the discrete formulas for the coupled system including the discretization at the interface. The solution method, the Uzawa smoother and its analysis by means of LFA, are presented in Section 4.4. In Section 4.5, several numerical experiments are performed to show the efficiency of the algorithm. Conclusions are drawn in Section 4.6.

4.2 Problem formulation

We restrict ourselves to the two-dimensional Darcy-Stokes problem. The proposed solution strategy can be straightforwardly extended to a three-dimensional setting.

We consider the Darcy-Stokes problem on a bounded domain $\Omega \subset \mathbb{R}^2$, and assume that Ω is subdivided into two disjoint subdomains Ω^d and Ω^f , corresponding to the porous medium and free flow regions, respectively. Let Γ denote the interface between the two subregions, that is, $\Gamma = \partial\Omega^d \cap \partial\Omega^f$. The geometry of the problem is represented in Figure 4.1, where we also display \mathbf{n}^f and \mathbf{n}^d , denoting the unit outward normal vectors on $\partial\Omega^f$ and $\partial\Omega^d$, respectively. At the interface Γ , we have $\mathbf{n}^f = -\mathbf{n}^d$.

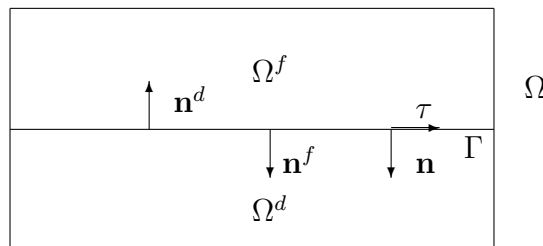


Figure 4.1: Geometry of the Darcy-Stokes problem. Subdivision of the domain Ω into a free flow subregion Ω^f and a porous medium subdomain Ω^d , by an internal interface Γ .

We describe the porous media and free flow models considered on the different subdomains, including the boundary conditions for the outer boundaries, in Sections 4.2.1 and 4.2.2, and the internal interface conditions governing the interactions between the fluid and the porous medium, in Section 4.2.3.

4.2.1 Porous medium description

The fluid flow through a rigid and saturated porous medium Ω^d is described by Darcy's law, which is an expression of conservation of momentum. The mixed formulation of the Darcy problem is natural for computations in the porous medium region since it allows to directly approximate the velocity. In this work, we will consider this formulation which reads

$$\begin{aligned}\mathbb{K}^{-1}\mathbf{u}^d + \nabla p^d &= \mathbf{0} & \text{in } \Omega^d, \\ \nabla \cdot \mathbf{u}^d &= f^d & \text{in } \Omega^d,\end{aligned}\tag{4.1}$$

where $\mathbf{u}^d = (u^d, v^d)$ describes the velocity and p^d the fluid pressure inside the porous medium. \mathbb{K} is the hydraulic conductivity tensor, representing the properties of the porous medium and the fluid. Here, the case $\mathbb{K} = K\mathbb{I}$, $K > 0$ is considered. Sinks and sources are described by the force term f^d .

We assume that the boundary $\partial\Omega^d \setminus \Gamma$ is the union of two disjoint subsets Γ_D^d and Γ_N^d , where Dirichlet and Neumann boundary conditions are imposed. More concretely, we consider the following boundary conditions

$$\begin{aligned}p^d &= g_D^d & \text{on } \Gamma_D^d, \\ \mathbf{u}^d \cdot \mathbf{n}^d &= g_N^d & \text{on } \Gamma_N^d.\end{aligned}\tag{4.2}$$

4.2.2 Free flow description

The free flow subproblem is modeled by the Stokes equations for a viscous, incompressible, Newtonian fluid. It is a linearized form of the Navier-Stokes equations in the limit case when the nonlinear term becomes negligible. The Stokes flow in the region Ω^f is described by

$$\begin{aligned}-\nabla \cdot \boldsymbol{\sigma}^f &= \mathbf{f}^f & \text{in } \Omega^f, \\ \nabla \cdot \mathbf{u}^f &= 0 & \text{in } \Omega^f,\end{aligned}\tag{4.3}$$

where $\mathbf{u}^f = (u^f, v^f)$ is the fluid velocity, $\mathbf{f}^f = (f_1^f, f_2^f)$ represents a prescribed force, and the fluid stress tensor $\boldsymbol{\sigma}^f$ is given by

$$\boldsymbol{\sigma}^f = -p^f \mathbf{I} + 2\nu \mathbf{D}(\mathbf{u}^f),$$

with p^f denoting the fluid pressure, ν representing the fluid viscosity and where $\mathbf{D}(\mathbf{u}^f) = (\nabla \mathbf{u}^f + (\nabla \mathbf{u}^f)^T)/2$ is the strain tensor. The first equation

in (4.3) is the momentum equation and the second one is the continuity equation. By writing the stress tensor $\boldsymbol{\sigma}^f$ as

$$\boldsymbol{\sigma}^f := \begin{pmatrix} \sigma_{xx} & \sigma_{xy} \\ \sigma_{yx} & \sigma_{yy} \end{pmatrix}, \quad (4.4)$$

where

$$\sigma_{xx} = -p^f + 2\nu \frac{\partial u^f}{\partial x}, \quad \sigma_{xy} = \sigma_{yx} = \nu \left(\frac{\partial u^f}{\partial y} + \frac{\partial v^f}{\partial x} \right), \quad \sigma_{yy} = -p^f + 2\nu \frac{\partial v^f}{\partial y}, \quad (4.5)$$

we can rewrite (4.3) as follows

$$-\nu \left(\frac{\partial^2 u^f}{\partial x^2} + \frac{\partial^2 u^f}{\partial y^2} \right) + \frac{\partial p^f}{\partial x} = f_1^f \text{ in } \Omega^f, \quad (4.6)$$

$$-\nu \left(\frac{\partial^2 v^f}{\partial x^2} + \frac{\partial^2 v^f}{\partial y^2} \right) + \frac{\partial p^f}{\partial y} = f_2^f \text{ in } \Omega^f, \quad (4.7)$$

$$\frac{\partial u^f}{\partial x} + \frac{\partial v^f}{\partial y} = 0 \text{ in } \Omega^f. \quad (4.8)$$

For the free flow subproblem, we split $\partial\Omega^f \setminus \Gamma$ into two disjoint parts Γ_D^f and Γ_N^f , where we impose the following boundary conditions

$$\begin{aligned} \mathbf{u}^f &= \mathbf{g}_D^f & \text{on } \Gamma_D^f, \\ \boldsymbol{\sigma}^f \cdot \mathbf{n}^f &= \mathbf{g}_N^f & \text{on } \Gamma_N^f. \end{aligned} \quad (4.9)$$

4.2.3 Interface conditions

The Darcy and Stokes systems must be coupled across the internal interface Γ by adequate conditions. To describe them, we fix the normal vector to the interface to be $\mathbf{n} = \mathbf{n}^f = -\mathbf{n}^d$ and we denote by $\boldsymbol{\tau}$ (see Figure 4.1) the tangential unit vector at the interface Γ , obtained by rotating the normal vector in the counter-clockwise direction by 90° . Across Γ the continuity of fluxes and normal stresses must be imposed. This gives rise to the following two standard coupling conditions on Γ :

- Mass conservation:

$$\mathbf{u}^f \cdot \mathbf{n} = \mathbf{u}^d \cdot \mathbf{n} \quad \text{on } \Gamma. \quad (4.10)$$

- Balance of normal stresses:

$$-\mathbf{n} \cdot \boldsymbol{\sigma}^f \cdot \mathbf{n} = p^d \quad \text{on } \Gamma. \quad (4.11)$$

As the third coupling condition, the so-called *Beavers-Joseph-Saffman interface condition* is widely used, which is supported by experimental findings and rigorous mathematical theory of homogenization. This condition relates the tangential velocity along the interface with the fluid stresses, that is,

$$\gamma \mathbf{u}^f \cdot \boldsymbol{\tau} + \boldsymbol{\tau} \cdot \boldsymbol{\sigma}^f \cdot \mathbf{n} = 0 \quad \text{on } \Gamma, \quad (4.12)$$

where γ is a parameter which needs to be experimentally determined and depends on the properties of the porous medium.

An alternative to this third interface condition neglects the second term in (4.12), giving rise to a *no-slip interface condition*,

$$\mathbf{u}^f \cdot \boldsymbol{\tau} = 0 \quad \text{on } \Gamma. \quad (4.13)$$

4.3 Discretization

The finite volume method on a staggered grid [77] is considered as the discretization scheme for the Darcy-Stokes problem. By using this discretization we ensure that spurious oscillations do not appear in the numerical solution [49], and we obtain a mass conservative algorithm for the whole system. The computational domain is partitioned into square blocks of size $h \times h$, so that the grid is conforming at the interface Γ . For notational convenience, we choose equal-sized blocks but the description in the more general case would be straightforward. Different control volumes are defined depending on which variable is considered. In Figure 4.2, we represent in different colors the control volumes associated with the equations collocated with the primary variables u , v and p ². The pressure unknowns p are defined at the centers of the blocks (marked by \times -points in Figure 4.2), and the components of the velocity unknowns, u and v , are located at the centers of the block faces (denoted by the \circ - and \bullet -points in the same figure). For the description of the discrete scheme, we need to fix an adequate indexing for the unknowns, which can be seen in Figure 4.3,

²In the following figures, the superscript, either d or f , is omitted, as we have the same arrangement of unknowns for both sub-problems.

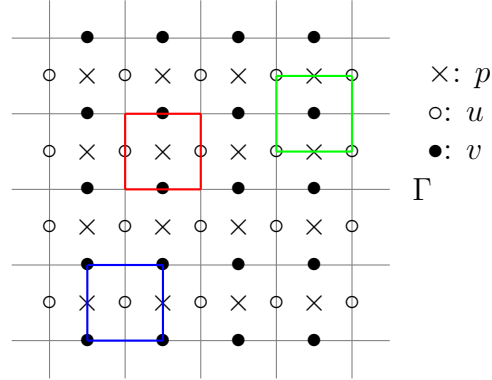


Figure 4.2: Staggered grid location of unknowns for the coupled model, and corresponding control volumes.

where each unknown is depicted together with the corresponding control volume and the different variables around it.

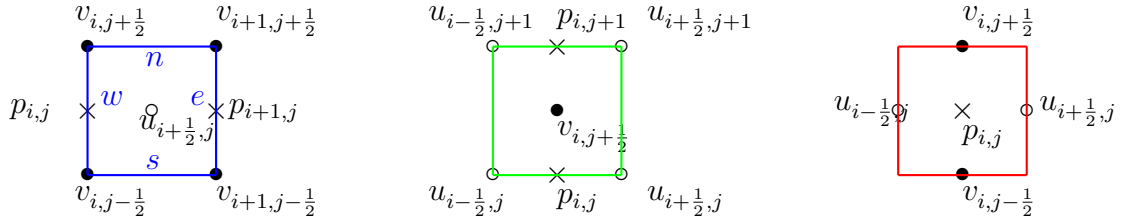


Figure 4.3: Control volumes for the primary unknowns: u (left), v (middle), p (right), together with the corresponding indexing for each variable.

We describe in detail the discretization for the mixed formulation of the Darcy problem in Section 4.3.1, the discrete scheme for the Stokes equations in Section 4.3.2, and the special discretization considered for the internal interface Γ in Section 4.3.3.

4.3.1 Discretization of Darcy equations

Since in the mixed formulation of the Darcy problem the pressure and the velocities are the primary variables, we describe the corresponding discretizations for each equation. Regarding the horizontal velocity unknown, let us consider control volume $V_{i+1/2,j}$ for variable $u_{i+1/2,j}^d$ (Figure 4.3, left side). By discretizing the first equation in (4.1) in such control volume, we

obtain,

$$K^{-1}u_{i+\frac{1}{2},j}^d + \frac{p_{i+1,j}^d - p_{i,j}^d}{h} = 0. \quad (4.14)$$

Similarly, by discretizing the equation for v^d in (4.1) over a control volume $V_{i,j+1/2}$ (Figure 4.3, middle), one obtains the discrete equation for the vertical velocity unknown $v_{i,j+1/2}^d$,

$$K^{-1}v_{i,j+\frac{1}{2}}^d + \frac{p_{i,j+1}^d - p_{i,j}^d}{h} = 0. \quad (4.15)$$

Equations (4.14) and (4.15) are associated with internal velocity unknowns. In the case of variables located at the external boundary where Dirichlet boundary conditions for the pressure are imposed, the corresponding control volumes to consider are half the size of the inner control volumes, and are treated accordingly.

Finally, the discrete equation corresponding to the pressure unknown $p_{i,j}^d$ is obtained by discretizing the second equation in (4.1) over control volume $V_{i,j}$ (Figure 4.3, right side), resulting in

$$\frac{u_{i+\frac{1}{2},j}^d - u_{i-\frac{1}{2},j}^d}{h} + \frac{v_{i,j+\frac{1}{2}}^d - v_{i,j-\frac{1}{2}}^d}{h} = f_{i,j}^d. \quad (4.16)$$

4.3.2 Discretization of Stokes equations

We proceed by briefly presenting the discretization of the Stokes equations. Regarding the mass balance equation, similarly as in the previous section, we discretize the second equation in (4.3) over control volume $V_{i,j}$ to obtain the following discrete equation,

$$\frac{u_{i+\frac{1}{2},j}^f - u_{i-\frac{1}{2},j}^f}{h} + \frac{v_{i,j+\frac{1}{2}}^f - v_{i,j-\frac{1}{2}}^f}{h} = 0. \quad (4.17)$$

Regarding the momentum equation in (4.3), we describe only the first component of the equation since the second one would be deduced in a similar way. Thus, discretizing such component over control volume $V_{i+\frac{1}{2},j}$ yields

$$-\left(\frac{(\sigma_{xx})_e - (\sigma_{xx})_w}{h} + \frac{(\sigma_{xy})_n - (\sigma_{xy})_s}{h} \right) = (f_1^f)_{i+\frac{1}{2},j}, \quad (4.18)$$

where σ_{xx} and σ_{xy} are components of the stress tensor. Approximating these components as

$$\begin{aligned} (\sigma_{xx})_e &= -p_{i+1,j}^f + 2\nu \frac{u_{i+\frac{3}{2},j}^f - u_{i+\frac{1}{2},j}^f}{h}, \\ (\sigma_{xx})_w &= -p_{i,j}^f + 2\nu \frac{u_{i+\frac{1}{2},j}^f - u_{i-\frac{1}{2},j}^f}{h}, \\ (\sigma_{xy})_n &= \nu \left(\frac{u_{i+\frac{1}{2},j+1}^f - u_{i+\frac{1}{2},j}^f}{h} + \frac{v_{i+1,j+\frac{1}{2}}^f - v_{i,j+\frac{1}{2}}^f}{h} \right), \\ (\sigma_{xy})_s &= \nu \left(\frac{u_{i+\frac{1}{2},j}^f - u_{i+\frac{1}{2},j-1}^f}{h} + \frac{v_{i+1,j-\frac{1}{2}}^f - v_{i,j-\frac{1}{2}}^f}{h} \right), \end{aligned}$$

and substituting them in (4.18), we obtain the following equation,

$$\begin{aligned} & -\frac{2\nu}{h^2}(u_{i+\frac{3}{2},j}^f - 2u_{i+\frac{1}{2},j}^f + u_{i-\frac{1}{2},j}^f) - \frac{\nu}{h^2}(u_{i+\frac{1}{2},j+1}^f - 2u_{i+\frac{1}{2},j}^f + u_{i+\frac{1}{2},j-1}^f) \\ & - \frac{\nu}{h^2}(v_{i+1,j+\frac{1}{2}}^f - v_{i,j+\frac{1}{2}}^f - v_{i+1,j-\frac{1}{2}}^f + v_{i,j-\frac{1}{2}}^f) + \frac{1}{h}(p_{i+1,j}^f - p_{i,j}^f) = (f_1^f)_{i+\frac{1}{2},j}. \end{aligned}$$

4.3.3 Discretization at the interface

In this section, we describe how we deal with the interface conditions. Our proposal is to obtain a *special discrete equation* for the unknowns at the internal interface. Due to the staggered arrangement of the unknowns, the only variables at the interface are the vertical components of the velocity, see Figure 4.4. For this purpose, we integrate the momentum equation of the Stokes system over a half volume, as displayed in red color in Figure 4.4, giving rise to the following equation

$$- \left(\frac{(\sigma_{xy})_e - (\sigma_{xy})_w}{h} + \frac{(\sigma_{yy})_n - (\sigma_{yy})_s}{h/2} \right) = (f_2^f)_{i,j+\frac{1}{2}}, \quad (4.19)$$

where, as can be seen in Figure 4.4, e and w denote locations at the interface, whereas n and s denote the locations of $p_{i,j+1}^f$ and $v_{i,j+\frac{1}{2}}^{d/f}$, respectively. The approximation of $(\sigma_{yy})_n$ is easily obtained as

$$(\sigma_{yy})_n = -p_{i,j+1}^f + \frac{2\nu}{h}(v_{i,j+\frac{3}{2}}^f - v_{i,j+\frac{1}{2}}^f), \quad (4.20)$$

Here, u_e^f can be obtained from (4.24) and substituted into the standard approximation of the stress $(\sigma_{xy})_e$, resulting in

$$\begin{aligned} (\sigma_{xy})_e &= \nu \left(\frac{u_{i+\frac{1}{2},j+1}^f - u_e^f}{h/2} + \frac{v_{i+1,j+\frac{1}{2}}^f - v_{i,j+\frac{1}{2}}^f}{h} \right) \\ &= \frac{2\nu\varsigma}{h} u_{i+\frac{1}{2},j+1}^f + \nu\varsigma \frac{v_{i+1,j+\frac{1}{2}}^f - v_{i,j+\frac{1}{2}}^f}{h}, \end{aligned} \quad (4.25)$$

where $\varsigma = \left(1 - \frac{2\nu}{h\gamma+2\nu}\right)$. The approximation of $(\sigma_{xy})_w$ can be calculated in a similar way. The discrete equation for the vertical velocities for the Stokes problem at the interface is thus obtained by substituting (4.20), (4.23) and (4.25) into equation (4.19), giving

$$\begin{aligned} & -\frac{2\nu\varsigma}{h^2} (u_{i+\frac{1}{2},j+1}^f - u_{i-\frac{1}{2},j+1}^f) - \frac{\nu\varsigma}{h^2} (v_{i+1,j+\frac{1}{2}}^f - 2v_{i,j+\frac{1}{2}}^f + v_{i-1,j+\frac{1}{2}}^f) \\ & + \frac{2}{h} (p_{i,j+1}^f - p_{i,j}^d) - \frac{4\nu}{h^2} (v_{i,j+\frac{3}{2}}^f - v_{i,j+\frac{1}{2}}^f) + \frac{1}{K} v_{i,j+\frac{1}{2}}^f = (f_2^f)_{i,j+\frac{1}{2}}, \end{aligned} \quad (4.26)$$

where we have used the interface condition $v_{i,j+\frac{1}{2}}^d = v_{i,j+\frac{1}{2}}^f$.

The discretization at the interface is of great importance and can be viewed as a relevant ingredient towards the construction of a highly efficient multigrid method. Since the coupled system is treated as a single problem, the equations of fluid dynamics, solid mechanics and their complex interaction are all included in one discrete formulation. By such a discretization, the fully coupled system possesses a saddle point structure which is suitable for monolithic multigrid.

4.4 Numerical method

This section is devoted to the design of a *monolithic geometric multigrid* for the Darcy-Stokes problem. For this purpose, we will first study the application of multigrid methods based on Uzawa smoothers to the Darcy and Stokes problems separately. In this analysis we will take into account the LFA technique to obtain suitable parameters for these methods. These algorithms will form the basis to construct a monolithic multigrid for the coupled problem. This will be possible since the individual Stokes and

Darcy systems, as well as the fully coupled problem, lead to saddle point linear systems of the form

$$\begin{pmatrix} A & B^T \\ B & 0 \end{pmatrix} \begin{pmatrix} \mathbf{u} \\ p \end{pmatrix} = \begin{pmatrix} \mathbf{g} \\ f \end{pmatrix}, \quad (4.27)$$

by choosing an adequate arrangement of the unknowns. For both problems B^T and B represent the discrete gradient and the minus discrete divergence operators, respectively, and A is the discrete representation of either the Laplace-type operator $-\nu\Delta$ for the Stokes equations, or $K^{-1}I$ for the Darcy equation. For the coupled problem, rearranging the vector of unknowns to order first the velocities for both problems and thereafter the pressure unknowns, we obtain the following linear system,

$$\begin{pmatrix} A^d & 0 & (B^d)^T & 0 \\ 0 & A^f & R & (B^f)^T \\ B^d & R & 0 & 0 \\ 0 & B^f & 0 & 0 \end{pmatrix} \begin{pmatrix} \mathbf{u}^d \\ \mathbf{u}^f \\ p^d \\ p^f \end{pmatrix} = \begin{pmatrix} \mathbf{0} \\ \mathbf{f}^f \\ f^d \\ 0 \end{pmatrix}, \quad (4.28)$$

where the system matrix in (4.28) has the same saddle point structure as in (4.27), by denoting

$$A = \begin{pmatrix} A^d & 0 \\ 0 & A^f \end{pmatrix}, \quad B = \begin{pmatrix} B^d & R \\ 0 & B^f \end{pmatrix}, \quad B^T = \begin{pmatrix} (B^d)^T & 0 \\ R & (B^f)^T \end{pmatrix}.$$

Here, R is a diagonal matrix containing the relations given by formula (4.26) between the vertical velocities v^f and the corresponding pressure unknowns in the Darcy domain p^d . So, most of its elements are zero, and the only nonzero diagonal terms are those corresponding to the Darcy pressure unknowns close to the internal interface, appearing in the equations of the vertical velocities on Γ . Due to this structure of the coupled problem, a geometric multigrid method together with an Uzawa smoother, as will be introduced in Section 4.4.1, can be applied for the whole system. As we will see, the choice of adequate relaxation parameters for the Uzawa smoother on each subproblem will be crucial for excellent multigrid convergence.

4.4.1 Multigrid based on Uzawa smoother

In order to develop an efficient multigrid solver, it is necessary to carefully define each component of multigrid, such as the smoothing operator and

the coarse-grid correction components (i.e., the restriction and prolongation operators, and the coarse grid operator). Regarding the coarse grid correction, geometric grid coarsening is chosen, as we will deal with regular Cartesian grids. The sequence of coarse grids is obtained by doubling the mesh size in each spatial direction. We further use well-known, proven, components for the transfer operators between the fine and coarse grids, that are dictated by the staggered grid arrangement, and focus our efforts on the analysis of the smoothing operator. In particular, the interplay between the relaxation method (the smoother) and the coarse grid correction is crucial for the multigrid performance.

Taking the staggered arrangement of the unknowns into account, the inter-grid transfer operators that act on the different unknowns are defined as follows: at velocity grid points six-point restrictions are considered, and at pressure grid points a four-point restriction is applied. In stencil notation, the restriction operators are given by

$$R_{h,2h}^u = \frac{1}{8} \begin{pmatrix} 1 & 2 & 1 \\ & * & \\ 1 & 2 & 1 \end{pmatrix}_h, \quad R_{h,2h}^v = \frac{1}{8} \begin{pmatrix} 1 & & 1 \\ 2 & * & 2 \\ 1 & & 1 \end{pmatrix}_h, \quad R_{h,2h}^p = \frac{1}{4} \begin{pmatrix} 1 & & 1 \\ & * & \\ 1 & & 1 \end{pmatrix}_h,$$

respectively. As the prolongation operators $P_{2h,h}^{u/v/p}$, we choose the adjoints of the restrictions.

The choice of smoother requires special attention due to the saddle point structure of the considered system. An Uzawa smoother, which was proposed for the Stokes problem in [41] and in Chapter 3 for poroelasticity, is considered for the coupled system.

Uzawa smoother We give a general description of the considered Uzawa smoother. We will see that this relaxation can be successfully applied in multigrid for both Stokes and Darcy systems, and also in the multigrid method for the coupled system. As presented in Chapter 3, the Uzawa smoother is obtained by splitting the discrete operator as follows

$$\begin{pmatrix} A & B^T \\ B & 0 \end{pmatrix} = \begin{pmatrix} M_A & 0 \\ B & -\omega^{-1} I \end{pmatrix} - \begin{pmatrix} M_A - A & -B^T \\ 0 & -\omega^{-1} I \end{pmatrix}, \quad (4.29)$$

where M_A is a typical smoother for A and ω is some positive parameter. M_A makes the approach less costly because of the inexact solve for velocities at each iteration.

From a given approximation of the solution to the system $(\mathbf{u}, p)^T$, the relaxed approximation $(\hat{\mathbf{u}}, \hat{p})^T$ is computed according to the decoupled Uzawa smoother in the following way

$$\begin{pmatrix} M_A & 0 \\ B & -\omega^{-1} I \end{pmatrix} \begin{pmatrix} \hat{\mathbf{u}} \\ \hat{p} \end{pmatrix} = \begin{pmatrix} M_A - A & -B^T \\ 0 & -\omega^{-1} I \end{pmatrix} \begin{pmatrix} \mathbf{u} \\ p \end{pmatrix} + \begin{pmatrix} \mathbf{g} \\ f \end{pmatrix}. \quad (4.30)$$

More concretely, a single step of the relaxation process is described as follows

- Relax the velocities by applying M_A : $\hat{\mathbf{u}} = \mathbf{u} + M_A^{-1} (\mathbf{g} - A\mathbf{u} - B^T p)$;
- Update the pressure: $\hat{p} = p + \omega(B\hat{\mathbf{u}} - f)$.

In general, the Uzawa method is equivalent to a stationary Richardson iteration applied to the Schur complement system. This relation allows to deduce an expression for parameter ω which minimizes the spectral radius of the corresponding iteration matrix, i.e.,

$$\omega = \frac{2}{\lambda_{\max} + \lambda_{\min}},$$

where λ_{\max} and λ_{\min} denote the largest and smallest eigenvalues of the Schur complement, respectively (see [7]). In the local Fourier analysis section we will estimate optimal relaxation parameter ω in the Uzawa smoother for the Darcy and Stokes problems, and we will also obtain a similar expression in which λ_{\max} and λ_{\min} are substituted by the largest and smallest eigenvalues but only on the high frequencies for smoothing analysis purposes.

M_A is based on the *symmetric Gauss-Seidel iterations* for A ; i.e.,

$$M_A = (D_A + L_A) D_A^{-1} (D_A + U_A), \quad (4.31)$$

where D_A , L_A and U_A are, respectively, the diagonal, the strictly lower, and the strictly upper parts of A . Numerical experiments in [41] revealed that, for essentially the same cost, the convergence associated with M_A in (4.31) is most efficient. So, this variant is the one that we extend to

the Darcy equation. The efficiency of the proposed Uzawa smoother for three-dimensional Stokes and Biot's poroelasticity equations was presented in [41] and [64], respectively.

We wish to mention the importance of the choice of an adequate value for the relaxation parameter ω to obtain a satisfactory performance of the Uzawa smoother. As in [41] for the Stokes equations, analytic expressions for ω can also be obtained by means of a theoretical analysis for the Darcy problem. We present this analysis first in a general way to make this work self-contained and later we will describe the particular case of the Darcy equations.

4.4.2 Local Fourier analysis

We briefly introduce the local Fourier analysis for staggered grids, before we focus on the analysis of the Uzawa smoother.

Basis of LFA To perform LFA, all discrete operators are assumed to be defined on an infinite grid G_h , and boundary conditions are neglected. Due to the arrangement of unknowns on a staggered grid, G_h is divided into three subsets $G_h^{\tilde{k}}$ defined as

$$G_h^{\tilde{k}} = \{\mathbf{x}_{(i,j)}^{\tilde{k}} = (i,j)h + \boldsymbol{\delta}^{\tilde{k}}h \mid i,j \in \mathbb{Z}\}, \text{ with } \boldsymbol{\delta}^{\tilde{k}} = \begin{cases} (1/2, 0), & \text{if } \tilde{k} = 1, \\ (0, 1/2), & \text{if } \tilde{k} = 2, \\ (0, 0), & \text{if } \tilde{k} = 3, \end{cases} \quad (4.32)$$

such that $G_h = G_h^1 \cup G_h^2 \cup G_h^3$. Corresponding to Figure 4.2, the velocities $u^{d/f}$ and $v^{d/f}$ are situated at nodes $\mathbf{x}_{i,j}^1$ and $\mathbf{x}_{i,j}^2$, respectively, whereas $\mathbf{x}_{i,j}^3$ is for the pressure unknowns $p^{d/f}$. The basic idea of LFA is that all occurring multigrid components, the discrete approximation and its corresponding error or residual can be represented by formal linear combinations of Fourier modes. In the case of a staggered grid, considering $\boldsymbol{\varphi}_h^1(\boldsymbol{\theta}, \mathbf{x}_{i,j}) = (e^{i\boldsymbol{\theta} \cdot \mathbf{x}_{i,j}^1/h}, 0, 0)^T$, $\boldsymbol{\varphi}_h^2(\boldsymbol{\theta}, \mathbf{x}_{i,j}) = (0, e^{i\boldsymbol{\theta} \cdot \mathbf{x}_{i,j}^2/h}, 0)^T$, and $\boldsymbol{\varphi}_h^3(\boldsymbol{\theta}, \mathbf{x}_{i,j}) = (0, 0, e^{i\boldsymbol{\theta} \cdot \mathbf{x}_{i,j}^3/h})^T$, the Fourier modes are defined as

$$\boldsymbol{\varphi}_h(\boldsymbol{\theta}, \mathbf{x}_{i,j}) := [\boldsymbol{\varphi}_h^1(\boldsymbol{\theta}, \mathbf{x}_{i,j}) \quad \boldsymbol{\varphi}_h^2(\boldsymbol{\theta}, \mathbf{x}_{i,j}) \quad \boldsymbol{\varphi}_h^3(\boldsymbol{\theta}, \mathbf{x}_{i,j})], \quad (4.33)$$

where $\mathbf{x}_{i,j} = (\mathbf{x}_{i,j}^1, \mathbf{x}_{i,j}^2, \mathbf{x}_{i,j}^3)$ and $\boldsymbol{\theta} \in \boldsymbol{\Theta} := (-\pi, \pi]^2$, which form a unitary basis of the space of infinite grid functions. The Fourier space generated by Fourier modes is given by $\mathcal{F}(G_h) := \text{span}\{\boldsymbol{\varphi}_h(\boldsymbol{\theta}, \cdot) | \boldsymbol{\theta} \in \boldsymbol{\Theta}\}$.

The analysis is similar as in Section 3.4.1. The smoothing factor μ is defined as:

$$\mu := \sup_{\boldsymbol{\theta} \in \boldsymbol{\Theta}_{high}^{2h}} \rho(S_h(\boldsymbol{\theta})), \quad (4.34)$$

where high frequency component $\boldsymbol{\Theta}_{high}^{2h}$ is defined in (3.17), and $S_h(\boldsymbol{\theta})$ represents the Fourier symbol of the relaxation operator. In our case, the Uzawa smoothing iteration can be written as $S_h = I_h - M_h^{-1}L_h$, where L_h is the discrete operator given by the system matrix in (4.27) and M_h represents the iteration matrix in (4.30).

We can analyze the behavior of multigrid by investigating the effect of the multigrid components acting on the Fourier space. The iteration operator of the two-grid method is similar as (3.21), thus the LFA two-grid convergence factor can be obtained as (3.22).

LFA for the Uzawa smoother A detailed study of the Uzawa smoother in the framework of LFA was already done in [41]. In that work, it was proved that

$$\mu \leq \bar{\mu} = \max\left((\mu_A)^{1/2}, \mu_S\right), \quad (4.35)$$

where μ_A is the smoothing factor of M_A and μ_S can be interpreted as the smoothing factor of the Richardson iteration for the Schur complement,

$$\mu_S := \sup_{\boldsymbol{\Theta}_{high}^{2h}} \rho\left(I - \omega(BA^{-1}B^T)\right). \quad (4.36)$$

There are no particular difficulties to obtain bounds for μ_A , since LFA results for many scalar elliptic PDEs are available in the literature, see for example [100]. However, to estimate μ_S is somewhat involved since information about the eigenvalues of the Schur complement is needed. In particular, the bound of μ_S is determined by the maximum and minimum

eigenvalues *on the high frequencies*, that is,

$$\max_{\boldsymbol{\theta} \in \Theta_{high}^{2h}} \left(\widetilde{B}(\boldsymbol{\theta}) \widetilde{A^{-1}}(\boldsymbol{\theta}) \widetilde{B^T}(\boldsymbol{\theta}) \right) \leq \beta_{\max}, \quad (4.37)$$

$$\min_{\boldsymbol{\theta} \in \Theta_{high}^{2h}} \left(\widetilde{B}(\boldsymbol{\theta}) \widetilde{A^{-1}}(\boldsymbol{\theta}) \widetilde{B^T}(\boldsymbol{\theta}) \right) \geq \beta_{\min}, \quad (4.38)$$

with $\widetilde{B}(\boldsymbol{\theta})$, $\widetilde{A^{-1}}(\boldsymbol{\theta})$ and $\widetilde{B^T}(\boldsymbol{\theta})$ the symbols or Fourier representations of operators B , A^{-1} and B^T for a fixed frequency $\boldsymbol{\theta}$. Let ζ be a positive real number such that $\zeta < 2$. By defining $\kappa_\beta = \frac{\beta_{\max}}{\beta_{\min}}$, the following bound for μ_S is obtained (see [41] for more details),

$$\mu_S \leq \max \left(\zeta - 1, 1 - \frac{\zeta}{\kappa_\beta} \right). \quad (4.39)$$

Note that the choice of $\zeta < 2$ is to ensure that $\mu_S < 1$. Then, by choosing a value of ζ to minimize the expression in (4.39), we obtain an optimal relaxation parameter for the Uzawa smoother as follows

$$\omega = \frac{2}{\beta_{\max} + \beta_{\min}}. \quad (4.40)$$

Next, we apply this analysis to obtain approximations of the smoothing factor of the Uzawa smoother for our problem, as well as optimal relaxation parameters for the Richardson iteration involved in the relaxation process.

In [41], the following bound for the smoothing factor of the Uzawa smoother was obtained in the case of *Stokes equations*, $\bar{\mu} = \max(0.5, \zeta - 1)$, by choosing the optimal relaxation parameter $\omega = \zeta\nu$. Notice that $\mu_A = 0.25$ for the symmetric Gauss-Seidel for the Laplace operator, and therefore $(\mu_A)^{1/2} = 0.5$. These results can be directly used for our free flow problem.

Uzawa smoother analysis for Darcy equation We work out the analysis for Darcy's equation in order to obtain a suitable parameter ω for the part corresponding to the Richardson iteration for the pressure, as well as an approximation for the smoothing factor of the Uzawa smoother.

Following the general analysis in the previous section to obtain β_{\max} and β_{\min} in (4.37)-(4.38), we will make use of the following equality

$$\widetilde{B}(\boldsymbol{\theta}) \widetilde{A^{-1}}(\boldsymbol{\theta}) \widetilde{B^T}(\boldsymbol{\theta}) = K \widetilde{B}(\boldsymbol{\theta}) \widetilde{B^T}(\boldsymbol{\theta}) = -K \widetilde{\Delta}(\boldsymbol{\theta}). \quad (4.41)$$

From this result, it is straightforward to obtain $\beta_{max} = \frac{8K}{h^2}$ and $\beta_{min} = \frac{2K}{h^2}$, which implies

$$\kappa_\beta = \frac{\beta_{max}}{\beta_{min}} = 4 . \quad (4.42)$$

Choosing $\zeta = 1.6$, which gives the lowest value of the maximum in (4.39), the smoothing factor is bounded by 0.6, independently of the value of K . This theoretical bound for the smoothing factor $\bar{\mu}$ matches perfectly with the value μ predicted by the local Fourier analysis. Moreover, following (4.40) the relaxation parameter is given by the expression $\omega = \frac{h^2}{5K}$. Parameter ω depends on the grid size, and therefore it will be different on each grid of the hierarchy used in the multigrid method.

4.4.3 Multigrid for the coupled Darcy-Stokes problem

Due to the saddle point structure of the coupled problem, a geometric multigrid method together with an Uzawa smoother, as introduced in Section 4.4.1, can be applied for the whole system. For this purpose, it is important to note that to keep the structure of the matrix of the saddle point system on the whole grid hierarchy, interface Γ has to be present on each grid level. Regarding the smoothing process, all velocity unknowns are relaxed before the pressure unknowns will be updated. The relaxation parameter ω for the Richardson iteration for the Schur complement has to be chosen differently if we are updating pressure unknowns from the Darcy or the Stokes problems. For the other components, the same operators can be used at every grid point since the discretization for both problems is performed with the same staggered arrangement of unknowns.

In the monolithic multigrid method we do not distinguish the subproblems and the internal interface. All the unknowns play essentially the same role. Only the relaxation parameter of the smoother is different for each subproblem. For the discretization at the interface, the unknowns for both subproblems are included in one equation. We keep the same philosophy for the other components in the monolithic multigrid. For example, to restrict the unknowns at the interface, six points from both subgrids around it are employed. A suitable discretization for the unknowns at the interface of the coupled system is a key step in achieving robustness and efficiency of our approach.

The proposed multigrid method for the coupled Darcy-Stokes problem can also be implemented as a *multiblock* version in which the Darcy and Stokes domains are assumed to be two different blocks. This is appealing from a practical point of view, for example when one has to solve the coupled problem by using two different codes. Moreover, this multiblock approach is easily parallelizable. Next, we describe in detail how this implementation can be done.

Multiblock multigrid algorithm We divide our domain into two different blocks corresponding to the Darcy and Stokes domains. In this way, the original staggered grid is split into two different subgrids. Starting with an approximation on the partitioned grid, it is trivial to compute a new iterate for the interior points of each subgrid. Near the boundary of each subgrid, the old approximations at those points belonging to the neighboring subgrid are needed. It is standard within a grid-partitioning framework [94] for a subgrid to not only store its own data but also a copy of the data located in a strip of the neighboring subgrid in an overlap region. Thus, the mesh corresponding to the Stokes domain is extended by adding an overlap region of *one cell length*, as can be seen in Figure 4.5. After a full iteration, on each grid level, the copies in the overlap region have to be updated by communication so that a next iteration can be carried out.

Next, we explain in detail the two-grid version of the multiblock algorithm. For simplicity in the presentation of the algorithm, we use pre-smoothing but no post-smoothing. By recursion, the multigrid version follows straightforwardly.

Multiblock two-grid algorithm: (with pre-smoothing but no post-smoothing)

1. Relax velocity unknowns for both blocks.
2. *Stokes to Darcy transfer*: vertical Stokes velocity unknowns at the interface are transferred to the Darcy block (see the red dots in Figure 4.5).
3. Update pressure unknowns by the Richardson iteration with the optimal relaxation parameters corresponding to each block.

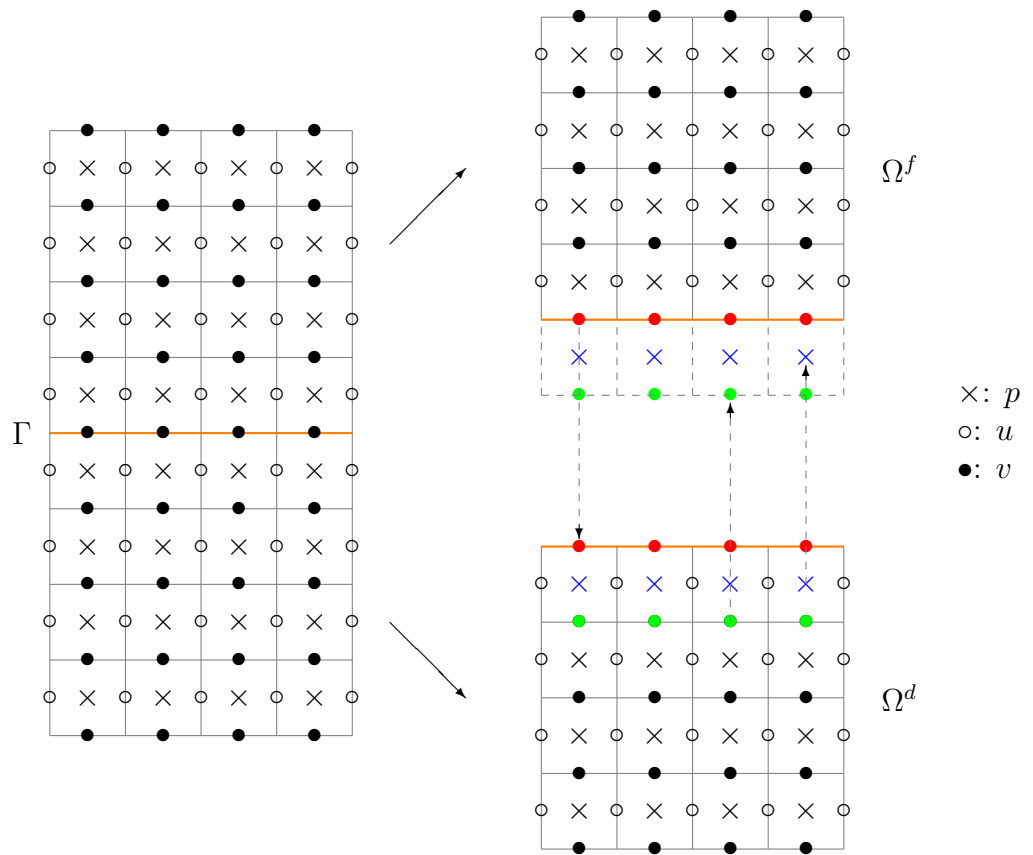


Figure 4.5: Communications between two partitioned subgrids.

4. *Darcy to Stokes transfer*: Darcy pressure unknowns are transferred to the Stokes overlap region (see the blue crosses in Figure 4.5).
5. Compute the residual.
6. *Darcy to Stokes transfer*: the residual of the vertical Darcy velocity unknowns is transferred to the Stokes overlap region (see the green dots in Figure 4.5).
7. Restrict the residual.
8. Solve exactly the defect equation on the coarsest grid.
9. *Stokes to Darcy transfer*: vertical Stokes velocity unknowns at the interface are transferred to the Darcy block.
10. Interpolate the error and correct the approximation to the solution.

This multiblock algorithm requires only little data communication. In particular, each communication step involves transfer of information in only one way. Moreover, each stage in the algorithm can be performed in parallel since the data required for each operation is available in the same process. Finally, although this multiblock approach can be cast into the class of domain decomposition (DD) methods, we wish to emphasize that in our case the communication between both Darcy and Stokes problems is performed *on each level in the hierarchy* instead of only on the finest grid as usual in the DD methods. This is crucial to achieve a highly efficient solver for this coupled problem, as we will see in the numerical experiments section.

Local Fourier analysis results In this section, we confirm that the asymptotic convergence factor of the monolithic multigrid based on the Uzawa smoother for the coupled problem can be estimated with a high accuracy by means of the worst of the two-grid convergence factors predicted by LFA for the individual Darcy and Stokes subproblems. In Table 4.1, we display the two-grid convergence factors predicted by the LFA for the Darcy problem varying the hydraulic conductivity K , and for the Stokes equations for different values of the viscosity ν . These results are obtained for different

$\nu_1 + \nu_2$	Darcy			Stokes		
	$K = 1$	$K = 10^{-3}$	$K = 10^{-6}$	$\nu = 1$	$\nu = 10^{-3}$	$\nu = 10^{-6}$
2	0.600	0.600	0.600	0.304	0.304	0.304
3	0.360	0.360	0.360	0.143	0.143	0.143
4	0.216	0.216	0.216	0.081	0.081	0.081

Table 4.1: Two-grid convergence factors, ρ , predicted by LFA for the Darcy and Stokes subproblems, separately, for different values of the parameters K and ν and different numbers of smoothing steps, $\nu_1 + \nu_2$.

	K	1			10^{-3}			10^{-6}		
	ν	1	10^{-3}	10^{-6}	1	10^{-3}	10^{-6}	1	10^{-3}	10^{-6}
$\nu_1 + \nu_2$	2	0.59	0.59	0.59	0.59	0.59	0.59	0.59	0.59	0.59
	3	0.36	0.36	0.36	0.36	0.36	0.36	0.36	0.36	0.36
	4	0.21	0.21	0.21	0.21	0.21	0.21	0.21	0.21	0.21

Table 4.2: Asymptotic convergence factors, ρ_h , for the multigrid W -cycle based on the Uzawa smoother for the coupled Darcy-Stokes problem, for different values of the physical parameters K and ν and different numbers of smoothing steps $\nu_1 + \nu_2$.

numbers of smoothing steps, $\nu_1 + \nu_2$. From this table, we can observe the robustness of the multigrid method based on the Uzawa smoother for each subproblem, separately.

In Table 4.2, we show the asymptotic convergence factors experimentally obtained by using the monolithic multigrid W -cycle based on Uzawa smoother for the Darcy-Stokes coupled problem. These values have been computed on a fine-grid of size $h = 1/128$, and by using a random initial guess and zero right-hand side in order to avoid round-off errors. We display the convergence factors obtained after 100 multigrid cycles, since in each test case the numerical convergence has stabilized. Comparing Tables 4.1 and 4.2, we observe that these factors match perfectly with the worst of the two-grid convergence factors predicted by LFA for both separate subproblems. This means that the treatment of the discretization at the interface as well as the implementation of the Uzawa smoother for the whole coupled problem have been performed in the most efficient way.

Discussion and comparison with other methods In this section we discuss alternative solution methods to the proposed monolithic multigrid approach.

In the discussion we include, on the one hand, monolithic multigrid methods with different smoothers, and, on the other hand, domain decomposition techniques and preconditioning strategies.

In a monolithic multigrid method we aim to solve the multi-physics system all-at-once. The choice of the smoother is important for the performance of the multigrid method. The proposed smoother in our work is based on Uzawa relaxation, but different relaxation schemes can be considered. The Braess-Sarazin method [1, 10] is an example of another relaxation method. More concretely, the Braess-Sarazin is based on the matrix system

$$\begin{pmatrix} N_A & B^T \\ B & 0 \end{pmatrix}$$

as the smoothing iteration matrix for saddle point system (4.27), where N_A is usually of the form $N_A := \chi \text{diag}(A)$ or $N_A := \chi I$, with $\chi \in \mathbb{R}$ a parameter which is not smaller than the maximum eigenvalue of A . For the solution of the pressure it is then necessary to solve a system whose matrix involves the Schur complement $BN_A^{-1}B^T$. However, in practice, an inexact solve is sufficient. In that case, an inexact Braess-Sarazin smoother is comparable to the Uzawa iteration and seems an appealing alternative to the Uzawa smoother. Next to the Braess-Sarazin smoother, the well-known coupled Vanka smoother [95] is based on solving several small-sized and local saddle point problems in a block Gauss-Seidel fashion. Originally proposed for the incompressible Navier-Stokes equations, this approach can be easily extended to solving the Darcy-Stokes system. The interface conditions, discretized on a staggered grid, can be naturally incorporated within the coupled Vanka smoothing approach. In particular, in the staggered case that we consider, five unknowns (pressure $p_{i,j}$ and velocities $u_{i-\frac{1}{2},j}$, $u_{i+\frac{1}{2},j}$, $v_{i,j-\frac{1}{2}}$ and $v_{i,j+\frac{1}{2}}$) that are simultaneously updated (see Figure 4.3), which results in solving 5×5 -systems for each cell in the grid. A coupled smoother is often somewhat more expensive than an equation-wise smoother. We will compare the Uzawa smoother with the Vanka smoother, in terms of computational efficiency, in the numerical section. Note, however, that the performance of a point-wise coupled smoother is not satisfactory when stretched grids or anisotropic problem parameters are encountered (see [39] for example), and their extension to line-wise Vanka relaxation gives rise to a significant increase in computational cost, since several lines of unknowns have to be updated simultaneously.

As mentioned in the introduction, other approaches for solving coupled problems are based on domain decomposition methods, splitting the multiphysics system into separate subproblems that are treated mainly independently, as specific preconditioning techniques for the global saddle point problem. In this context, preconditioned GMRES methods with block or constraint preconditioners [18, 23, 24] usually show a mesh-independent convergence rate, yielding an effective approach for solving Darcy-Stokes problem. However, in the literature it can be observed that these methods can exhibit some parameter specific convergence, depending on the values of the physical parameters (see [19] for example). Our monolithic method provides convergence characteristics independent of parameters K and ν . Even for very small parameter values, when the subproblems are strongly coupled, the multigrid convergence is excellent. One of the advantages of the considered monolithic multigrid method is thus the robustness with respect to the values of the physical parameters.

Remark 4.1. *As is commonly done, we mainly focus on the case of constant hydraulic conductivity K . The proposed multigrid solution method can however be generalized to varying K -values and also to the case where the hydraulic conductivity is prescribed by a full tensor \mathbb{K} . In [64], see also Chapter 3, we applied a variant of the Uzawa smoother for porous media flow when anisotropies due to grid stretching appeared. Also heterogeneous coefficients were considered in that chapter. Grid anisotropies basically have the same impact as anisotropic conductivity. Therefore, the proposed algorithm can be adapted to such setting. When a full SPD (symmetric positive definite) tensor \mathbb{K} is encountered, the same solution strategy may be applied since \mathbb{K} can be diagonalized. For the case of a heterogeneous porous medium, some multigrid results are presented in Section 4.5.4.*

4.5 Numerical experiments

We present three numerical tests in order to study the accuracy of the discrete scheme and the convergence and robustness of the proposed multigrid method based on the Uzawa smoother with respect to different values of the kinematic viscosity ν and the hydraulic conductivity K . For the implementation, we will consider the optimal relaxation parameters for the Richardson iteration defined in Section 4.4, with values of $\zeta = 1$ for Stokes

and $\zeta = 1.6$ for the Darcy problem. For Stokes it follows that $\omega = \nu$, that is, the relaxation parameter is fixed on all grids and equal to the viscosity of the fluid. This is due to the fact that the Schur complement is spectrally equivalent to the identity matrix for the considered discretization, and therefore the eigenvalues are bounded from below and above by positive constants which do not depend on the mesh size. We have $\omega = \frac{h^2}{5K}$ in the Darcy domain, so ω depends on K which is the hydraulic conductivity of the porous media and on the size of the grid (different on each mesh in the hierarchy).

In all numerical experiments, the initial solution is chosen to be random, and the stopping criterion is

$$\frac{\|\text{residual}\|_\infty}{\|\text{right-hand side}\|_\infty} \leq \text{tolerance} \cdot \frac{\|\text{initial residual}\|_\infty}{\|\text{right-hand side}\|_\infty}, \quad (4.43)$$

where the tolerance is chosen as 10^{-10} . Moreover, for simplicity we consider uniform meshes with grid-size h in both directions on each subdomain.

4.5.1 No-slip interface condition

In this first numerical experiment we deal with a coupled Darcy-Stokes problem with a known analytic solution on the domain $\Omega = (0, 1) \times (0, 2)$, which is a benchmark test widely used to assess the behavior of different numerical algorithms, see [19, 32, 33] for example. The domain Ω is divided into two subdomains by the interface $\Gamma = (0, 1) \times \{1\}$. The Stokes region is the upper part $\Omega^f = (0, 1) \times (1, 2)$ whereas the Darcy region is the bottom part $\Omega^d = (0, 1) \times (0, 1)$. We choose the right-hand side terms and the boundary conditions so that the exact solution is given by

$$\begin{aligned} \mathbf{u}^f(x, y) &= \begin{pmatrix} u^f(x, y) \\ v^f(x, y) \end{pmatrix} = \begin{pmatrix} y^2 - 2y + 1 \\ x^2 - x \end{pmatrix}, \\ p^f(x, y) &= 2\nu(x + y - 1) + \frac{1}{3K}, \\ \mathbf{u}^d(x, y) &= \begin{pmatrix} u^d(x, y) \\ v^d(x, y) \end{pmatrix} = \begin{pmatrix} (2x - 1)(y - 1) - 2K\nu \\ (x^2 - x) - y^2 + 2y - 1 \end{pmatrix}, \\ p^d(x, y) &= \frac{1}{K}((x - x^2)(y - 1) + \frac{y^3}{3} - y^2 + y) + 2\nu x. \end{aligned} \quad (4.44)$$

Dirichlet boundary conditions for velocity are prescribed at $\partial\Omega^f \setminus \Gamma$ and at the bottom boundary $(0, 1) \times \{0\}$. Neumann boundary conditions for pressure are imposed at the remaining parts, i.e., the lateral boundaries of the porous medium. Moreover, a simplified no-slip interface condition (4.13), together with (4.10) and (4.11) are considered here at the internal interface.

First of all, we compare the numerical solution with the given exact solution for fixed values of viscosity $\nu = 1$ and hydraulic conductivity $K = 1$. For different grid-sizes, in Table 4.3 we display the maximum norm of the error for each variable. As expected, second-order accuracy is obtained for

	32×64	64×128	128×256	256×512
u^d	2.03×10^{-4}	5.38×10^{-5}	1.39×10^{-5}	3.51×10^{-6}
v^d	3.11×10^{-4}	8.81×10^{-5}	2.34×10^{-5}	6.02×10^{-6}
p^d	2.43×10^{-4}	6.09×10^{-5}	1.52×10^{-5}	3.81×10^{-6}
u^f	2.29×10^{-4}	5.91×10^{-5}	1.50×10^{-5}	3.78×10^{-6}
v^f	3.11×10^{-4}	8.81×10^{-5}	2.34×10^{-5}	6.02×10^{-6}
p^f	3.61×10^{-2}	1.81×10^{-2}	9.07×10^{-3}	4.54×10^{-3}

Table 4.3: Maximum norm errors of variables $u^{d/f}$, $v^{d/f}$, $p^{d/f}$ for different grid-sizes, by considering fixed values $\nu = 1$ and $K = 1$.

Darcy problem, whereas for the Stokes problem, we achieve second-order accuracy for velocities and first-order for the pressure field. The maximum errors for vertical velocities are the same in both subdomains due to the fact that the maximum is achieved at the internal interface Γ .

Now we focus on the study of the behavior of the proposed multigrid method for the Darcy-Stokes problem. First, a multigrid W -cycle with two pre- and two post-smoothing steps is applied in order to see the h -independent convergence of the algorithm for fixed values $\nu = K = 1$. In Figure 4.6 we show the history of the convergence for different grid-sizes $h = 1/2^{k_l}$ for $k_l = 5, 6, 7, 8$. The maximum norm of the residuals divided by the maximum norm of the right-hand sides is plotted in logarithmic scale against the number of multigrid cycles necessary to fulfill the stopping criterion. It can be seen that the convergence rate is independent of the space discretization parameter, and that the proposed multigrid method

performs well for the coupled problem, since only 15 iterations are needed to achieve the desired convergence.

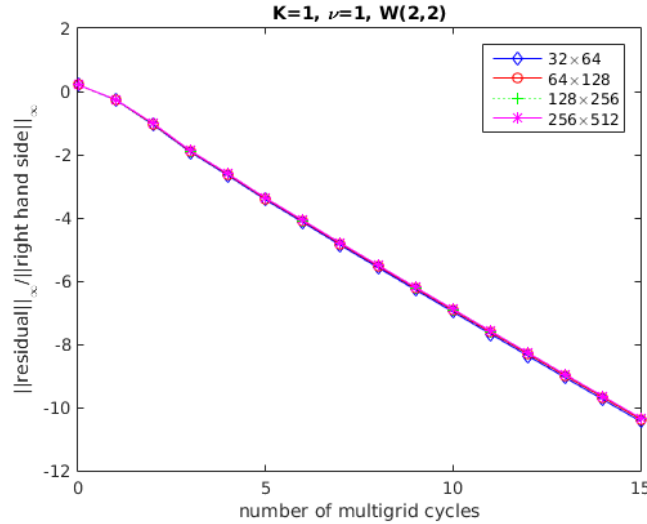


Figure 4.6: History of the convergence of the $W(2, 2)$ -multigrid method for different grids.

Next, we investigate the robustness of the multigrid algorithm with respect to a wide range of values of the physical parameters ν and K . This is important since the values of the parameters that are relevant for geoscientific applications are typically very small. For example, $K = 10^{-2}$ is the hydraulic conductivity for sand and $K = 10^{-5}$ for limestone, and $\nu = 10^{-6}$ is the viscosity of water. In Table 4.4, we show the number of iterations necessary to reach the stopping criterion for different values of ν and K , and for different multigrid cycles and numbers of pre- and post-smoothing steps. All these results are obtained on a grid with space discretization parameter $h = \frac{1}{128}$.

As it can be observed, the proposed multigrid method results in a robust solver when W -cycles are used. If V -cycles are chosen, we can also observe a satisfactory behavior of the multigrid method. Moreover, very good results are obtained for small values of the physical parameters. In order to analyze the efficiency of the proposed method, we have done a comparison of the number of arithmetic operations needed for both cycles. The most efficient multigrid cycle in Table 4.4 is the $V(3, 3)$ -cycle. Therefore, we choose this cycle to compare the efficiency of the proposed multigrid based on the Uzawa smoother with a multigrid algorithm based on the Vanka smoother. For these two methods, the only difference is the smoothing part, on each

K	ν	$W(1, 1)$	$W(1, 2)$	$W(2, 2)$	$V(2, 2)$	$V(3, 3)$
1	1	38	21	15	22	13
10^{-3}	1	38	20	14	28	13
1	10^{-3}	45	24	17	32	14
10^{-3}	10^{-3}	38	20	14	23	10
10^{-2}	10^{-6}	39	21	15	24	11
10^{-4}	10^{-6}	37	20	14	22	9
10^{-6}	10^{-6}	37	20	14	22	9
10^{-7}	10^{-6}	37	20	14	22	9

Table 4.4: Number of iterations necessary to achieve the desired convergence for different values of the parameters ν and K , by using W - and V -cycles with different numbers of pre- and post-smoothing steps.

level of the hierarchy. By calculating the computational work per V -cycle, we observe that the Uzawa smoother is approximately 30% cheaper than the Vanka smoother. In Table 4.5, the number of multigrid cycles necessary to achieve the desired accuracy is presented. Overall, the method based on the Uzawa relaxation needs 50% fewer operations than the Vanka based multigrid method. Therefore, in our present test case the use of the Uzawa smoother is preferred to the Vanka relaxation.

K	1	10^{-3}	1	10^{-3}	10^{-2}	10^{-4}	10^{-6}	10^{-7}
ν	1	1	10^{-3}	10^{-3}	10^{-6}	10^{-6}	10^{-6}	10^{-6}
Uzawa	13	13	14	10	11	9	9	9
Vanka	12	11	13	11	12	11	11	11

Table 4.5: Number of iterations necessary to achieve the desired convergence for different values of the parameters ν and K , by using a $V(3, 3)$ -cycle with both Uzawa and Vanka smoothers.

4.5.2 Beavers-Joseph-Saffman interface condition

Now we consider a more complicated and realistic numerical test in which the Beavers-Joseph-Saffman interface condition is prescribed instead of the no-slip condition previously considered. In this case, the domain $\Omega = (0, 1) \times (-1, 1)$ is divided into a porous medium part $\Omega^d = (0, 1) \times (-1, 0)$ and a free-flow subdomain $\Omega^f = (0, 1) \times (0, 1)$ by the interface $\Gamma = (0, 1) \times \{0\}$. The source terms and the boundary conditions are chosen such that the analytic solution of the Darcy-Stokes problem is as follows,

$$\begin{aligned} \mathbf{u}^d(x, y) &= \begin{pmatrix} u^d(x, y) \\ v^d(x, y) \end{pmatrix} = \begin{pmatrix} -K e^y \cos x \\ -K e^y \sin x \end{pmatrix}, \\ p^d(x, y) &= e^y \sin x, \\ \mathbf{u}^f(x, y) &= \begin{pmatrix} u^f(x, y) \\ v^f(x, y) \end{pmatrix} = \begin{pmatrix} \lambda'(y) \cos x \\ \lambda(y) \sin x \end{pmatrix}, \\ p^f(x, y) &= 0, \end{aligned} \tag{4.45}$$

where $\lambda(y) = -K - \frac{y}{2\nu} + (-\frac{\gamma}{4\nu^2} + \frac{K}{2})y^2$. At the outer boundaries of the free-flow domain, Dirichlet boundary conditions for velocities are prescribed. In the case of the porous medium, the pressure is fixed at the bottom $(0, 1) \times \{-1\}$, whereas Dirichlet conditions for velocities are imposed at the lateral walls. Along the internal interface Γ , the Beavers-Joseph-Saffman condition (4.12) is taken into account.

By comparing the numerical solution with the given exact solution for fixed values of the parameters $\nu = K = 1$ and for different grid-sizes $h = 1/2^{k_l}$ for $k_l = 5, 6, 7, 8$, second-order accuracy is again obtained for all variables except for the pressure in the free-flow subdomain where we achieve first-order accuracy. This time the errors for the vertical velocities do not reach their maximum at the interface as in the previous numerical test in which the no-slip condition was imposed instead the Beavers-Joseph-Saffman condition.

Regarding the performance of the monolithic multigrid method for the coupled problem considered in this numerical test, we display in Figure 4.7 the history of the convergence of the algorithm by using a $W(2, 2)$ -cycle for different grids and $\nu = K = 1$. The $W(2, 2)$ -cycle is chosen here since it gives a more robust multigrid method. It is clear that the convergence is independent of the mesh size and that the method performs efficiently

since it only needs around 13 iterations to achieve the required stopping criterion. In Figure 4.8 the robustness of the proposed multigrid method

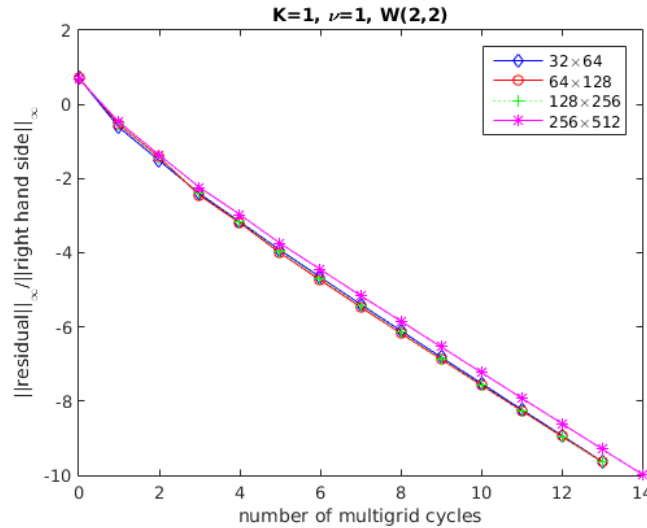


Figure 4.7: History of the convergence of the $W(2, 2)$ -multigrid method when the Beavers-Joseph-Saffman interface condition is considered.

is displayed, since for different values of ν and K and different grid-sizes the convergence of the algorithm is highly satisfactory and independent of the parameters. We can observe that with the more complicated Beavers-Joseph-Saffman condition at the interface Γ , the results provided by the proposed multigrid method for the Darcy-Stokes problem are also highly satisfactory.

4.5.3 Realistic test: cross-flow membrane filtration model

This test addresses the coupling of Darcy and Stokes problem which is in a *cross-flow filtration* setting. The cross-flow filtration can be applied in a wide range of industrial applications ranging from oil production to medical treatment. The data in this test are taken from the experiment presented in [48] which is a micro-membrane filtration model. It is used to clean fluids that are difficult to filter and to separate fine matter such as cells, proteins, enzymes and viruses [48].

The domain of the coupled problem is shown in Figure 4.9. Ω^f represents a channel on the top where the flow can go through, while Ω^d represents a filter. Since the lengths of the free flow domain and the porous medium are

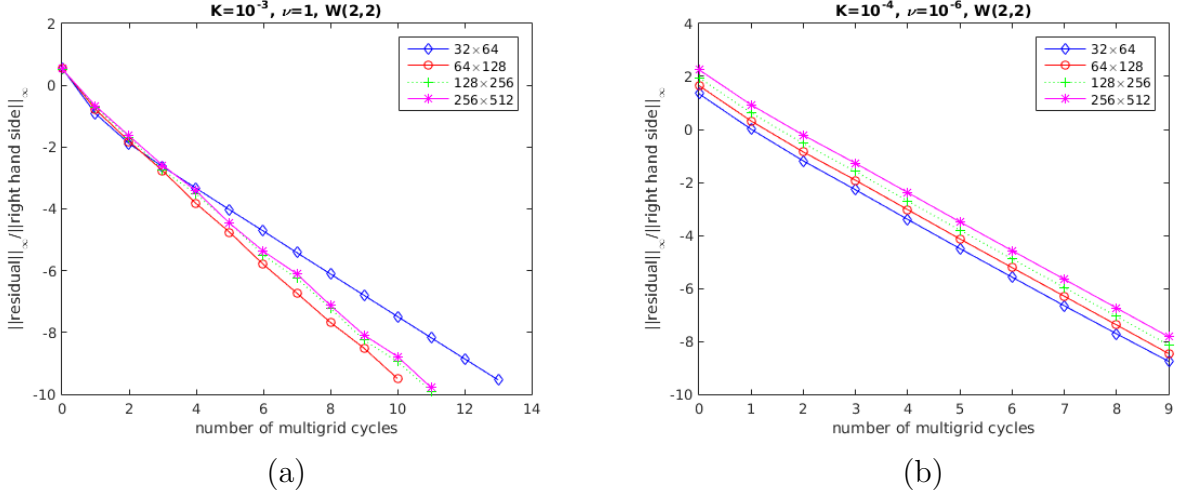


Figure 4.8: History of the convergence of the $W(2, 2)$ -multigrid method when the Beavers-Joseph-Saffman interface condition is considered for different values of the physical parameters: (a) $\nu = 1$, $K = 10^{-3}$, and (b) $\nu = 10^{-6}$, $K = 10^{-4}$.

not the same, the coupled domain is divided into four different blocks corresponding to the Darcy (*Block1*) and Stokes (*Block2*, *Block3* and *Block4*) domains. The two-block multigrid algorithm described in Section 4.4.3 can be straightforwardly adapted to the four blocks. The information transfer between *Block1* and *Block3* is the same as before. For the Stokes domain, two artificial boundaries are generated by the partitioning. As the communication between the subgrids in Ω^f is necessary, an overlap region of one cell length is created for *Block2* and *Block4* along the artificial boundaries. The data located in the overlap region is computed and transferred from the neighboring subgrid in *Block3*.

The unknowns at the artificial boundaries, i.e., u^f , are updated in *Block2* and *Block4*, and then sent to *Block3*. The communication is implemented on each level of the multigrid algorithm. The inflow entering into the domain Ω^f is specified. At the interface, the Beavers-Joseph condition is imposed. At the bottom of the porous medium, the pore pressure is set to zero. There is an exit (see Figure 4.9 in a dashed line) at the right-vertical boundary of the free flow domain. The height of the exit is 0.00125 which is quite small compared to the inlet. The stress-free boundary condition is employed at the exit where the flow may leave the domain freely. All the other imposed conditions are shown in Figure 4.9.

Two values of hydraulic conductivity $K = 0.1$ and $K = 10^{-6}$ are con-

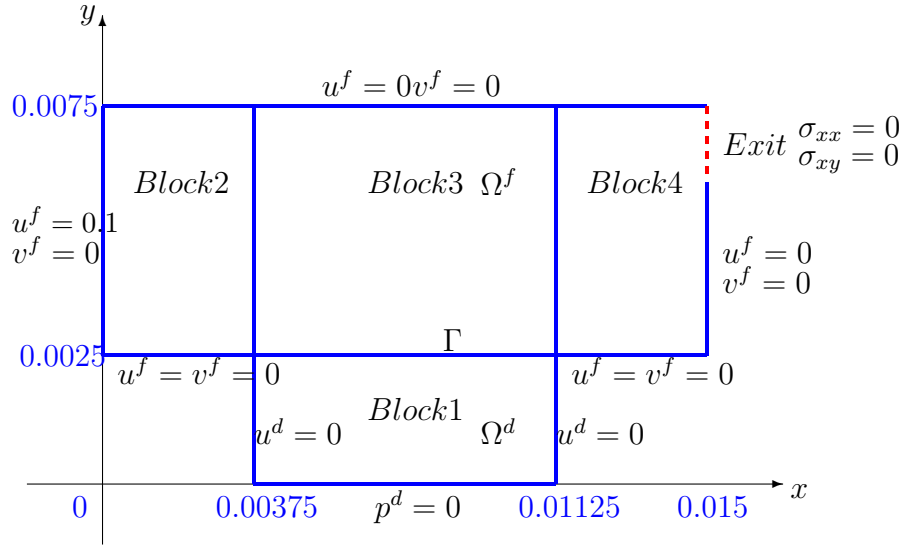


Figure 4.9: Geometry of the cross-flow membrane filtration model. Subdivision of the domain Ω into a free flow subregion Ω^f and a filter subdomain Ω^d , by an internal interface Γ .

sidered in the numerical experiment. The fluid viscosity is chosen as 10^{-6} . The solutions are investigated on four grids as shown in Table 4.6. For the test with $K = 0.1$, the velocity components along the vertical and horizontal centerlines are shown in Figure 4.10. It can be seen that the solutions for *Grid3* and *Grid4* do not differ much. This indicates that the numerical solution is convergent with the increase of the grid cells on these grids. For a multigrid $W(2, 2)$ -cycle, the multigrid convergence factor is around 0.2 for all cases, and the multigrid method exhibits a highly satisfactory behavior. This is in accordance with the previous tests.

	<i>Block1</i>	<i>Block2</i>	<i>Block3</i>	<i>Block4</i>
<i>Grid1</i>	192×64	96×128	192×128	96×128
<i>Grid2</i>	96×32	48×64	96×64	48×64
<i>Grid3</i>	48×16	24×32	48×32	24×32
<i>Grid4</i>	24×8	12×16	24×16	12×16

Table 4.6: Different grids in the computational tests.

In Figure 4.11, we show the velocity vector corresponding to $K = 0.1$. Since the hydraulic conductivity of the porous medium is quite high, when the fluid travels tangentially across the interface, the majority of the flow

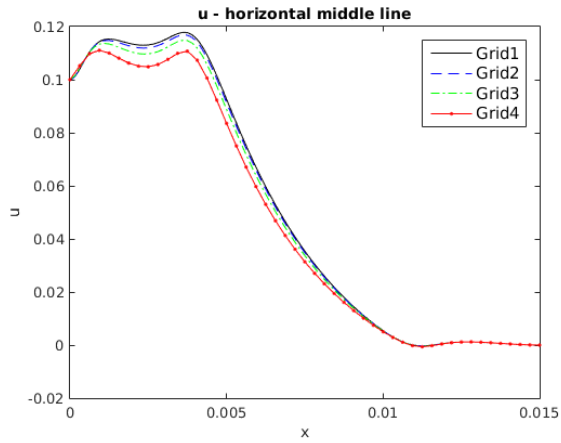
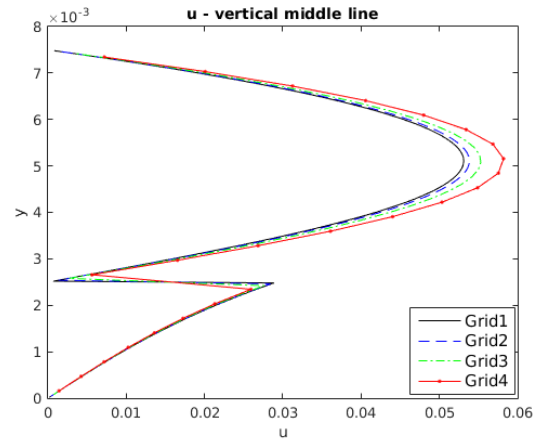
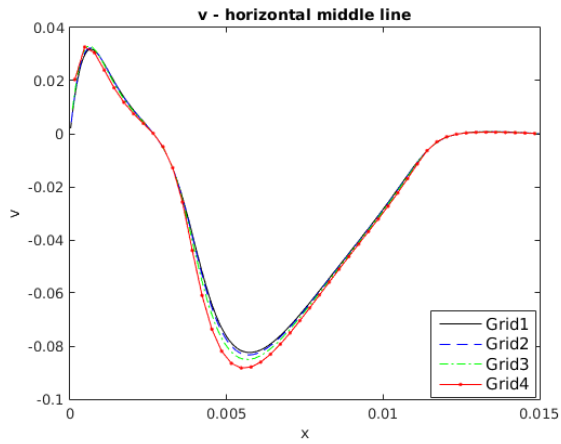
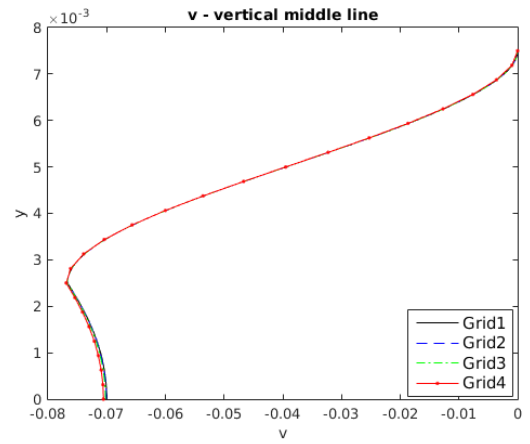
(a) $x = 0.0075$ (b) $y = 0.00375$ (c) $x = 0.0075$ (d) $y = 0.00375$

Figure 4.10: Velocity component (a) u along the vertical centerline in the coupled domain, (b) u along the horizontal centerline in the coupled domain, (c) v along the vertical centerline in the coupled domain, and (d) v along the horizontal centerline in the coupled domain.

seeps into the filter. While only a small amount of fluid goes through the exit of the channel.

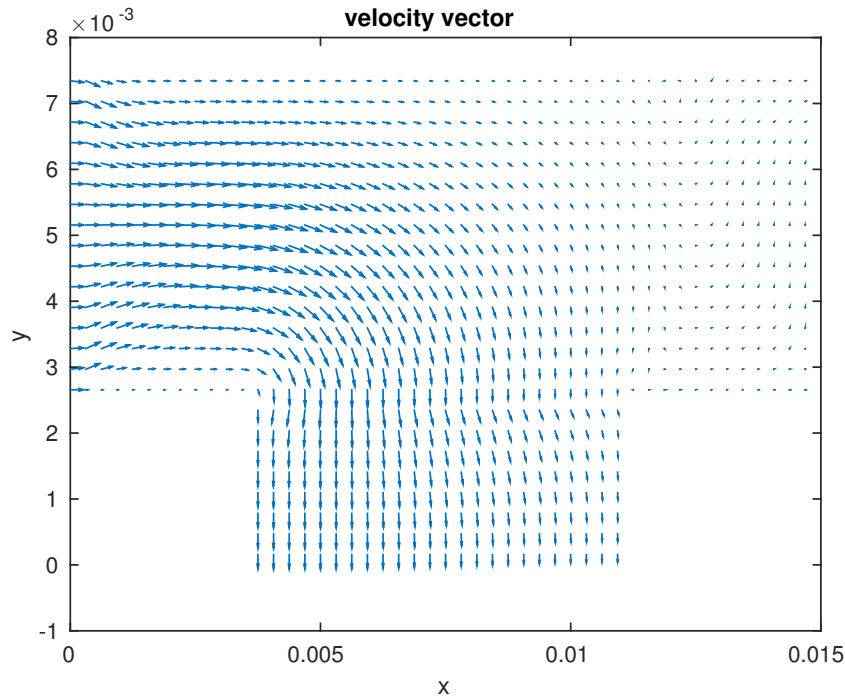


Figure 4.11: Velocity vectors over the cross-flow filtration domain with hydraulic conductivity $K = 0.1$.

In Figure 4.12, the velocity vector corresponding to $K = 10^{-6}$ is represented. With such a low hydraulic conductivity of the porous medium, the minority of the flow penetrates the interface. Whereas most of the fluid flows towards the small exit of the channel.

4.5.4 Heterogeneity test

Often, a porous medium is defined by complicated material properties. Here we therefore consider a porous medium with a random heterogeneous hydraulic conductivity K . Our aim is to study the effect of this heterogeneity model on the multigrid convergence. To simulate heterogeneity in the porous medium, a statistical approach is chosen. In order to generate random spatial data, here, a Gaussian model characterized by parameters

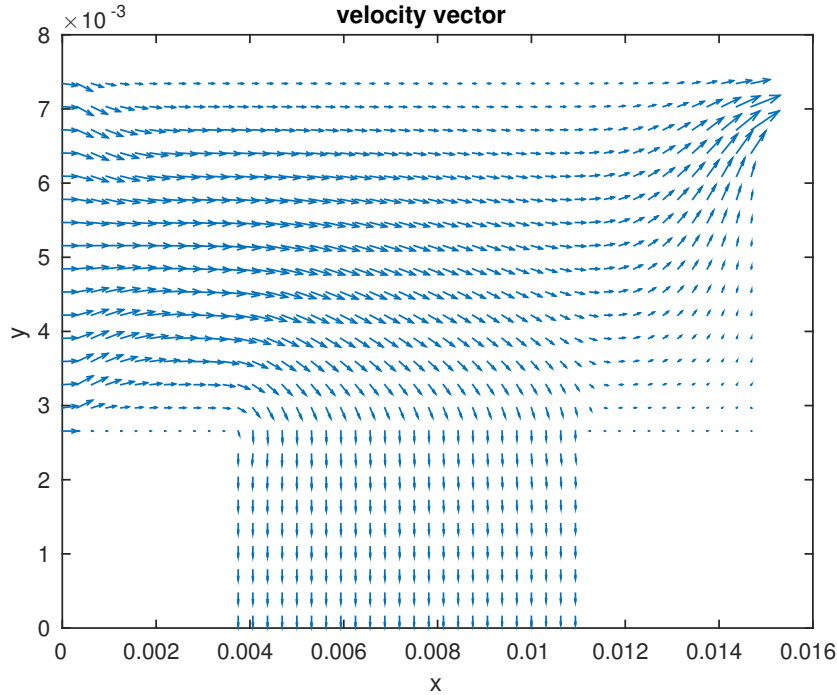


Figure 4.12: Velocity vectors over the cross-flow filtration domain with hydraulic conductivity $K = 10^{-6}$. For a better sight, the vectors have been scaled by 1.5.

λ_g and σ_g^2 is considered, i.e.,

$$C(d_g) = \sigma_g^2 \exp \left(-\frac{d_g^2}{\lambda_g} \right), \quad (4.46)$$

where d_g is the distance between two points, λ_g defines the correlation length and σ_g^2 represents the variance. By using a so-called circulant embedding technique, outlined in [83], we generate a random field on a vertex-centered grid which is twice as fine as the computational grid.

As an example, in Figure 4.13 we present a possible random sample of the hydraulic conductivity K corresponding to the porous medium in Figure 4.9 with parameters $\lambda_g = 0.3$ and $\sigma_g^2 = 1$. Dark blue in Figure 4.13 represents a higher value of the hydraulic conductivity, whereas dark red is for low conductivity.

Note that when our multigrid algorithm with the Uzawa smoother is applied, the relaxation parameter ω is varied in the Darcy domain, because ω depends on the hydraulic coefficient K . The corresponding suitable relaxation parameters for each grid point on each grid level can be calculated and used within the Uzawa smoother. Moreover, the random field should

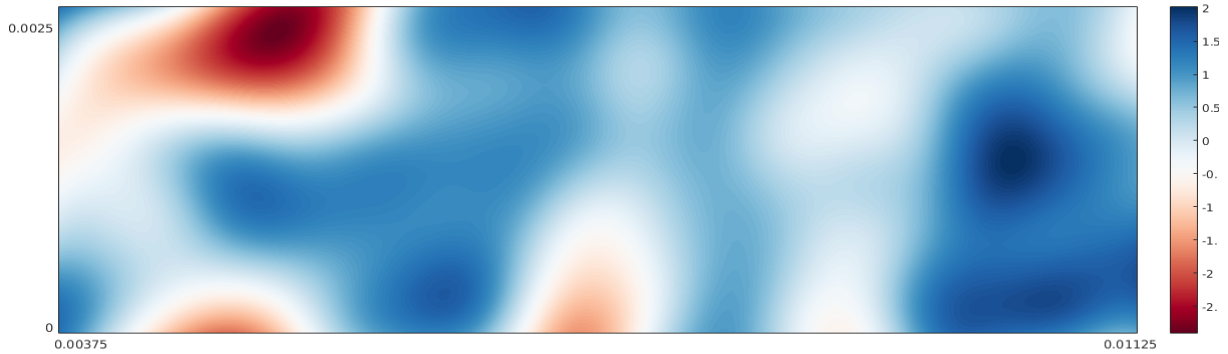


Figure 4.13: Example of random field of hydraulic conductivity K in log-scale.

be transferred from the finest grid to the other grid levels, to present the same characteristics of the porous medium on fine and coarse grids. Conductivity K is restricted to each grid level as the average value of four neighbouring fine grid points [58].

In our current experiment, for solving the problem in Section 4.5.3, two different values for parameter λ_g are chosen to analyze the multigrid convergence results; $\lambda_g = 0.1$ denotes a more heterogeneous porous medium than $\lambda_g = 0.3$. Solutions are computed on three grids, as indicated in Table 4.6. For each case, 50 realizations of the random field are generated and we record the multigrid convergence factors of the $W(2, 2)$ -cycle. The mean value of the convergence factors is presented in Table 4.7. Since fine grids are able to represent the field more accurately, the convergence results are improved with grid refinement. Multigrid exhibits better convergence for the less heterogeneous porous medium. In Figure 4.14, the solutions for $\lambda_g = 0.3$ are depicted. As expected, the velocity in the porous medium is higher (blue and white color in Figure 4.14) where the value of hydraulic conductivity is higher (Figure 4.13).

	$\lambda_g = 0.3$	$\lambda_g = 0.1$
<i>Grid1</i>	0.19	0.20
<i>Grid2</i>	0.19	0.21
<i>Grid3</i>	0.20	0.29

Table 4.7: Mean value of the multigrid convergence factors after 50 realizations of the random field.

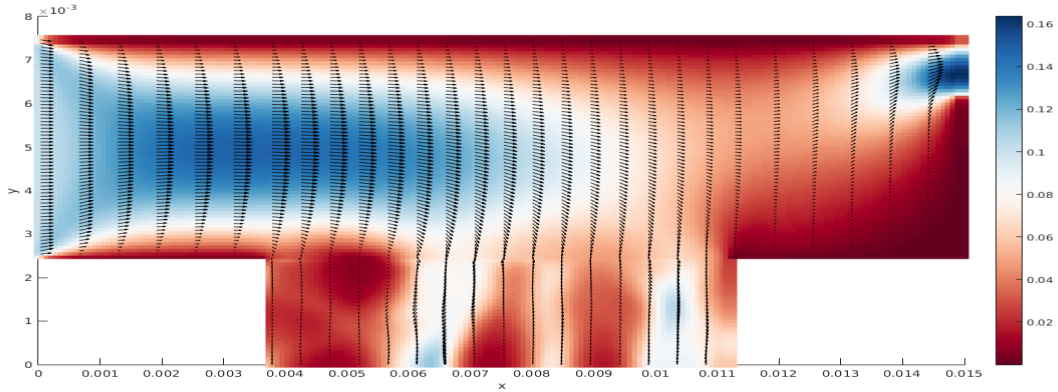


Figure 4.14: L_2 -norm of the velocity vectors over the cross-flow filtration domain with randomly distribution of hydraulic conductivity K ($\lambda_g = 0.3$).

4.6 Conclusions

In this chapter, we investigated the multigrid convergence of a coupled system consisting of a porous medium and incompressible flow. For this purpose, a coupled model based on the Darcy equation and the incompressible Stokes equations with appropriate internal interface conditions was formulated. The model was discretized by finite volumes on a staggered grid, and special care has been taken regarding the accurate discretization at the interface. We focused on an efficient multigrid algorithm for the coupled problem. A decoupled Uzawa smoother is employed, which is based on symmetric Gauss-Seidel smoothing for the velocity components and a simple Richardson iteration on the Schur complement to update the pressure field. By local Fourier analysis we have selected suitable relaxation parameters for both systems, and we have confirmed the global convergence of the monolithic multigrid which results to be the worst of the convergence factors between both the individual Darcy and Stokes subproblems. Numerical tests have shown a highly satisfactory convergence of our multigrid method for the coupled system. The algorithm performed very well in numerical experiments for a wide range of physical parameter values and for different interface conditions.

Monolithic Multigrid Method for the Coupled Stokes Flow and Deformable Porous Medium System

The interaction between fluid flow and a deformable porous medium is a complicated multi-physics problem, which can be described by a coupled model based on the Stokes and poroelastic equations. In this chapter, a monolithic multigrid method together with either a coupled Vanka smoother or a decoupled Uzawa smoother is employed as an efficient numerical technique for the linear discrete system obtained by finite volumes on staggered grids. A specialty in our modeling approach is that at the interface of the fluid and poroelastic medium, two unknowns from the different subsystems are defined at the same grid point. We propose a special discretization at and near the points on the interface, which combines the approximation of the governing equations and the considered interface conditions. For the decoupled Uzawa smoother, local Fourier analysis (LFA) helps us again to select optimal values of the relaxation parameter appearing. To implement the monolithic multigrid method, grid partitioning is used to deal with the interface updates when communication is required between two subdomains. Numerical experiments show that the proposed numerical method has an excellent convergence rate. The efficiency and robustness of the method are confirmed in numerical experiments with typically small realistic values of the physical coefficients.¹

¹The contents of this chapter have been written in a paper [65]: P. Luo, C. Rodrigo, F.J. Gaspar and C.W. Oosterlee. Monolithic Multigrid Method for the Coupled Stokes Flow and Deformable Porous Medium System. *Submitted for publication*, 2017.

5.1 Introduction

The interaction between a free fluid and a poroelastic material is attracting researchers' attention because of the wide range of applications. In order to detect or control the flow and the deformation of the porous medium, it is of great importance to understand the mechanism of the coupled dynamical process.

To model the incompressible and Newtonian free flow, the Stokes equations are considered here. The behavior of the deformable fluid-saturated porous medium is described by the well-developed Biot's model [8, 9], in which the fluid motion and solid deformation are taken into account. In Biot's model, the fluid in the pores is modeled by the Darcy equation, and the deformation by elasticity, resulting in the poroelastic equations. It is a challenge to couple the Stokes and poroelasticity systems properly at the interface. For this purpose, the conservation of mass and momentum, and a balance of normal stress and tangential stress equilibria are imposed at the interface. To our knowledge, the coupled model has not been widely studied yet, probably due to the complex coupling at the interface. In [85], Showalter models the interaction between the Stokes and the Biot's poroelasticity equations, and shows the model to be a mathematical well-posed problem which is amenable to analysis and computation.

From the computational viewpoint, the finite volume method on a staggered grid is taken into consideration as the discretization scheme for the coupled Stokes-poroelasticity system. A challenge is to deal with the discretization at the interface, since two unknowns belonging to different subsystems are placed at the same location. In this special discrete system, the governing equations of both free fluid and deformable porous medium, and their complex interaction are all included, showing a strong coupling between the two subsystems. Based on the discretization, a linear system of saddle point structure is obtained. Saddle point systems [7] arise in a wide variety of computational science and engineering fields, for example, in fluid and solid mechanics.

In [72], a DD approach using the SIMPLE-algorithm [76] on a cell-centered grid for the Stokes equations and a multigrid solver on a staggered grid for the Biot equations is employed. The authors in [4] adopt an extended DD method for the fluid-poroelastic structure interaction (FPSI)

problem without considering the fluid motion in the porous medium. It is a modular approach which only requires interface data transfer between the two existing fluid and structure codes, without any modification of the sources. In [71], partitioning strategies based on a Nitsche's coupling approach are developed for the coupled Stokes-Biot system, while in [17] a loosely coupled finite element solver by considering a Lie operator splitting scheme is proposed for the coupled fluid-structure interaction.

Another approach is to consider monolithic methods. These are algorithms that are developed for solving the fully coupled system at once. As a highly efficient solver for a saddle point system, the monolithic multigrid method is chosen in this chapter. Methods of this type have been successfully applied for the system of Stokes equations [95, 68], and also for poroelasticity equations [64, 38, 39]. In this chapter, both the coupled and decoupled smoothers are considered for the Stokes-poroelasticity system. With respect to the coupled smoothers, the Vanka smoother [95], in which the unknowns appearing in the discrete divergence operator are relaxed simultaneously, is popular and robust. Here, we also consider the Uzawa smoother for the coupled system. In [64], [68], [41], and Chapter 3 and 4, the Uzawa smoother was successfully applied for solving poroelastic equations and Stokes problems, respectively. To choose optimal values of the parameters, local Fourier analysis (LFA) is applied.

Finally, from the implementation point of view, we consider a monolithic multigrid based on grid partitioning [94], where communication between neighboring subdomains is needed on each multigrid level.

The chapter is organized as follows. First of all, we introduce the governing equations of free fluid and deformable porous medium, as well as the interface conditions in Section 5.2. The discretization of the coupled Stokes-poroelasticity system is shown in Section 5.3. In particular, we present the details about how we deal with the interface. The monolithic multigrid method, together with the coupled and decoupled smoothers, is shown in Section 5.4. After that, several numerical experiments are given to confirm the efficiency and robustness of our proposed method. Conclusions are drawn in Section 5.6. Some finer details on the discretizations and on the communication within grid partitioning are found in the appendices.

5.2 Problem formulation

The Stokes-poroelasticity problem is considered on a bounded domain $\Omega \subset \mathbb{R}^2$. It is again assumed that Ω is subdivided into two disjoint subdomains Ω^f and Ω^p , separated by a common interface $\Gamma = \partial\Omega^f \cap \partial\Omega^p$. Subregions Ω^f and Ω^p represent the free flow region and poroelastic medium, respectively. A model geometry of the problem is shown in Figure 5.1, where we also displayed \mathbf{n}^f and \mathbf{n}^p , denoting the unit outward normal vectors on $\partial\Omega^f$ and $\partial\Omega^p$, respectively. At the interface Γ , we have $\mathbf{n}^f = -\mathbf{n}^p$. Notice that compared to Figure 4.1, the domains used for Stokes-poroelasticity are reversed.

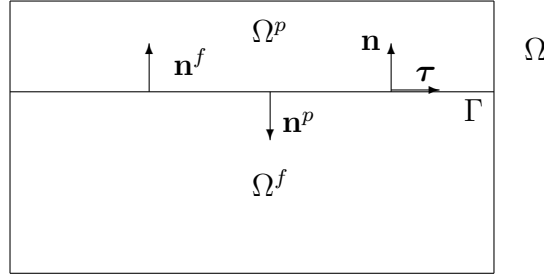


Figure 5.1: Example of a model geometry of the Stokes-poroelasticity problem. Subdivision of the domain Ω into a free flow subregion Ω^f and a porous medium subdomain Ω^p , separated by an internal interface Γ .

The description of the free flow and poroelasticity models on the different subdomains, including the boundary conditions for the outer boundaries, are presented in Sections 5.2.1 and 5.2.2. The internal interface conditions governing the interactions between the fluid and the porous medium are given in Section 5.2.3.

5.2.1 Stokes flow description

The 2D free flow subproblem is modeled by the Stokes equations for a viscous, incompressible, Newtonian fluid. It is a linearized form of the Navier-Stokes equations in the limit case when the nonlinear term becomes negligible. The motion of the Stokes flow in the region Ω^f is described by

$$\begin{aligned} \rho \frac{\partial \mathbf{u}^f}{\partial t} - \nabla \cdot \boldsymbol{\sigma}^f &= \mathbf{f}^f \quad \text{in } \Omega^f, \quad 0 < t \leq T, \\ \nabla \cdot \mathbf{u}^f &= 0 \quad \text{in } \Omega^f, \quad 0 < t \leq T, \end{aligned} \tag{5.1}$$

where ρ is the fluid density, $\mathbf{u}^f = (u^f, v^f)$ is the fluid velocity, $\mathbf{f}^f = (f_1^f, f_2^f)$ represents a prescribed force, and the fluid stress tensor $\boldsymbol{\sigma}^f$ is given by $\boldsymbol{\sigma}^f = -p^f \mathbf{I} + 2\nu \mathbf{D}(\mathbf{u}^f)$, with p^f denoting the fluid pressure, ν representing the fluid viscosity and where $\mathbf{D}(\mathbf{u}^f) = (\nabla \mathbf{u}^f + (\nabla \mathbf{u}^f)^T)/2$ is the strain tensor. The first formula in (5.1) represents the momentum equations and the second one is the continuity equation.

We assume that the boundary $\partial\Omega^f \setminus \Gamma$ is the union of two disjoint subsets Γ_D^f and Γ_N^f , where Dirichlet and Neumann boundary conditions are imposed, respectively. More concretely, we consider the following boundary conditions

$$\begin{aligned} \mathbf{u}^f &= \mathbf{g}_D^f & \text{on } \Gamma_D^f, \quad 0 < t \leq T, \\ \boldsymbol{\sigma}^f \cdot \mathbf{n}^f &= \mathbf{g}_N^f & \text{on } \Gamma_N^f, \quad 0 < t \leq T. \end{aligned} \quad (5.2)$$

5.2.2 Poroelastic flow description

We consider the 2D quasi-static Biot's model to represent the behavior of a deformable fluid-saturated porous medium. Biot's model is based on the coupling between the coherent solid skeleton and the pore fluid flow. The porous medium is assumed to be linearly elastic, homogeneous and isotropic, and the fluid is supposed to be incompressible and viscous. The governing equations in subdomain Ω^p are given by

$$\begin{aligned} -\nabla \cdot \boldsymbol{\sigma}^p &= \mathbf{f}^p & \text{in } \Omega^p, \quad 0 < t \leq T, \\ \frac{\partial}{\partial t}(\nabla \cdot \mathbf{u}^p) + \nabla \cdot \mathbf{q}^p &= f^p & \text{in } \Omega^p, \quad 0 < t \leq T, \\ \mathbf{q}^p &= -K \nabla p^p & \text{in } \Omega^p, \quad 0 < t \leq T. \end{aligned} \quad (5.3)$$

The stress tensor of the poroelastic medium is $\boldsymbol{\sigma}^p = \boldsymbol{\sigma}^e - p^p \mathbf{I}$, where $\boldsymbol{\sigma}^e$ denotes the effective stress tensor and p^p is the fluid pressure. The right-hand side $\mathbf{f}^p = (f_1^p, f_2^p)$ represents the external body forces, whereas the source term f^p corresponds to a forced fluid extraction or injection process. Since the porous skeleton is assumed to be deformable, the effective stress tensor $\boldsymbol{\sigma}^e$ is characterized by the displacement $\mathbf{u}^p = (u^p, v^p)$, i.e. $\boldsymbol{\sigma}^e(\mathbf{u}^p) = 2G\mathbf{D}(\mathbf{u}^p) + \lambda \text{tr}(\mathbf{D}(\mathbf{u}^p))\mathbf{I}$, where λ and G denote the Lamé coefficients for the solid framework and $\mathbf{D}(\mathbf{u}^p) = (\nabla \mathbf{u}^p + (\nabla \mathbf{u}^p)^T)/2$. Parameter K is the hydraulic conductivity, representing the properties of the porous medium and the fluid. The flux \mathbf{q}^p is the relative velocity of the fluid within the porous matrix.

For the poroelasticity subproblem, at the outer boundary, $\partial\Omega^p \setminus \Gamma$, we prescribe combinations of the following boundary conditions,

$$\begin{aligned} \mathbf{u}^p &= \mathbf{g}_D^p, \quad 0 < t \leq T, \\ p^p &= g_D^p, \quad 0 < t \leq T, \\ \boldsymbol{\sigma}^p \cdot \mathbf{n}^p &= \mathbf{g}_N^p, \quad 0 < t \leq T, \\ \mathbf{q}^p \cdot \mathbf{n}^p &= g_N^p, \quad 0 < t \leq T. \end{aligned} \tag{5.4}$$

5.2.3 Interface conditions

To solve the coupled system, proper internal interface conditions are needed to be set up at the interface Γ . Here we denote by $\mathbf{n} = \mathbf{n}^f = -\mathbf{n}^p$ the outward normal vector to the fluid domain and by $\boldsymbol{\tau}$ the tangential unit vector on the interface Γ , which is obtained by rotating the normal vector in the counter-clockwise direction by 90° . It is natural to consider the continuity of velocities and stresses at the interface of the fluid and the poroelastic medium.

- For mass conservation, the continuity of normal fluid flux across the interface is required,

$$(\mathbf{u}^f - \frac{\partial \mathbf{u}^p}{\partial t}) \cdot \mathbf{n} = \mathbf{q}^p \cdot \mathbf{n}, \tag{5.5}$$

where $\frac{\partial \mathbf{u}^p}{\partial t}$ is the velocity of the skeleton, and the flux \mathbf{q}^p denotes the filtration velocity.

- Regarding the exchange of stresses, the normal components of the stress in the fluid phase should be in balance

$$\mathbf{n} \cdot \boldsymbol{\sigma}^f \mathbf{n} = -p^p. \tag{5.6}$$

- The conservation of momentum prescribes the balance of contact forces, i.e. the stress of the porous medium is balanced by the stress of the fluid, that is,

$$\mathbf{n} \cdot \boldsymbol{\sigma}^f \mathbf{n} - \mathbf{n} \cdot \boldsymbol{\sigma}^p \mathbf{n} = 0, \tag{5.7}$$

and

$$\boldsymbol{\tau} \cdot \boldsymbol{\sigma}^f \mathbf{n} - \boldsymbol{\tau} \cdot \boldsymbol{\sigma}^p \mathbf{n} = 0. \tag{5.8}$$

- A no-slip interface boundary condition is considered,

$$\mathbf{u}^f \cdot \boldsymbol{\tau} = \frac{\partial \mathbf{u}^p}{\partial t} \cdot \boldsymbol{\tau} , \quad (5.9)$$

for the cases in which there is no tangential flow.

Remark 5.1. *Besides to the no-slip interface conditions, also the Beavers-Joseph-Saffman interface condition*

$$-\boldsymbol{\tau} \cdot \boldsymbol{\sigma}^f \mathbf{n} = \vartheta (\mathbf{u}^f - \frac{\partial \mathbf{u}^p}{\partial t}) \cdot \boldsymbol{\tau} , \quad (5.10)$$

is sometimes used in problems where porous media and free flow domains are connected (see also Chapter 4). The slip rate coefficient ϑ quantifies the resistance of the porous medium to the flow of the fluid in tangential direction. The parameter that needs to be determined in this interface condition is non-trivial and often connected to real experiments. We do not consider the Beavers-Joseph-Saffman condition here for the Stokes-poroelasticity multi-physics experiments. We would like to note, however, that the strategy proposed in this work can be also applied if the Beavers-Joseph-Saffman interface condition would be employed.

5.3 Discretization

We consider the finite volume method on a staggered grid [77] as the spatial discretization scheme for the coupled Stokes-poroelasticity problem. The staggered grid location of the unknowns has been shown in Figure 4.2.

Our aim is to obtain a special discrete equation for the unknowns at and near the internal interface Γ . Details for the discretization of the interior points of the poroelastic and Stokes equations are shown in Appendix 5.A and 5.B. Due to the staggered arrangement of the unknowns, the only variables at the interface are the vertical components of each system. Note that at the interface, two unknowns v^p and v^f share the same location, so we have two different governing equations at one grid point, see Figure 5.2.

Remark 5.2. *For the case in which the interface does not match with the grid points, we refer to the modeling as done in [72, 59]. In [72], a cell-centered grid in the fluid region and a staggered grid in the porous domain*

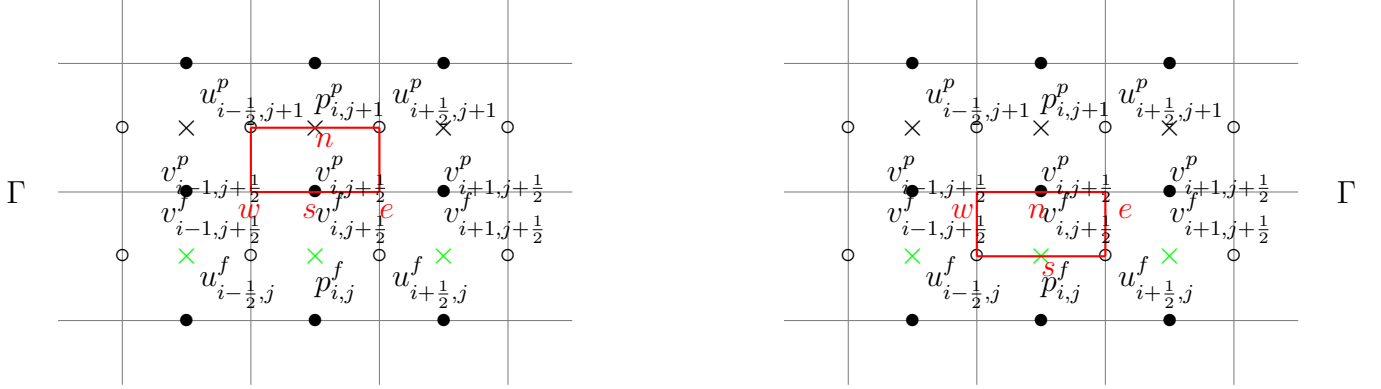


Figure 5.2: Staggered grid location of the unknowns and the control volume of v^p (left) and v^f (right) at the interface.

are used for the coupled system. To deal with the discretization of the interface conditions, the authors introduce some specific grid points at the interface, where the information between the two subdomains is exchanged. The coupling with these additional points is done by means of a matching function, which can, for example, be a bilinear interpolation. Alternatively, the Mortar finite element method [59] is a suitable technique for interface problems when considering the coupling of different discretization schemes or non-matching meshes.

5.3.1 Discretization for v^p and v^f at the interface

First of all, we describe the discretization for the poroelastic unknown v^p at the interface. Note that in the following discrete formula, the superscript \bar{m} represents the values at current time, while $\bar{m} - 1$ denotes the solutions from a previous time step. For simplicity, we consider uniform meshes with time step τ and grid size h in both directions on each subdomain. The y -momentum equation of the poroelastic system is integrated over a half volume, as displayed in red color in Figure 5.2 (left), giving rise to the following equation

$$-\left(\frac{(\sigma_{xy}^{p,\bar{m}})_e - (\sigma_{xy}^{p,\bar{m}})_w}{h} + \frac{(\sigma_{yy}^{p,\bar{m}})_n - (\sigma_{yy}^{p,\bar{m}})_s}{h/2} \right) = (f_2^{p,\bar{m}})_s, \quad (5.11)$$

where, as can be seen in Figure 5.2 (left), e and w denote locations at the interface, and n and s denote the location of $p_{i,j+1}^p$ and $v_{i,j+\frac{1}{2}}^p/v_{i,j+\frac{1}{2}}^f$, respectively. In the discrete formula, for example, we denote the approximation of v^p in the grid point $(i, j + \frac{1}{2})$ at the interface as $v_{i,j+\frac{1}{2}}^p$. Similar

notations are used for the other variables. $(\sigma_{yy}^{p,\bar{m}})_n$ is easily approximated by the existing variables as follows,

$$(\sigma_{yy}^{p,\bar{m}})_n = \frac{\lambda}{h}(u_{i+\frac{1}{2},j+1}^{p,\bar{m}} - u_{i-\frac{1}{2},j+1}^{p,\bar{m}}) + \frac{\lambda + 2G}{h}(v_{i,j+\frac{3}{2}}^{p,\bar{m}} - v_{i,j+\frac{1}{2}}^{p,\bar{m}}) - p_{i,j+1}^{p,\bar{m}}. \quad (5.12)$$

For the remaining components of the stress tensor, the interface conditions are required. By applying the interface conditions (5.6) and (5.7), $(\sigma_{yy}^{p,\bar{m}})_s$ is obtained as,

$$(\sigma_{yy}^{p,\bar{m}})_s = (\sigma_{yy}^{f,\bar{m}})_s = -p_s^{p,\bar{m}}. \quad (5.13)$$

The stress tensors $(\sigma_{xy}^{p,\bar{m}})_e$ and $(\sigma_{xy}^{p,\bar{m}})_w$ are related to the horizontal displacements $u_e^{p,\bar{m}}$ and $u_w^{p,\bar{m}}$ at the interface as,

$$(\sigma_{xy}^{p,\bar{m}})_e = G \left(\frac{u_{i+\frac{1}{2},j+1}^{p,\bar{m}} - u_e^{p,\bar{m}}}{h/2} + \frac{v_{i+1,j+\frac{1}{2}}^{p,\bar{m}} - v_{i,j+\frac{1}{2}}^{p,\bar{m}}}{h} \right), \quad (5.14)$$

$$(\sigma_{xy}^{p,\bar{m}})_w = G \left(\frac{u_{i-\frac{1}{2},j+1}^{p,\bar{m}} - u_w^{p,\bar{m}}}{h/2} + \frac{v_{i,j+\frac{1}{2}}^{p,\bar{m}} - v_{i-1,j+\frac{1}{2}}^{p,\bar{m}}}{h} \right). \quad (5.15)$$

Substituting (5.12)-(5.15) into (5.11) gives rise to the following discrete equation for $v_{i,j+\frac{1}{2}}^{p,\bar{m}}$,

$$\begin{aligned} & -\frac{2(\lambda + G)}{h^2}(u_{i+\frac{1}{2},j+1}^{p,\bar{m}} - u_{i-\frac{1}{2},j+1}^{p,\bar{m}}) + \frac{2G}{h^2}(u_e^{p,\bar{m}} - u_w^{p,\bar{m}}) - \frac{G}{h^2}(v_{i+1,j+\frac{1}{2}}^{p,\bar{m}} + v_{i-1,j+\frac{1}{2}}^{p,\bar{m}}) \\ & - \frac{2(\lambda + 2G)}{h^2}v_{i,j+\frac{3}{2}}^{p,\bar{m}} + \left(\frac{2G}{h^2} + \frac{2(\lambda + 2G)}{h^2} \right) v_{i,j+\frac{1}{2}}^{p,\bar{m}} + \frac{2}{h}(p_{i,j+1}^{p,\bar{m}} - p_s^{p,\bar{m}}) = (f_2^{p,\bar{m}})_s. \end{aligned} \quad (5.16)$$

Since pressure $p_s^{p,\bar{m}}$ and the two displacements $u_e^{p,\bar{m}}$ and $u_w^{p,\bar{m}}$ are not known at the interface, we approximate them with the help of the interface conditions. From the interface condition (5.5), the approximation of $p_s^{p,\bar{m}}$ reads

$$p_s^{p,\bar{m}} = p_{i,j+1}^{p,\bar{m}} + \frac{h}{2K}v_{i,j+\frac{1}{2}}^{f,\bar{m}} - \frac{h}{2K\tau}(v_{i,j+\frac{1}{2}}^{p,\bar{m}} - v_{i,j+\frac{1}{2}}^{p,\bar{m}-1}). \quad (5.17)$$

To approximate the horizontal displacement, we need to use the conservation of momentum (5.8) and the no-slip interface condition (5.9). Thus, by applying (5.8) and (5.9) at the location denoted by e in Figure 5.2 (left), we obtain the expressions of $u_e^{p,\bar{m}}$ and $u_e^{f,\bar{m}}$ as

$$u_e^{p,\bar{m}} = G\tau\xi(2u_{i+\frac{1}{2},j+1}^{p,\bar{m}} + v_{i+1,j+\frac{1}{2}}^{p,\bar{m}} - v_{i,j+\frac{1}{2}}^{p,\bar{m}}) - \nu\tau\xi(-2u_{i+\frac{1}{2},j}^{f,\bar{m}} + v_{i+1,j+\frac{1}{2}}^{f,\bar{m}} - v_{i,j+\frac{1}{2}}^{f,\bar{m}}) + 2\nu\xi u_e^{p,\bar{m}-1}, \quad (5.18)$$

and

$$u_e^{f,\bar{m}} = G\xi(2u_{i+\frac{1}{2},j+1}^{p,\bar{m}} + v_{i+1,j+\frac{1}{2}}^{p,\bar{m}} - v_{i,j+\frac{1}{2}}^{p,\bar{m}}) - \nu\xi(-2u_{i+\frac{1}{2},j}^{f,\bar{m}} + v_{i+1,j+\frac{1}{2}}^{f,\bar{m}} - v_{i,j+\frac{1}{2}}^{f,\bar{m}}) - 2G\xi u_e^{p,\bar{m}-1}, \quad (5.19)$$

where $\xi = \frac{1}{2\nu+2G\tau}$. The approximation of the horizontal velocity at the location w can be calculated in a similar way. Then, by applying (5.17), (5.18) and the approximation of $u_w^{p,\bar{m}}$ to (5.16), we have the discrete formula for the interface unknown $v_{i,j+\frac{1}{2}}^{p,\bar{m}}$. This discretization does not only include the poroelastic unknowns but also the unknowns of the Stokes system. When implementing the discretization for one subsystem, the information from the other subsystem is required. Strong coupling is thus guaranteed through the interface conditions.

For the discretization of the second unknown, v^f , at the interface, we obtain (5.20) by integrating the corresponding equation over a half volume as displayed in red color in Figure 5.2 (right),

$$-\left(\frac{(\sigma_{xy}^{f,\bar{m}})_e - (\sigma_{xy}^{f,\bar{m}})_w}{h} + \frac{(\sigma_{yy}^{f,\bar{m}})_n - (\sigma_{yy}^{f,\bar{m}})_s}{h/2}\right) + \frac{\varrho}{\tau}(v_{i,j+\frac{1}{2}}^{f,\bar{m}} - v_{i,j+\frac{1}{2}}^{f,\bar{m}-1}) = (f_2^{f,\bar{m}})_n. \quad (5.20)$$

Following the same technique to approximate the components of the stress tensor as above, we again obtain a formulation where three variables $u_e^{f,\bar{m}}$, $u_w^{f,\bar{m}}$ and $p_n^{p,\bar{m}}$ are not known at the interface. The variables $u_e^{f,\bar{m}}$ and $u_w^{f,\bar{m}}$ can be calculated from the interface conditions (5.8) and (5.9). By applying these expressions to (5.20), the unknowns for both subproblems are included in the coupling between the two systems.

5.3.2 Discretization for u^p and u^f near the interface

The discretizations for the unknowns near the interface are also special and of great importance. Considering the control volume in Figure 5.3 (left) in red, the governing equation for $u_{i+\frac{1}{2},j+1}^p$ is equation (5.30), which is shown in Appendix 5.A. The related stress components $(\sigma_{xx}^{p,\bar{m}})_e$, $(\sigma_{xx}^{p,\bar{m}})_w$ and $(\sigma_{xy}^{p,\bar{m}})_n$ are similar to the equations in (5.31)-(5.33). However, component $(\sigma_{xy}^{p,\bar{m}})_s$ is now written as

$$(\sigma_{xy}^{p,\bar{m}})_s = G\left(\frac{u_{i+\frac{1}{2},j+1}^{p,\bar{m}} - u_s^{p,\bar{m}}}{h/2} + \frac{v_{i+1,j+\frac{1}{2}}^{p,\bar{m}} - v_{i,j+\frac{1}{2}}^{p,\bar{m}}}{h}\right), \quad (5.21)$$

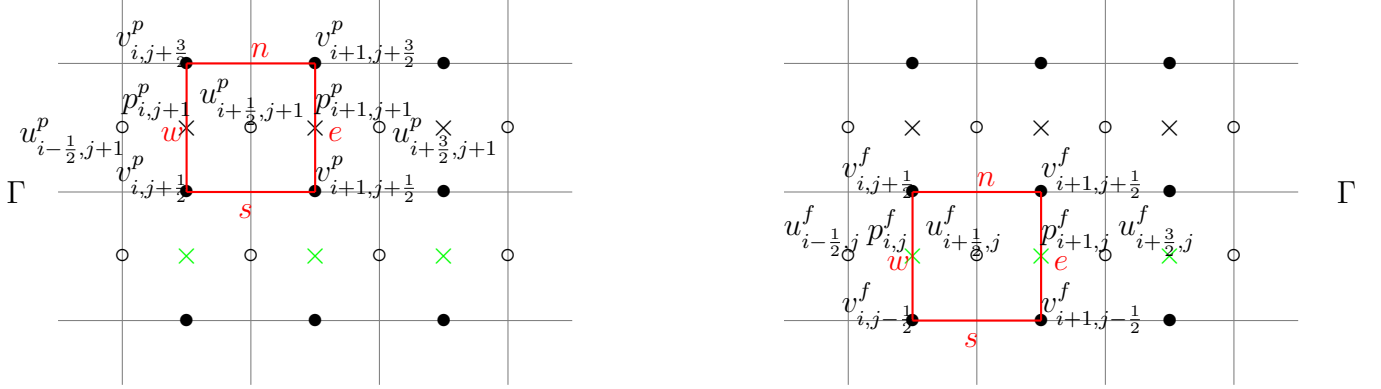


Figure 5.3: Staggered grid location of the unknowns and the control volume of u^p (left) and u^f (right) near the interface.

where the horizontal displacement $u_s^{p,\bar{m}}$ at the interface is needed. A similar expression for $u_s^{p,\bar{m}}$ can be obtained by using two interface conditions. Since $u_s^{p,\bar{m}}$ includes the Stokes unknowns, the discrete equation for $u_{i+\frac{1}{2},j+1}^{p,\bar{m}}$ is also coupled with the free fluid system.

Similarly, for the discretization of $u_{i+\frac{1}{2},j}^f$ in Figure 5.3 (right), only $(\sigma_{xy}^{f,\bar{m}})_n$ in (5.36) needs to be redefined as

$$(\sigma_{xy}^{f,\bar{m}})_n = \nu \left(\frac{u_n^{f,\bar{m}} - u_{i+\frac{1}{2},j}^{f,\bar{m}}}{h/2} + \frac{v_{i+1,j+\frac{1}{2}}^{f,\bar{m}} - v_{i,j+\frac{1}{2}}^{f,\bar{m}}}{h} \right), \quad (5.22)$$

which relates the poroelastic system to $u_n^{f,\bar{m}}$.

5.3.3 Discretization for p^p and p^f near the interface

Following the notation in Figure 5.4, the discretization for $p_{i,j+1}^p$ is given by

$$\begin{aligned} \frac{1}{h\tau} (u_{i+\frac{1}{2},j+1}^{p,\bar{m}} - u_{i-\frac{1}{2},j+1}^{p,\bar{m}} + v_{i,j+\frac{3}{2}}^{p,\bar{m}} - v_{i,j+\frac{1}{2}}^{p,\bar{m}}) - \frac{K}{h^2} (p_{i+1,j+1}^{p,\bar{m}} + p_{i-1,j+1}^{p,\bar{m}} + p_{i,j+2}^{p,\bar{m}} \\ - 5p_{i,j+1}^{p,\bar{m}} + 2p_s^{p,\bar{m}}) = (f^{p,\bar{m}})_{i,j+1} + \frac{1}{h\tau} (u_{i+\frac{1}{2},j+1}^{p,\bar{m}-1} - u_{i-\frac{1}{2},j+1}^{p,\bar{m}-1} + v_{i,j+\frac{3}{2}}^{p,\bar{m}-1} - v_{i,j+\frac{1}{2}}^{p,\bar{m}-1}). \end{aligned} \quad (5.23)$$

From the interface condition (5.5), $p_s^{p,\bar{m}}$ can be approximated using the same strategy as in (5.17). For the Stokes pressure near the interface, the discrete equation remains the same as in (5.41) in Appendix 5.B.

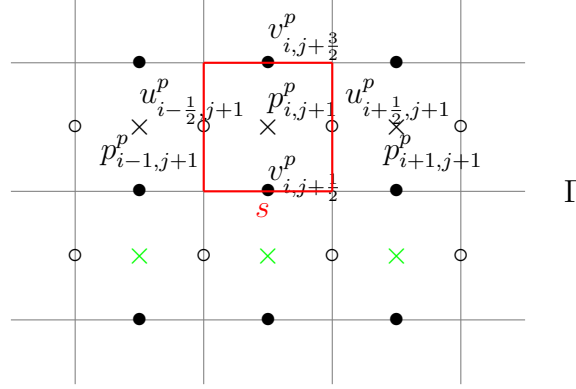


Figure 5.4: Staggered grid location of the unknowns and the control volume of p^p near the interface.

5.3.4 Saddle point structure

As already explained, for the individual poroelastic and Stokes systems, the discretization described in the previous subsections leads to a saddle point linear system at each time step, of the form,

$$\begin{pmatrix} A & B^T \\ B & -C \end{pmatrix} \begin{pmatrix} \mathbf{u} \\ p \end{pmatrix} = \begin{pmatrix} \mathbf{g} \\ f \end{pmatrix}. \quad (5.24)$$

For both subproblems B^T and B represent the discrete gradient and the negative discrete divergence operators, respectively. For the poroelastic system, A is the discrete representation of the elastic operator $-G\Delta - \nabla(\lambda + G)\nabla \cdot$, and C corresponds to the diffusion operator $-\tau\nabla \cdot (K\nabla p)$, whereas for the Stokes system, A represents the discretization of operator $\frac{\rho}{\tau}I - \nu\Delta$ and C is a zero block. Although the term in C is nonzero for the poroelasticity subsystem, it can become arbitrarily small because parameter K in the diffusion operator can be very small, as well as the time step.

Analogously to the individual systems, the coupled system is also governed by the saddle point structure by rearranging the vector of unknowns to order first the velocities and displacements and thereafter the pressure unknowns. Thus the following linear system is obtained,

$$\begin{pmatrix} A^f & R^T & (B^f)^T & (R')^T \\ R & A^p & 0 & (B^p)^T \\ B^f & 0 & 0 & 0 \\ R' & B^p & 0 & -C^p \end{pmatrix} \begin{pmatrix} \mathbf{u}^f \\ \mathbf{u}^p \\ p^f \\ p^p \end{pmatrix} = \begin{pmatrix} \mathbf{f}^f \\ \mathbf{f}^p \\ 0 \\ f^p \end{pmatrix}. \quad (5.25)$$

Obviously, (5.25) has the same structure as (5.24) by denoting

$$A = \begin{pmatrix} A^f & R^T \\ R & A^p \end{pmatrix}, B = \begin{pmatrix} B^f & 0 \\ R' & B^p \end{pmatrix}, -C = \begin{pmatrix} 0 & 0 \\ 0 & -C^p \end{pmatrix},$$

where R and R' are matrices containing the coupling for the unknowns at and near the interface. For each equation, most of the elements in R and R' are zero, whereas the nonzero elements correspond to the terms not belonging to the current subsystem, but appearing in the special interface discretizations. In particular, the nonzero elements are on the diagonal of R' . In the discretization of the vertical component of \mathbf{u}^f at the interface, the nonzero elements in R' represent the appearance of poroelastic pressure p^p , while in the discrete equation of p^p , the vertical component of velocity \mathbf{u}^f is present. R has more nonzero elements than R' , since the discretizations for \mathbf{u}^f and \mathbf{u}^p are more involved. For example, the Stokes velocity at three grid points is needed when discretizing the vertical component of \mathbf{u}^p at the interface, whereas in the discretization of the horizontal component of \mathbf{u}^p near the interface, only two Stokes velocities are necessary.

5.4 Fast solvers based on multigrid

Our aim is again to design a monolithic geometric multigrid method for the coupled Stokes-poroelasticity problem. To obtain an efficient multigrid solver, it is necessary to carefully select the components of the algorithm. In this section, the smoothing operator, the restriction and prolongation operators and the coarse-grid discretization are all presented.

5.4.1 Smoother

Basically, there are two types of robust smoothers developed for our problem, classified as coupled and decoupled smoothers.

Coupled smoothers

Vanka smoother Regarding coupled smoothers, the Vanka smoother is considered here. It can be straightforwardly applied to solving the Stokes-poroelasticity problem. For the staggered arrangement of variables, this approach is based on updating all equations of the system for each grid cell

simultaneously. Particularly, five unknowns are relaxed at the same time. The relaxation is implemented in a block Gauss-Seidel fashion and for each cell in the grid, a 5×5 -system is solved. For the poroelasticity system, a multigrid method based on the Vanka smoother has been applied in [39] and in Chapter 4 showing a very robust performance.

Decoupled smoother

Uzawa smoother Regarding the decoupled smoothers, we focus on the Uzawa smoother, which is an equation-wise relaxation method. The Uzawa smoother was proposed for Stokes problems in fluid dynamics in [68], [41]. In [64], a multigrid method with an Uzawa smoother was successfully applied for solving poroelastic equations in Chapter 3. Thus, it seems natural to assume that this relaxation is also suitable for the coupled Stokes-poroelasticity problem. Details have been presented in Section 3.3.2.

Optimal relaxation parameter In [64], [41] and Chapter 3, different analytic expressions of the relaxation parameters ω appearing within the Uzawa smoother for the individual Stokes and poroelastic systems are obtained by a theoretical analysis that we can use directly for the coupled system as well. Local Fourier analysis helps to predict the asymptotic convergence factor of the multigrid algorithm and provides a concrete formula for the optimal relaxation parameter. In [64] and Chapter 3, the optimal parameter for the poroelastic system is given by

$$\omega^p = \frac{h^2(\lambda + 2G)}{5K\tau(\lambda + 2G) + h^2}, \quad (5.26)$$

with the parameters K , λ , G , h , τ as previously introduced. Meanwhile, the optimal parameter for the Stokes system is obtained from [41] as follows

$$\omega^f = \nu + \frac{\varrho h^2}{8\tau}. \quad (5.27)$$

From (5.26) and (5.27), it can be seen that the relaxation parameters do not only depend on the model coefficients but also on the grid size and on time step τ , thus ω^p and ω^f are different on each grid of the hierarchy in the multigrid method.

Remark 5.3. *Besides the smoothers presented in this thesis, other relaxations may be considered, for example, the distributive Gauss-Seidel smoother (DGS). DGS is a smoother which, after an operator transformation, results in a decoupled, equation-wise relaxation method and it has been designed for discretizations on staggered grids. Distributive smoothing methods for incompressible flow problems or poroelasticity systems have been presented in [94, 13] and [39]. However, for the coupled Stokes-poroelasticity system, DGS method is rather challenging. It is not clear how to define the operator transformation due to the involved coupling of the poroelasticity and Stokes unknowns at and near the interface.*

Communication

The computational domain is divided into (at least) two different blocks corresponding to the Stokes and poroelasticity domains. The points at and near Γ have special discretizations that contain the variables from the neighboring subdomain. Therefore, it is necessary for each subgrid to store not only the data from its own but also a copy of data of the neighboring subgrid in an overlap region. The size of this overlap region should however be one grid cell only. The communication between two individual subsystems is based on the grid partitioning technique.

In Figure 5.5, the two subgrids are extended by adding “one cell” overlap regions that are drawn in dashed lines. The red circles, dots and crosses represent the unknowns of the Stokes system, while the blue circles, dots and crosses denote the poroelastic unknowns. Notice that this communication pattern is a little different from that in Figure 4.5. In the Stokes subdomain Ω^f , for example, the color of the unknowns in the overlap region (blue) is different from the color of those in Ω^f (red). Since u^p , v^p and p^p appear in the discrete formula for the Stokes velocity v^f at the interface, the values of these three poroelastic unknowns are transferred to the extra region of the Stokes domain, represented by blue arrows in Figure 5.5. For the poroelastic part, the transfer strategy is the same. The difference is that only velocities u^f and v^f are needed in the special discretizations for the poroelastic unknowns. So, the fluid pressure p^f is not transferred to the overlap region in Ω^p . The communication from the Stokes subsystem to the poroelastic subsystem is indicated by the red arrows in Figure 5.5.

In the monolithic multigrid method, we choose the grids so that Γ is

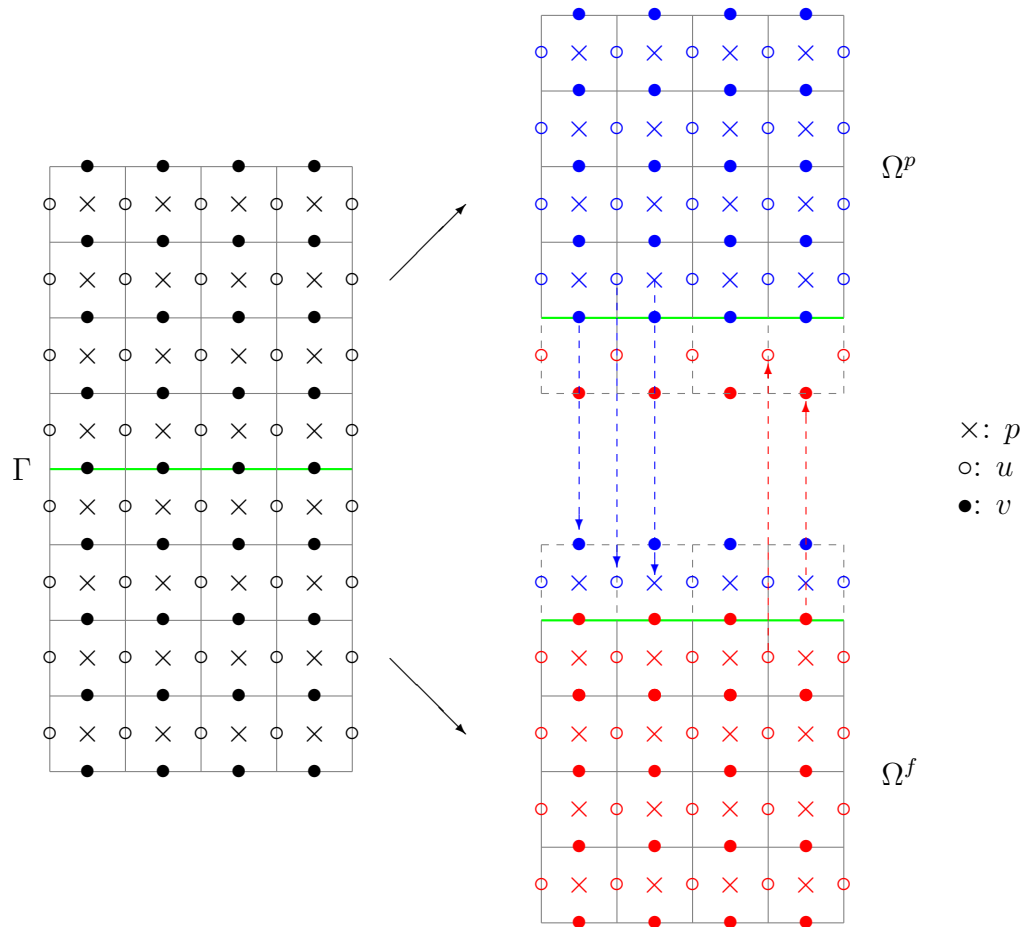


Figure 5.5: Communications between two partitioned subgrids.

present on the complete grid hierarchy. The communication between the Stokes and poroelasticity problems is performed at each grid level instead of only at the finest grid. After the smoothing process on each grid level, the values of unknowns in the overlap region are updated by communication.

Comparing the communication steps of the two smoothers, the Vanka smoother needs less communication than the Uzawa smoother. Here we wish to precisely describe the relaxation order of the unknowns in the Uzawa smoother which is different from that for the Vanka smoother. In the Uzawa smoothing process, all velocity and displacement unknowns are updated before all pressure unknowns are relaxed. Different relaxation parameters $\omega^{f/p}$ for the Richardson iteration for the Schur complement are chosen when updating the pressure unknowns in the Stokes and poroelastic domains. In a full smoothing iteration, we thus first relax the velocity \mathbf{u}^f in Ω^f , then the updates are transferred to the overlap region in Ω^p . With these values, we update the displacement unknowns \mathbf{u}^p , and transfer them to the overlap region in Ω^f . After that, we return to Ω^f to update the pressure p^f by using relaxation parameter ω^f in (5.27), then we move to Ω^p to relax p^p by using ω^p in (5.26). Finally, we return the updated values of p^p to the overlap region in Ω^f before a new smoothing iteration can be carried out. We wish to emphasize again that this smoothing process with the data communication is implemented on each grid level in the hierarchy. There is no difference in the performance of the Uzawa smoother if we would start the relaxation method with the poroelasticity part.

Comparing the communication steps of the two smoothers, the Vanka smoother needs less communication than the Uzawa smoother. In a complete smoothing iteration on the whole domain, the Vanka smoother requires two communication phases. After the smoothing of the Stokes subsystem, the data is transferred to the overlap region. Then, the transfer is needed again when the poroelastic part is updated. Conversely, the Uzawa smoother requires four communication stages in the smoothing process since it is an equation-wise smoother. In a sequential implementation, we see no significant difference in CPU time between a Vanka smoother and an Uzawa smoother iteration. If the algorithm would be performed in parallel, the Vanka smoother could be more efficient, as the Vanka smoother requires fewer communication phases which implies less communication start-up time. Generally, a coupled smoother is often somewhat more ex-

pensive than a decoupled smoother, if we need to consider line-wise or plane-wise smoothing within a multigrid algorithm.

5.4.2 Coarse-grid correction

Regarding the discrete operators on the coarser grids in the hierarchy, direct discretization of the continuous operators is considered. At the coarsest level of the grid, a direct solver is implemented, which is easy, accurate and cheap.

Besides the smoother, other important components in multigrid are the inter-grid transfer operators. For the staggered arrangement of the unknowns, the transfer operators between two levels in the grid hierarchy are defined as follows: at displacement or velocity grid points six-point restrictions are applied and at pressure grid points one considers a four-point restriction. The restriction operators have been shown in the stencil notation in Section 4.4.1. As the prolongation operators $P_{2h,h}^{u/v/p}$, we choose the adjoints of the restrictions. The interpolation and restriction operators must be accordingly altered at boundary points or neighbors of boundary points.

In particular, the unknowns at the interface are treated as boundary points of their own subdomains. For the unknowns v^p at the interface, the restriction operator is adapted to

$$R_{h,2h}^{v^p} = \frac{1}{8} \begin{pmatrix} 1 & & 1 \\ 2 & * & 2 \\ 0 & & 0 \end{pmatrix}_h,$$

which has the same structure as those stencils for the inner grid points, but we set the weights of the points outside the poroelastic subdomain Ω^p to be zero. Following the same rule for the Stokes unknowns v^f at the interface,

$$R_{h,2h}^{v^f} = \frac{1}{8} \begin{pmatrix} 0 & & 0 \\ 2 & * & 2 \\ 1 & & 1 \end{pmatrix}_h,$$

is obtained as the restriction in that case.

Remark 5.4. *As is commonly done, we mainly deal with the case of constant physical parameters, such as parameter K . However, the proposed*

multigrid solution method can be generalized to varying K -values. In Chapter 4 (and in [57]), we have performed numerical experiments for the coupled Darcy-Stokes system in which the porous medium was modeled by a random heterogeneous hydraulic conductivity K . When the multigrid algorithm with Uzawa smoother is applied, the optimal relaxation parameter ω is varied within the poroelastic domain, because ω depends on K . Additionally, the random field values should be transferred from fine to coarse grid levels in an accurate way, for an efficient multigrid method. Therefore, the corresponding suitable relaxation parameters for each grid point on each grid level should be calculated.

5.5 Numerical experiments

Three numerical experiments are presented in this section. We aim to study the accuracy of the discretization scheme, the convergence performance of the proposed multigrid method with the coupled and decoupled smoothers, and the application of the method for some test cases that may resemble realistic situations. The efficiency and robustness of the monolithic multigrid method with respect to different values of the physical parameters are also investigated.

In all numerical experiments, the initial approximation is chosen to be random, and the stopping criterion is given by,

$$\frac{||\text{residual}||_{\infty}}{||\text{right-hand side}||_{\infty}} \leq \text{tolerance} \cdot \frac{||\text{initial residual}||_{\infty}}{||\text{right-hand side}||_{\infty}}, \quad (5.28)$$

where the tolerance is chosen to be 10^{-10} . Moreover, for simplicity we consider uniform meshes with grid size h in both directions on each sub-domain.²

5.5.1 Analytic test

In the first numerical experiment, we deal with a coupled Stokes-poroelasticity problem with a known analytic solution on the domain $\Omega = (0, 1) \times (0, 2)$. The domain is divided into a free flow part $\Omega^f = (0, 1) \times (0, 1)$ and a porous

²In [64] and Chapter 3, we applied the multigrid method for porous medium flow when anisotropies due to grid stretching appeared. It is thus straightforward to generalize the proposed method for the coupled system to an anisotropic grid setting.

medium subdomain $\Omega^p = (0, 1) \times (1, 2)$ by the interface $\Gamma = (0, 1) \times \{1\}$. The exact solution is chosen to be

$$\begin{cases} u^f = u^p = (y^2 - y)e^t, \\ v^f = v^p = 0, \\ p^f = p^p = xe^t, \end{cases} \quad (5.29)$$

and the source terms have been subsequently determined. Dirichlet boundary conditions are imposed at the exterior boundaries of the coupled geometry. At the internal interface, equations (5.5)-(5.9), are considered. In this test, the analytic solution satisfies all interface conditions when $G = \nu$.

Errors on different grid sizes First of all, we compare the numerical solution with the given exact solution for the following values of the coefficients, $K = \lambda = G = \nu = \varrho = 1$. The final time is $T = 1$. The errors in maximum norm for each unknown on different meshes are shown in Table 5.1. As we

	Grid-size			
	$16 \times 32 \times 1$	$32 \times 64 \times 4$	$64 \times 128 \times 16$	$128 \times 256 \times 64$
u^f	2.45×10^{-3}	7.58×10^{-4}	2.00×10^{-4}	5.04×10^{-5}
v^f	4.22×10^{-3}	1.28×10^{-3}	3.34×10^{-4}	8.43×10^{-5}
p^f	1.60×10^{-1}	6.99×10^{-2}	3.02×10^{-2}	1.37×10^{-2}
u^p	2.38×10^{-3}	6.30×10^{-4}	1.62×10^{-4}	4.09×10^{-5}
v^p	9.45×10^{-4}	2.31×10^{-4}	5.89×10^{-5}	1.49×10^{-6}
p^p	5.64×10^{-4}	1.81×10^{-4}	4.94×10^{-5}	1.28×10^{-5}

Table 5.1: Maximum norm errors of variables $u^{f/p}$, $v^{f/p}$ and $p^{f/p}$ for different grid sizes with parameters $K = 1$, $\lambda = 1$, $G = 1$, $\nu = 1$ and $\varrho = 1$.

expected, by decreasing the time step with a factor 4 and the spatial mesh width by a factor 2, second-order accuracy is confirmed for poroelasticity problem, whereas for the Stokes problem, we achieve second-order accuracy for velocities and first-order for the pressure field.

Local Fourier analysis results In this section, we confirm that the asymptotic convergence factor of the monolithic multigrid based on the Uzawa smoother for the coupled problem can be predicted by means of the worst

$\nu_1 + \nu_2$	Poroelasticity			Stokes		
	$K = 1$	$K = 10^{-3}$	$K = 10^{-6}$	$\nu = 1$	$\nu = 10^{-3}$	$\nu = 10^{-6}$
2	0.36	0.36	0.36	0.20	0.20	0.78
3	0.22	0.22	0.22	0.09	0.09	0.51
4	0.14	0.14	0.14	0.06	0.05	0.37

Table 5.2: Two-grid convergence factors, ρ predicted by LFA for poroelastic and Stokes subproblems, separately, for different values of the parameters K and ν and different numbers of smoothing steps, $\nu_1 + \nu_2$.

of the two-grid convergence factors obtained by LFA for the individual poroelastic and Stokes subproblems. For different values of the hydraulic conductivity K and viscosity ν , the two-grid convergence factors predicted by LFA are presented for the poroelastic and Stokes problems separately in Table 5.2. The results are obtained for different numbers of smoothing steps, $\nu_1 + \nu_2$. From the table, it is observed that the multigrid method based on Uzawa smoother is robust for each subproblem.

In Table 5.3, the asymptotic convergence factors obtained by using the monolithic multigrid W -cycle together with Uzawa smoother for the coupled Stokes-poroelasticity problem are presented. Homogeneous Dirichlet boundary conditions are applied at the exterior boundaries of the coupled domain. To avoid round-off errors, a random initial guess and zero right-hand sides are chosen on a fine-grid of size $h = 1/128$. We show the convergence factors after 100 multigrid cycles so that the asymptotic convergence rates can be reached. Comparing Table 5.2 and 5.3, we observe that these factors match the worst of the two-grid convergence factors predicted by LFA for the individual subproblems. When ν is small, the numerical convergence factors can be estimated by LFA at a high accuracy. The slight discrepancy for some test cases is due to the involved coupling at the interface. The discretization scheme at the interface as well as the implementation of the Uzawa smoother for the whole coupled problem lead to an efficient solver.

Comparison between different cycles Next, we investigate the efficiency of the multigrid W - and V -cycles with different pre- and post-smoothing steps. We employ the Vanka as well as the Uzawa smoother in the monolithic multigrid algorithm for the coupled problem. More realistic and

	K	1			10^{-3}			10^{-6}		
	ν	1	10^{-3}	10^{-6}	1	10^{-3}	10^{-6}	1	10^{-3}	10^{-6}
$\nu_1 + \nu_2$	2	0.40	0.40	0.71	0.40	0.40	0.72	0.40	0.40	0.72
	3	0.27	0.27	0.49	0.27	0.27	0.49	0.26	0.26	0.49
	4	0.23	0.23	0.36	0.23	0.23	0.36	0.22	0.22	0.36

Table 5.3: Asymptotic convergence factors, ρ_h , for the multigrid W -cycle based on Uzawa smoother for the coupled Stokes-poroelasticity problem, for different values of the physical parameters K and ν and different numbers of smoothing steps $\nu_1 + \nu_2$.

difficult values of the coefficients are chosen for this test. In particular $K = 10^{-3}$, $\nu = 0.035$, $\lambda = 10^6$ and $G = 2.5 \times 10^5$. In Table 5.4, the number of iterations necessary to reach the stopping criterion as well as the average multigrid convergence factors (in brackets) are shown for different smoothers, multigrid cycles and pre- and post-smoothing steps. The results are computed on a 64×128 -grid with only one time step. As it can be seen from the table, generally highly satisfactory results are obtained for both Vanka and Uzawa smoothers. Taking into account both the convergence rates and their computational cost, the $W(2, 2)$ -cycle results to be fastest among the different choices. We compare the CPU time of a $W(2, 2)$ -cycle with either the Vanka or the Uzawa smoother. For the Vanka smoother, it takes around 0.86s, whereas for the Uzawa smoother, it takes 1.08s. It has been implemented on a MacBook Pro with a 2.6 GHz Intel Core i5 processor.

$K = 10^{-3}$, $\lambda = 10^6$, $G = 2.5 \times 10^5$, $\nu = 0.035$ and $\varrho = 1$					
Smoother	$W(1, 1)$	$W(1, 2)$	$W(2, 2)$	$V(2, 2)$	$V(3, 3)$
Vanka	19 (0.31)	14 (0.22)	13 (0.20)	19 (0.35)	16 (0.29)
Uzawa	25 (0.45)	18 (0.33)	15 (0.26)	26 (0.48)	20 (0.38)

Table 5.4: Number of iterations necessary to achieve the desired convergence (and convergence factors in brackets) by using W - and V -cycles with different numbers of pre- and post-smoothing steps on a $64 \times 128 \times 1$ -grid.

Multigrid convergence with different parameters We are interested in the multigrid performance with respect to different values of the physical parameters. In geoscientific applications, parameters K and ν are typically

very small numbers. It is a challenge for any solution method to deal with these small parameters and exhibit rapid convergence. In Figure 5.6, for different grid sizes $h = 1/2^{k_l}$ ($k_l = 5, 6, 7, 8$), the robustness of the proposed multigrid method with the Vanka smoother is displayed for different values of K and ν and different grid sizes. The maximum norm of the residual divided by the maximum norm of the right-hand side is plotted in logarithmic scale against the number of multigrid cycles necessary to fulfill the stopping criterion. The multigrid convergence rate is independent of the physical parameters and the grid sizes, and approximately 13 iterations are needed to reduce the residual by 11 orders of magnitude for these more difficult cases.

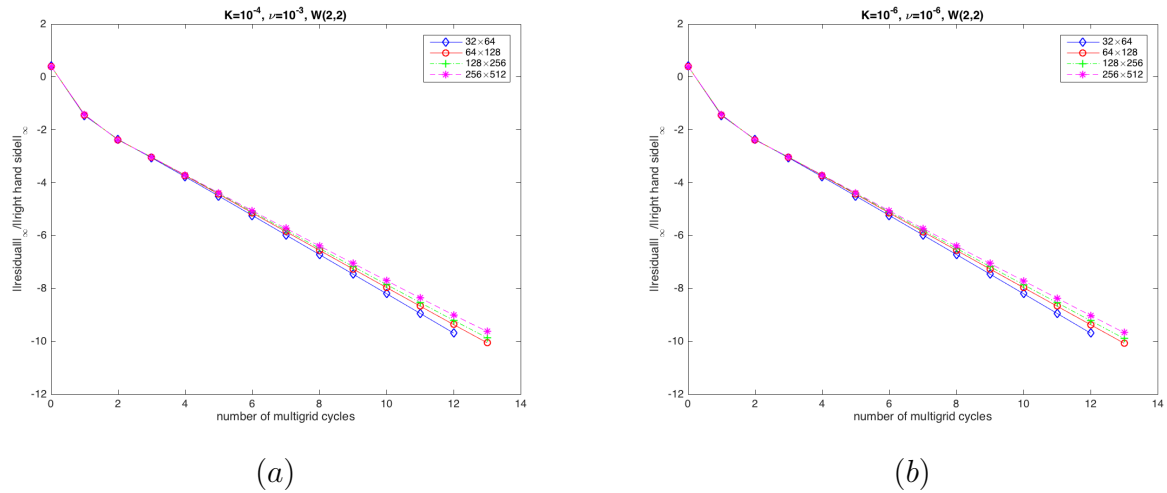


Figure 5.6: History of the convergence of the $W(2, 2)$ -multigrid method for different values of the physical parameters: (a) $K = 10^{-4}$, $\nu = 10^{-3}$, and (b) $K = 10^{-6}$, $\nu = 10^{-6}$.

Convergence results with different time steps Four different values of the time step $\tau = 10^{-3}$, 5×10^{-4} , 2.5×10^{-4} , 1.25×10^{-4} are chosen to check the convergence behavior of multigrid with the two smoothers. As it can be observed from Table 5.5, where the number of iterations needed to fulfill the stopping criterion together with the mean convergence rate (in brackets) are shown, the proposed method is stable and robust with the varying time step.

$K = 10^{-3}$, $\lambda = 10^6$, $G = 2.5 \times 10^5$, $\nu = 10^{-3}$ and $\varrho = 1$				
τ	10^{-3}	5×10^{-4}	2.5×10^{-4}	1.25×10^{-4}
Vanka	16 (0.20)	16 (0.20)	16 (0.20)	16 (0.20)
Uzawa	19 (0.28)	19 (0.28)	19 (0.28)	19 (0.28)

Table 5.5: Convergence results with different values of time step τ .

5.5.2 Two-block realistic test

In the next numerical test, we simulate the dynamical coupling process in a straight pipe with deformable porous media at the boundaries. To reduce the computational effort, we consider a halved domain with symmetry boundary conditions. This domain for the coupled problem is depicted in Figure 5.7, where Ω^f represents a pipe with free flow inside, while Ω^p is a thin porous medium layer at the top. The Neumann condition is imposed at the inlet of free flow system, while at the outlet a homogeneous Neumann condition is applied.

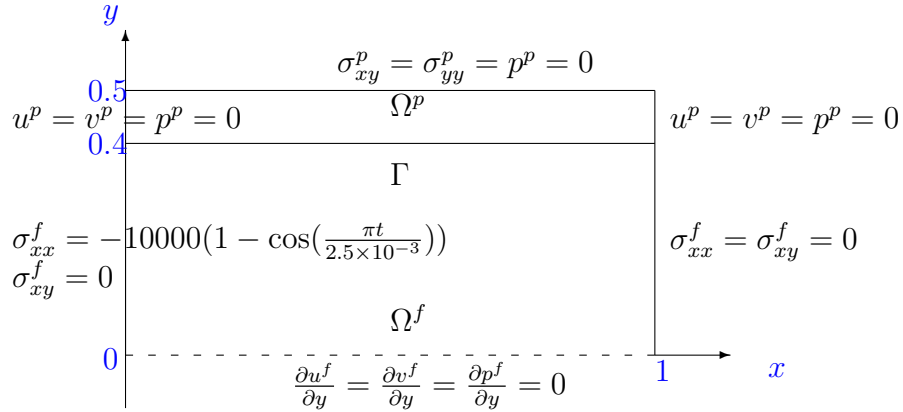


Figure 5.7: Geometry of the coupled two-block Stokes-poroelasticity problem. Subdivision of the domain into a free flow subregion Ω^f and a porous medium subdomain Ω^p , separated by an internal interface Γ .

We take the data from the experiment in [4]. The final time is $T = 0.01$ and the time step is $\tau = 1.25 \times 10^{-3}$. The values of the physical parameters are chosen as $K = 10^{-4}$, $\lambda = 10^6$, $G = 2.5 \times 10^5$, $\nu = 0.0035$ and $\varrho = 1$. Within the porous medium, the fluid velocity in the pores is related to the pressure gradient and can thus be computed and visualized too. In Figures 5.8 and 5.9, velocity vectors and corresponding streamlines of the

fluid flow in the whole domain Ω are shown at two different time points, $t = 0.0025$ and $t = 0.005$. Since the inlet stress is periodic, we have $\sigma_{xx}^f = 20000$ at times $t = 0.0025$ and $t = 0.0075$, whereas $\sigma_{xx}^f = 0$ when $t = 0.005$ and $t = 0.01$. A 160×80 -grid is considered as the finest grid, and a 5-level multigrid method is used in this test. By using the multigrid $W(2,2)$ -cycle, a similar highly satisfactory convergence is obtained as for the first test.

For the case with the large stress value at the inlet (Figure 5.8), the fluid penetrates the porous medium and we see deformation in the porous material near the interface (Figure 5.10 (a)). The pressure solutions are presented in Figure 5.10 (b). When the inlet stress is zero (Figure 5.9), the flow hardly seeps into the porous medium. Due to periodicity, at $t = 2.5 \times 10^{-3}$ and $t = 7.5 \times 10^{-3}$, the solutions are similar, as expected.

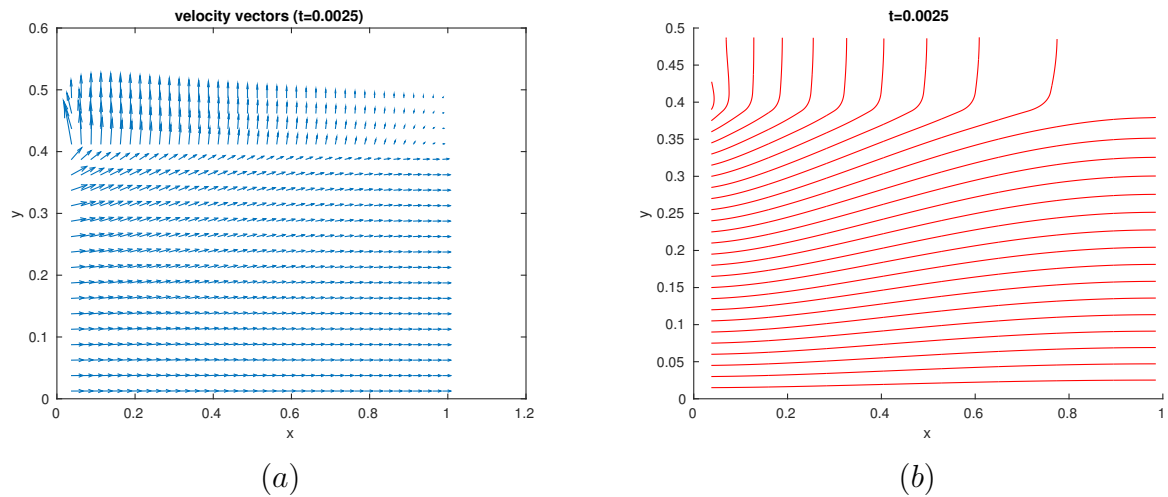


Figure 5.8: For $t = 0.0025$: (a) Velocity vectors in the domain Ω . For a better view, the velocity vectors in the porous medium are multiplied by 4. (b) Corresponding streamlines of the fluid flow.

5.5.3 Multi-block realistic test

Here we investigate the performance of the proposed multigrid method for the coupled system for a more complex geometry. The domain of the coupled problem is shown in Figure 5.11. Since the length of the free flow domain Ω^f and the porous medium Ω^p are not identical, the domain is divided into four different blocks corresponding to the Stokes (*Block1*,

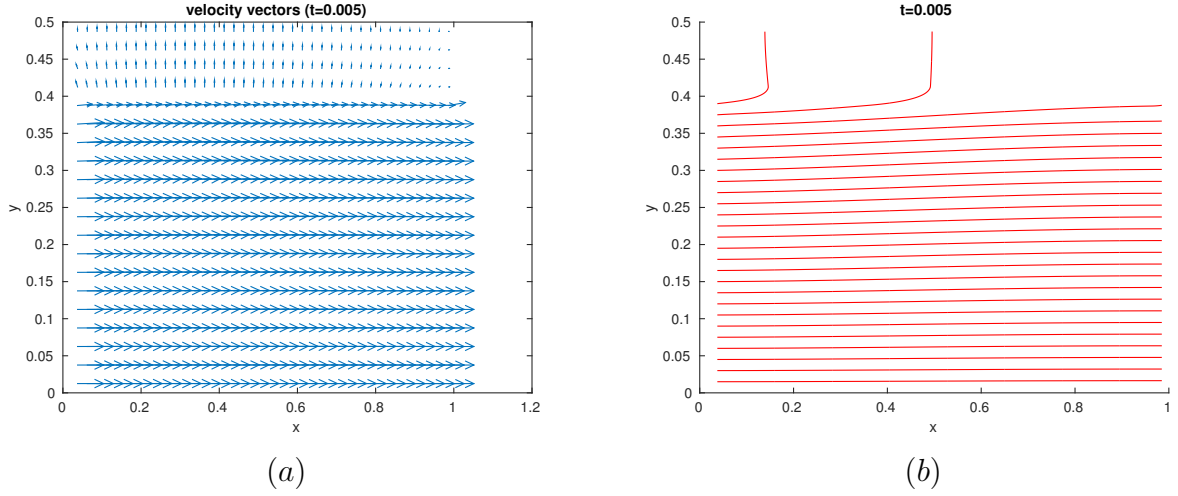


Figure 5.9: For $t = 0.005$: (a) Velocity vectors in the domain Ω . For a better view, the velocity vectors in the porous medium are multiplied by 4. (b) Corresponding streamlines of the fluid flow.

Block2 and *Block3*) and porous medium (*Block4*) domains, respectively. A strategy similar to the one used in the previous two-block test can be straightforwardly adapted for the four block case. The information transferred between *Block2* and *Block4* is the same as before. For the Stokes domain, two artificial boundaries are generated by the grid partitioning approach. As communication between the subgrids in Ω^f is necessary, an overlap region of one cell length is created on each grid level along the arti-

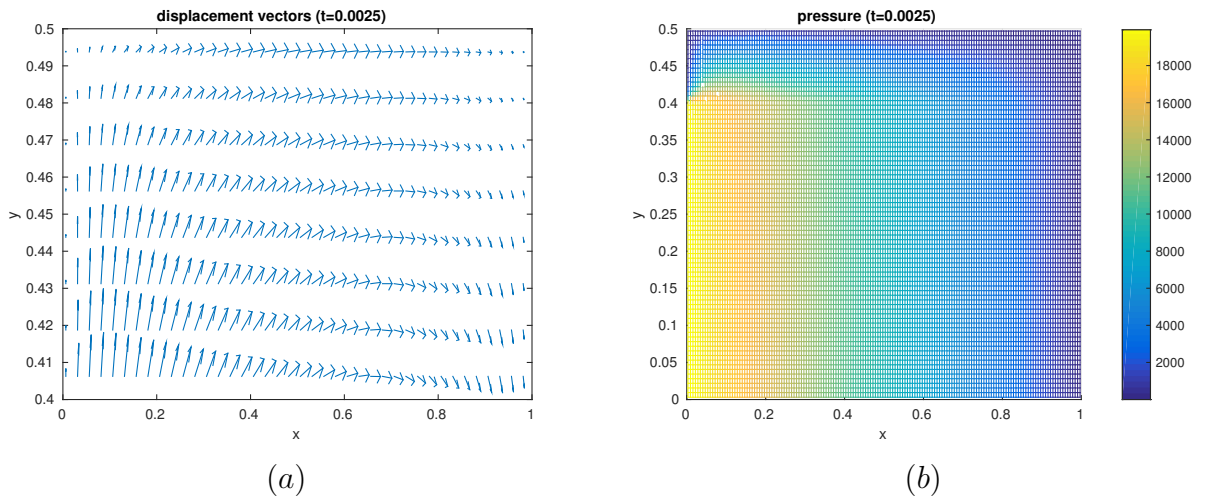


Figure 5.10: For $t = 0.0025$: (a) Displacement vectors in Ω^p , and (b) pressure in the domain Ω .

cial boundaries. The fluid inflow in Ω^f is specified by $\sigma_{xx}^f = -20000$. There is an small exit at the right-side vertical boundary of the fluid flow domain, where the stress-free boundary is imposed. The height of the exit is 0.1. All the other boundary conditions are specified in Figure 5.11. We are interested in the motion of the fluid flow under different parameter settings. In particular, we examine whether we can mimic two different conditions for the porous medium, i.e., we prescribe either permeable or impermeable conditions at the exterior boundary of Ω^p . The values for the physical parameters (except the hydraulic conductivity K) are as in the two-block pipe flow test. The solution is computed on the target grid shown in Table 5.6.

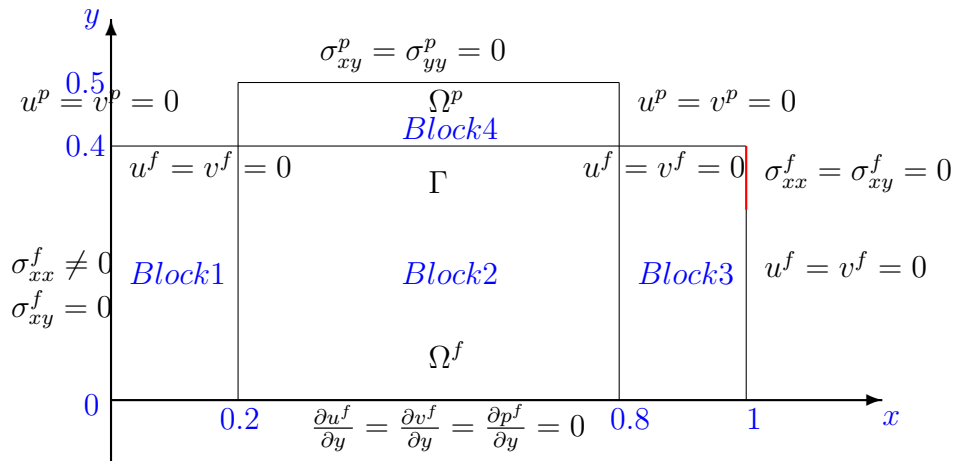


Figure 5.11: Geometry of the coupled multi-block Stokes-poroelasticity problem.

The numbers of iterations necessary to achieve the desired convergence by using the $W(2,2)$ -cycle with both Uzawa and Vanka smoothers are very similar for all multi-block tests. For the Vanka smoother, 20 iterations are required, whereas for the Uzawa smoother we need 22 iterations. Both smoothers perform highly satisfactory. The Vanka smoother is again somewhat more robust when the physical parameters are extremely small.

	<i>Block1</i>	<i>Block2</i>	<i>Block3</i>	<i>Block4</i>
<i>Grid</i>	64×128	192×128	64×128	192×32

Table 5.6: Fine grid in the computational tests.

Permeable conditions on the exterior boundary of Ω^p

We first impose drained conditions ($p^p = 0$) for the pressure on the exterior boundary of the porous medium. This test addresses a tangential flow filtration setting. Tangential flow filtration can be used in applications, as waste water treatment or protein purification.

We present time-varying flow fields. The velocity vectors in the computational domain, together with the streamlines are shown in Figures 5.12 and 5.14 at different times. It is observed that at the beginning (Figure 5.12) there is much flow seeping into the porous medium. The flow in the top filter then leaves the porous medium through the exterior boundary. The deformation of the porous medium is presented in Figure 5.13 (a). As expected, deformation occurs at the left part of the porous medium. The pressure solutions in the domain are shown in Figure 5.13 (b). The velocity of the flow in the porous medium is much smaller than the velocity of the fluid, see Figure 5.14.

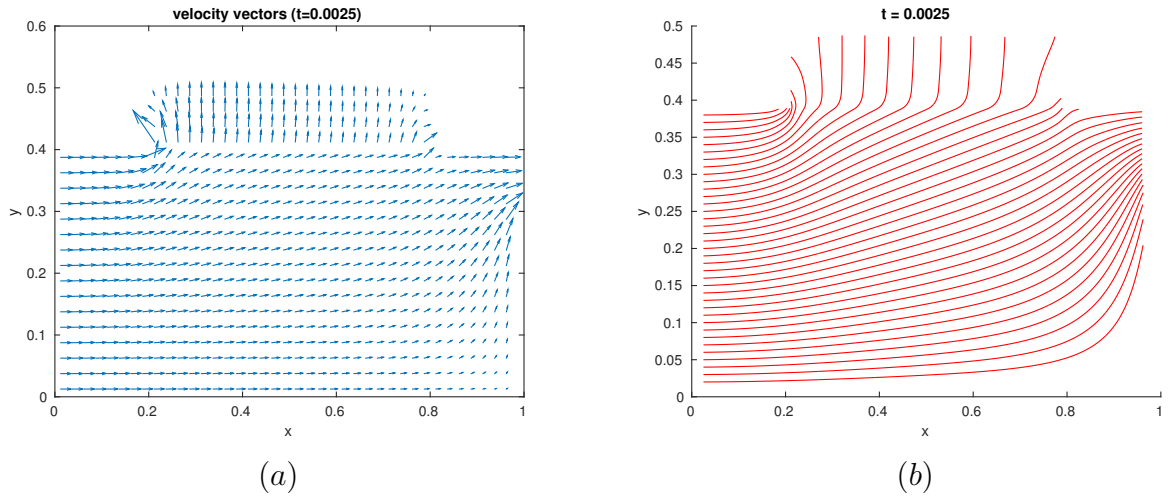


Figure 5.12: For $K = 10^{-4}$ and $t = 0.0025$: (a) Velocity vectors in the domain Ω . For a better view, the velocity vectors in the porous medium are multiplied by 4. (b) Corresponding streamlines of the fluid flow.

Impermeable conditions on the exterior boundary of Ω^p

Next, impermeable conditions are imposed on the exterior boundary of the porous medium, which can be applied in a reservoir simulation. We study the fluid motion with different values of hydraulic conductivity K .

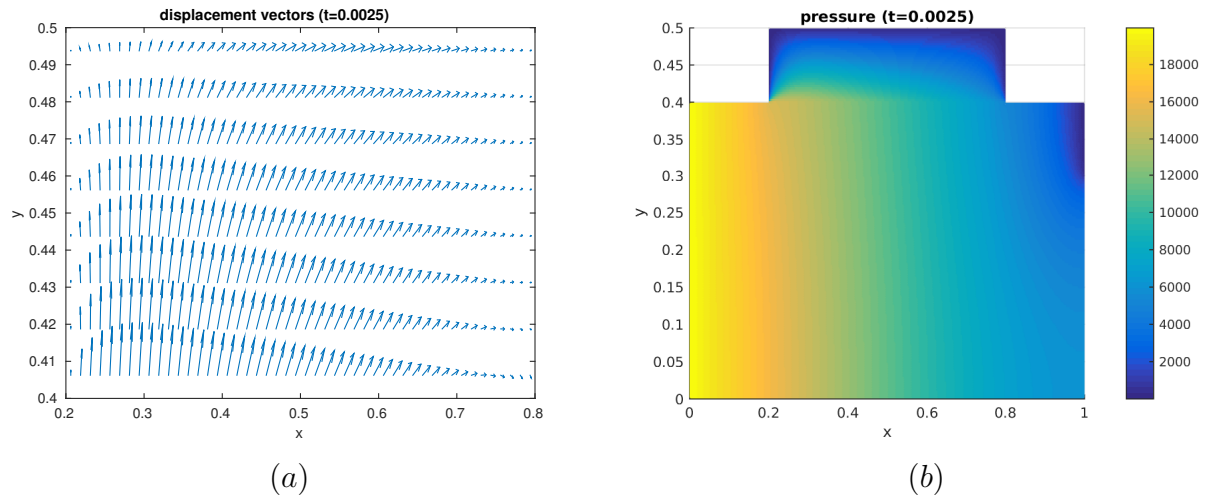


Figure 5.13: For $K = 10^{-4}$ and $t = 0.0025$: (a) Displacement vectors in Ω^p , and (b) pressure in the domain Ω .

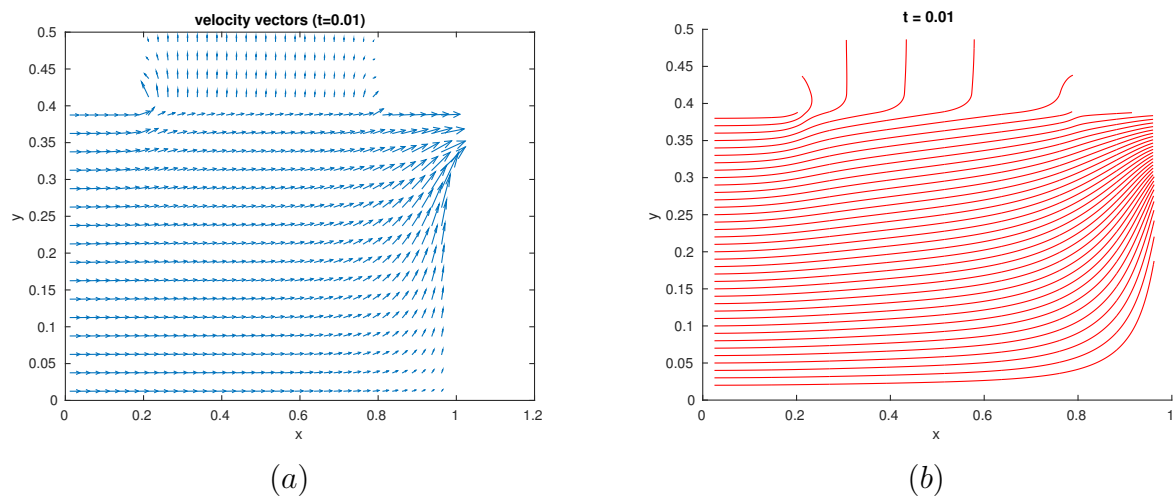


Figure 5.14: For $K = 10^{-4}$ and $t = 0.01$: (a) Velocity vectors in the domain Ω . For a better view, the velocity vectors in the porous medium are multiplied by 4. (b) Corresponding streamlines of the fluid flow.

In Figures 5.15 and 5.16, we show the results corresponding to $K = 0.01$. With such a high hydraulic conductivity of the porous medium, the free flow can easily penetrate the porous medium. The values of the velocity in Ω^f and Ω^p do not differ much. Since it is supposed there is no Darcy flow across the external boundary of Ω^p , the fluid is forced to leave the porous medium through the interface, then flows towards the exit of the Stokes domain, see Figure 5.15. The pressure (Figure 5.16 (b)) drops more or less linearly throughout the domain.

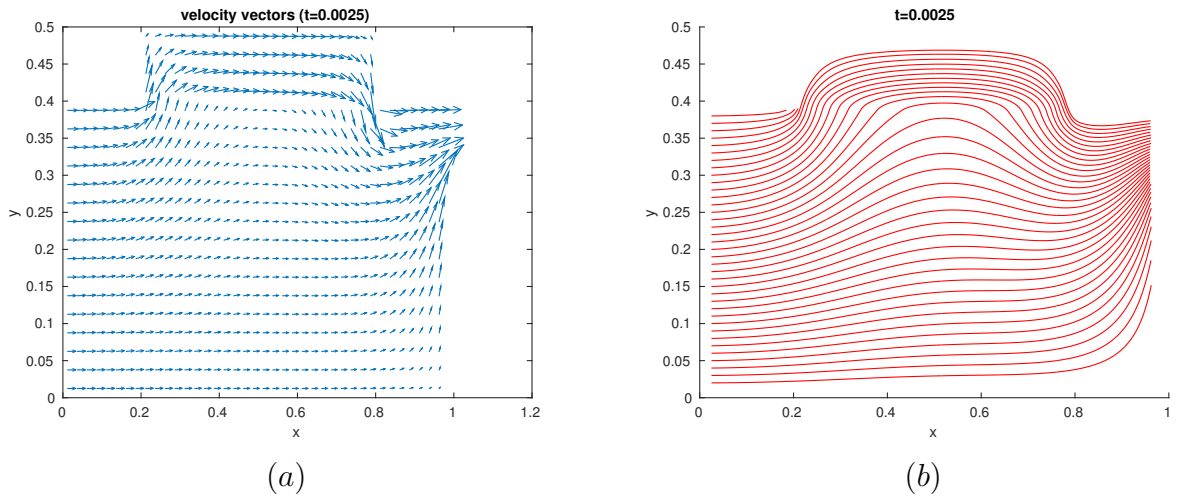


Figure 5.15: For $K = 0.01$ and $t = 0.0025$: (a) Velocity vectors in the domain Ω . All vectors have been scaled by 2. (b) Corresponding streamlines of the fluid flow.

In Figure 5.17, the velocity solutions corresponding to $K = 10^{-4}$ are represented. Since the hydraulic conductivity of the porous medium is very low, the velocity of the Darcy flow is one to two orders of magnitude smaller compared with the velocity of the Stokes flow. A bulk of fluid goes through the exit of the channel directly. The deformation of the porous medium for smaller values of K is bigger than that for higher values of K . The higher the hydraulic conductivity, the smaller resistance of the porous medium to the fluid flow and thus, the smaller the stresses are. Lower stresses imply smaller deformation or displacements.

5.6 Conclusions

In this chapter, an efficient monolithic multigrid method was developed for a coupled system composed of a free fluid flow and a deformable porous

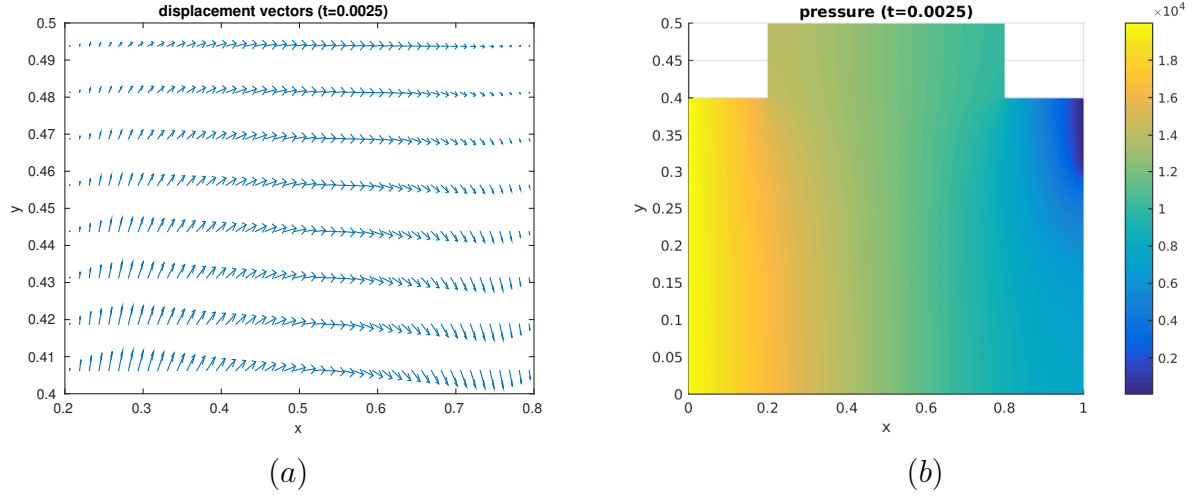


Figure 5.16: For $K = 0.01$ and $t = 0.0025$: (a) Displacement vectors in Ω^p , and (b) pressure in the domain Ω .

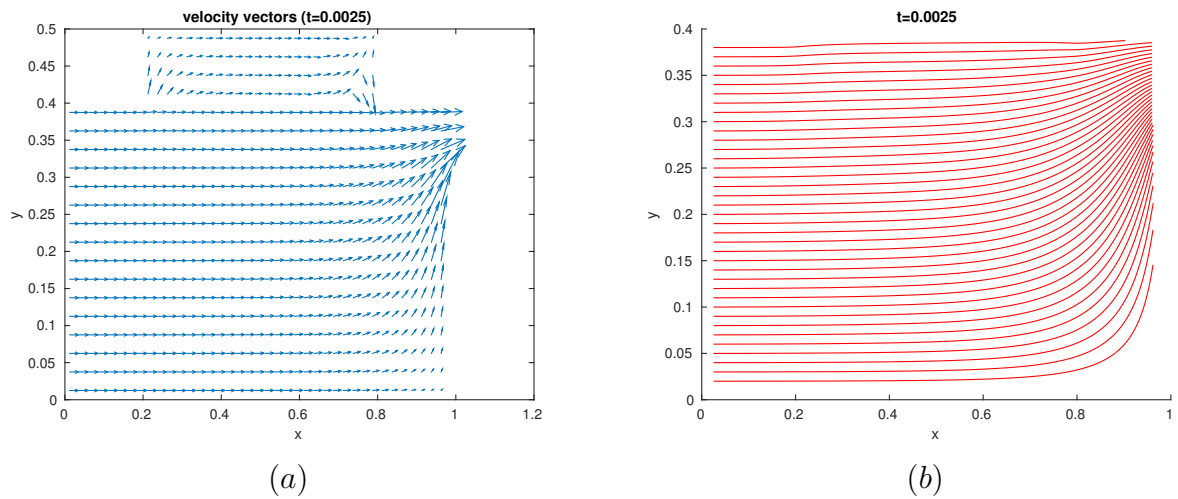


Figure 5.17: For $K = 10^{-4}$ and $t = 0.0025$: (a) Velocity vectors in the domain Ω . For a better view, velocity vectors in the porous medium are multiplied by 18. (b) Corresponding streamlines of the fluid flow.

medium flow. A model based on the Stokes equations and poroelastic equations was formulated with appropriate interface conditions. The finite volume method on a staggered grid was chosen as the discretization scheme for the coupled problem. For the variables near the interface, special discretizations are required based on the interface conditions. Note that in our work at the interface two unknowns belonging to different subsystems were defined at the same grid point. To solve the Stokes-poroelasticity system, a monolithic multigrid method with either a coupled Vanka or a decoupled Uzawa smoother was employed and these smoothers were compared. Both smoothers perform highly satisfactory for many parameter sets; only for extremely small parameters the coupled smoother exhibited a more robust convergence.

In the smoothing process, the two subsystems were coupled based on the grid partitioning technique. To achieve an excellent multigrid convergence behavior, the information is exchanged between neighboring subdomains on each grid level. Numerical experiments confirmed that the discretization scheme is stable and accurate. Moreover, a highly satisfactory convergence of the monolithic multigrid method was obtained for the coupled system. Particularly, for some realistic and difficult problems where the values of the physical parameters are typically small, the proposed method performs very well.

Appendix

5.A Discretization of poroelastic equations at interior points

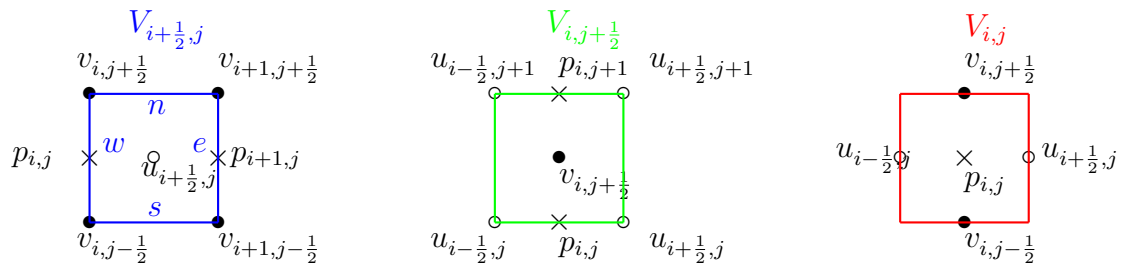


Figure 5.18: Control volumes for the primary unknowns: u (left), v (middle), p (right), together with the corresponding indexing for each variable.

Here we briefly present the staggered discretization of the poroelastic equation. We take the horizontal displacement $u_{i+\frac{1}{2},j}^p$ as an example, since the discretization for the vertical component can be deduced in a similar way. The control volume $V_{i+\frac{1}{2},j}$ in Figure 5.18 is considered. By discretizing the x -momentum equation, we have

$$-\left(\frac{(\sigma_{xx}^{p,\bar{m}})_e - (\sigma_{xx}^{p,\bar{m}})_w}{h} + \frac{(\sigma_{xy}^{p,\bar{m}})_n - (\sigma_{xy}^{p,\bar{m}})_s}{h}\right) = (f_1^{p,\bar{m}})_{i+\frac{1}{2},j}, \quad (5.30)$$

where $(\sigma_{xx}^{p,\bar{m}})$ and $(\sigma_{xy}^{p,\bar{m}})$ are components of the stress tensor, respectively. Approximating these components as

$$(\sigma_{xx}^{p,\bar{m}})_e = \frac{\lambda + 2G}{h}(u_{i+\frac{3}{2},j}^{p,\bar{m}} - u_{i+\frac{1}{2},j}^{p,\bar{m}}) + \frac{\lambda}{h}(v_{i+1,j+\frac{1}{2}}^{p,\bar{m}} - v_{i+1,j-\frac{1}{2}}^{p,\bar{m}}) - p_{i+1,j}^{p,\bar{m}}, \quad (5.31)$$

$$(\sigma_{xx}^{p,\bar{m}})_w = \frac{\lambda + 2G}{h}(u_{i+\frac{1}{2},j}^{p,\bar{m}} - u_{i-\frac{1}{2},j}^{p,\bar{m}}) + \frac{\lambda}{h}(v_{i,j+\frac{1}{2}}^{p,\bar{m}} - v_{i,j-\frac{1}{2}}^{p,\bar{m}}) - p_{i,j}^{p,\bar{m}}, \quad (5.32)$$

$$(\sigma_{xy}^{p,\bar{m}})_n = \frac{G}{h}(u_{i+\frac{1}{2},j+1}^{p,\bar{m}} - u_{i+\frac{1}{2},j}^{p,\bar{m}} + v_{i+1,j+\frac{1}{2}}^{p,\bar{m}} - v_{i,j+\frac{1}{2}}^{p,\bar{m}}), \quad (5.33)$$

$$(\sigma_{xy}^{p,\bar{m}})_s = \frac{G}{h}(u_{i+\frac{1}{2},j}^{p,\bar{m}} - u_{i+\frac{1}{2},j-1}^{p,\bar{m}} + v_{i+1,j-\frac{1}{2}}^{p,\bar{m}} - v_{i,j-\frac{1}{2}}^{p,\bar{m}}), \quad (5.34)$$

and substituting them in (5.30), we will obtain the discrete formulation.

For the pressure unknowns $p_{i,j}^p$, the backward Euler scheme is considered for the time-dependent term in (5.3). The discrete equation is obtained by discretizing the second equation in (5.3) over control volume $V_{i,j}$ (Figure 5.18, right side), resulting in

$$\begin{aligned} \frac{1}{h\tau}(u_{i+\frac{1}{2},j}^{p,\bar{m}} - u_{i-\frac{1}{2},j}^{p,\bar{m}} + v_{i,j+\frac{1}{2}}^{p,\bar{m}} - v_{i,j-\frac{1}{2}}^{p,\bar{m}}) - \frac{1}{h\tau}(u_{i+\frac{1}{2},j}^{p,\bar{m}-1} - u_{i-\frac{1}{2},j}^{p,\bar{m}-1} + v_{i,j+\frac{1}{2}}^{p,\bar{m}-1} - v_{i,j-\frac{1}{2}}^{p,\bar{m}-1}) \\ - \frac{K}{h^2}(p_{i+1,j}^{p,\bar{m}} + p_{i-1,j}^{p,\bar{m}} + p_{i,j+1}^{p,\bar{m}} + p_{i,j-1}^{p,\bar{m}} - 4p_{i,j}^{p,\bar{m}}) = (f^{p,\bar{m}})_{i,j}. \end{aligned} \quad (5.35)$$

Superscripts \bar{m} and $\bar{m} - 1$ denote the current and the previous time steps respectively. The solutions at current time step \bar{m} can be calculated immediately from the values at the previous time.

In the case of variables located at the external boundary, where Neumann boundary conditions for the displacement are imposed, the corresponding control volumes are half the size of the inner control volumes, and are treated accordingly.

5.B Discretization of Stokes equations at interior points

Regarding the momentum equations in (5.1), we here describe the discretization for the first component of the equation. By discretizing the equation over control volume $V_{i+\frac{1}{2},j}$ (Figure 5.18, left side), the discrete equation for $u_{i+\frac{1}{2},j}^f$ yields

$$\frac{\rho}{\tau}(u_{i+\frac{1}{2},j}^{f,\bar{m}} - u_{i+\frac{1}{2},j}^{f,\bar{m}-1}) - \left(\frac{(\sigma_{xx}^{f,\bar{m}})_e - (\sigma_{xx}^{f,\bar{m}})_w}{h} + \frac{(\sigma_{xy}^{f,\bar{m}})_n - (\sigma_{xy}^{f,\bar{m}})_s}{h} \right) = (f_1^{f,\bar{m}})_{i+\frac{1}{2},j}. \quad (5.36)$$

The components of the stress tensor are approximated as

$$(\sigma_{xx}^{f,\bar{m}})_e = -p_{i+1,j}^{f,\bar{m}} + 2\nu \frac{u_{i+\frac{3}{2},j}^{f,\bar{m}} - u_{i+\frac{1}{2},j}^{f,\bar{m}}}{h}, \quad (5.37)$$

$$(\sigma_{xx}^{f,\bar{m}})_w = -p_{i,j}^{f,\bar{m}} + 2\nu \frac{u_{i+\frac{1}{2},j}^{f,\bar{m}} - u_{i-\frac{1}{2},j}^{f,\bar{m}}}{h}, \quad (5.38)$$

$$(\sigma_{xy}^{f,\bar{m}})_n = \nu \left(\frac{u_{i+\frac{1}{2},j+1}^{f,\bar{m}} - u_{i+\frac{1}{2},j}^{f,\bar{m}}}{h} + \frac{v_{i+1,j+\frac{1}{2}}^{f,\bar{m}} - v_{i,j+\frac{1}{2}}^{f,\bar{m}}}{h} \right), \quad (5.39)$$

$$(\sigma_{xy}^{f,\bar{m}})_s = \nu \left(\frac{u_{i+\frac{1}{2},j}^{f,\bar{m}} - u_{i+\frac{1}{2},j-1}^{f,\bar{m}}}{h} + \frac{v_{i+1,j-\frac{1}{2}}^{f,\bar{m}} - v_{i,j-\frac{1}{2}}^{f,\bar{m}}}{h} \right). \quad (5.40)$$

The discrete formula for the horizontal unknown $u_{i+\frac{1}{2},j}^{f,\bar{m}}$ then is obtained by substituting (5.37)-(5.40) into (5.36).

For the mass balance equation, the following discrete equation is obtained by discretizing the second equation in (5.1) over control volume $V_{i,j}$

$$\frac{u_{i+\frac{1}{2},j}^{f,\bar{m}} - u_{i-\frac{1}{2},j}^{f,\bar{m}}}{h} + \frac{v_{i,j+\frac{1}{2}}^{f,\bar{m}} - v_{i,j-\frac{1}{2}}^{f,\bar{m}}}{h} = 0. \quad (5.41)$$

Conclusions and Outlook

6.1 Conclusions

The numerical solution of multi-physics systems has received much attention due to a wide range of application fields and modern hardware on which obtaining multi-physics solutions is feasible nowadays. This thesis had its focus on the development of efficient and robust multigrid algorithms, in particular for the coupled free fluid flow and porous media flow system. We basically addressed three research objectives. In this chapter, the conclusions for each objective are drawn.

Multigrid method for nonlinear and linear poroelasticity equations

In the first part of the thesis, we focussed on the poroelasticity equations, with a nonlinear hydraulic conductivity. We discretized the equations on a collocated grid by the finite volume method. To avoid oscillations in the first time steps of the solution process, an artificial term was added to one of the continuous equations. To solve the nonlinear problem, the global linearization method combined with linear multigrid for the linearized system, “Newton Multigrid”, was employed, as well as the “Full Approximation Scheme” (FAS). Both methods lead to rapid multigrid convergence. Within the multigrid method, we employed the coupled Vanka box smoother as well as the point-wise Gauss-Seidel relaxation. Moreover, a heterogeneous nonlinear problem with random physical parameters was considered. From the numerical experiments we concluded that both nonlinear multigrid methods and both smoothing methods gave rise to very good multigrid convergence, independent of the mesh width in the compu-

tational grid.

Moreover, we investigated the multigrid performance when a decoupled Uzawa-type iteration was used as the smoother for linear poroelasticity equations, that were discretized on staggered grids. The Uzawa smoother is a combination of a symmetric Gauss-Seidel smoothing iteration for the poroelasticity displacements, together with a Richardson iteration, which contains a relaxation parameter, for the pressure solution. Since the relaxation parameter needs to be chosen with care within the Richardson iteration, we applied Local Fourier Analysis (LFA) to determine the suitable parameter. The optimal parameter values, that were estimated by smoothing factors and predicted multigrid convergence factors, could be obtained this way. The multigrid method was applied to both collocated and staggered grid discrete problems. Numerical tests confirmed our analysis results very well. Regarding the non-trivial heterogeneous media problem, an iterant recombination scheme was employed, resulting in very fine convergence acceleration of the underlying multigrid method.

Monolithic multigrid method for the coupled Darcy-Stokes system

Based on the knowledge from the previous chapters, we solved the coupled free fluid flow and the rigid porous media system, which was represented by the Darcy-Stokes model. The discrete formulas for the coupled multi-physics system, with a special discretization at the interface, were generated by finite volume discretization on a staggered grid. A monolithic multigrid method with the Uzawa smoother was applied to the multi-physics system, based on a multiblock multigrid algorithm. Optimal relaxation parameters in the Uzawa smoother were computed by LFA for each subproblem. The global convergence factor of multigrid was well approximated by the worst multigrid convergence factor of the individual subproblems by LFA, which forms an indication that our discretization and implementation for the coupled system were done in an efficient way. Moreover, a porous medium with a random heterogeneous hydraulic conductivity was studied. A highly efficient monolithic multgrid algorithm for the Darcy-Stokes problem on a staggered grid resulted.

Monolithic multigrid method for the coupled Stokes-poroelasticity system

Finally, as an extension of the Darcy-Stokes model, we worked on the coupled Stokes-poroelasticity system, based on the assumption that the porous media is also deformable. This means that the fluid motion and solid deformation are both considered. Different from the Darcy-Stokes problem, we here defined two unknowns belonging to different subsystems at the same grid point at the interface. Special discretizations were implemented, not only for the unknowns at the interface, but also for the variables close to the interface. For reference test cases, we could confirm that we achieved second-order spatial convergence. For this Stokes-poroelasticity system, monolithic multigrid methods with either a coupled Vanka or a decoupled Uzawa smoother were employed, and their convergence performance was compared. Both smoothers showed highly satisfactory results for a wide range of parameter values. The coupled smoother appeared more robust in the case of extreme parameters or computational grid cells.

6.2 Outlook

In this section, some suggestions for future research are presented.

Three-dimensional problems

Since the work in this thesis focuses on two-dimensional problems, a continuation to three-dimensional problems seems a logical research direction. It is worth noting that when the multigrid method with decoupled Uzawa smoother is applied, optimal relaxation parameters will be different but can be calculated in the framework of LFA for each subsystem. We expect that the coupling of the two subsystems in 3D will bring several additional research challenges.

Other smoothers in multigrid

In the multigrid method, the choice of the smoother is an important component. In this thesis, we focussed our attention to the coupled Vanka and decoupled Uzawa smoothers. Of course, other smoothers may also be interesting to investigate, like ILU smoothers or Braess-Sarazin smoothers.

Robustness with respect to stretched grids, or nonstaggered grid arrangements, are important research topics.

Parallel computing

The multiblock multigrid algorithm described in Chapter 4 can be performed in parallel, as mentioned before. In this algorithm, the information transfer in each step is only in one direction. The data required for each operation is available in the same process. So it is possible to consider high performance computing for large-scaled problems, and search for different ways of communicating information.

Unsaturated porous media

Another interesting coupling is between Stokes flow and the Richards equation by assuming that the porous medium is unsaturated. The Richards equation is a nonlinear partial differential equation, which will give us challenges in the numerical solution, the multi-physics coupling and also the multigrid solution.

Navier-Stokes equations in the coupled model

Instead of the Stokes equations, we may consider either the steady or unsteady Navier-Stokes equations in the coupled system. To deal with the non-zero convective terms in the Navier-Stokes equations, nonlinear multigrid methods are needed. However, we have gained experience on solving the nonlinear poroelasticity equations in the second chapter of this thesis. It may therefore be possible to solve a more challenging coupled system arising from the Navier-Stokes equations and nonlinear poroelasticity equations.

Bibliography

- [1] J. Adler, T. Benson, E. Cyr, S. MacLachlan, and R. Tuminaro. Monolithic multigrid methods for two-dimensional resistive magnetohydrodynamics. *SIAM Journal on Scientific Computing*, 38(1):B1–B24, 2016.
- [2] P. Angot. On the well-posed coupling between free fluid and porous viscous flows. *Applied Mathematics Letters*, 24(6):803–810, 2011.
- [3] O. Axelsson. *Iterative solution methods*. Cambridge University Press, 1996.
- [4] S. Badia, A. Quaini, and A. Quarteroni. Coupling Biot and Navier–Stokes equations for modelling fluid–poroelastic media interaction. *Journal of Computational Physics*, 228(21):7986–8014, 2009.
- [5] H. Barucq, M. Madaune-Tort, and P. Saint-Macary. On nonlinear biot’s consolidation models. *Nonlinear Analysis: Theory, Methods & Applications*, 63(5):e985–e995, 2005.
- [6] G. Batchelor. *An introduction to fluid dynamics*. Cambridge University Press, 2000.
- [7] M. Benzi, G. Golub, and J. Liesen. Numerical solution of saddle point problems. *Acta Numerica*, 14(1):1–137, 2005.
- [8] M. Biot. General theory of three-dimensional consolidation. *Journal of Applied Physics*, 12(2):155–164, 1941.
- [9] M. Biot. Theory of elasticity and consolidation for a porous anisotropic solid. *Journal of Applied Physics*, 26(2):182–185, 1955.

- [10] D. Braess and R. Sarazin. An efficient smoother for the Stokes problem. *Applied Numerical Mathematics*, 23(1):3–19, 1997.
- [11] A. Brandt. Multi-level adaptive technique (MLAT) for fast numerical solution to boundary value problems. In *Proceedings of the Third International Conference on Numerical Methods in Fluid Mechanics*, pages 82–89. Springer, 1973.
- [12] A. Brandt. Multi-level adaptive solutions to boundary-value problems. *Mathematics of Computation*, 31(138):333–390, 1977.
- [13] A. Brandt and N. Dinar. Multigrid solutions to elliptic flow problems. *Numerical Methods for PDEs*, pages 53–147, 1979.
- [14] A. Brandt and O. Livne. *Multigrid techniques: 1984 guide with applications to fluid dynamics*. SIAM, 2011.
- [15] A. Brandt and A. Lubrecht. Multilevel matrix multiplication and fast solution of integral equations. *Journal of Computational Physics*, 90(2):348–370, 1990.
- [16] W. Briggs, S. McCormick, and V. Henson. *A Multigrid Tutorial*. SIAM, 2000.
- [17] M. Bukač, I. Yotov, and P. Zunino. An operator splitting approach for the interaction between a fluid and a multilayered poroelastic structure. *Numerical Methods for PDEs*, 31(4):1054–1100, 2015.
- [18] M. Cai, M. Mu, and J. Xu. Preconditioning techniques for a mixed Stokes/Darcy model in porous media applications. *Journal of Computational and Applied Mathematics*, 233(2):346–355, 2009.
- [19] A. Caiazzo, V. John, and U. Wilbrandt. On classical iterative subdomain methods for the Stokes–Darcy problem. *Computational Geosciences*, 18(5):711–728, 2014.
- [20] Y. Cao, M. Gunzburger, X. Hu, F. Hua, X. Wang, and W. Zhao. Finite element approximations for Stokes–Darcy flow with Beavers–Joseph interface conditions. *SIAM Journal on Numerical Analysis*, 47(6):4239–4256, 2010.

- [21] Y. Cao, M. Gunzburger, F. Hua, and X. Wang. Coupled Stokes-Darcy model with Beavers-Joseph interface boundary condition. *Communications in Mathematical Sciences*, 8(1):1–25, 2010.
- [22] W. Chen, M. Gunzburger, F. Hua, and X. Wang. A parallel Robin-Robin domain decomposition method for the Stokes-Darcy system. *SIAM Journal on Numerical Analysis*, 49(3):1064–1084, 2011.
- [23] P. Chidyagwai, S. Ladenheim, and D. Szyld. Constraint preconditioning for the coupled Stokes–Darcy system. *SIAM Journal on Scientific Computing*, 38(2):A668–A690, 2016.
- [24] P. Chidyagwai and B. Rivière. Numerical modelling of coupled surface and subsurface flow systems. *Advances in Water Resources*, 33(1):92–105, 2010.
- [25] O. Coussy. *Poromechanics*. John Wiley & Sons, 2004.
- [26] S. Cowin. Bone poroelasticity. *Journal of Biomechanics*, 32(3):217–238, 1999.
- [27] J. Curtis. Fractured shale-gas systems. *AAPG Bulletin*, 86(11):1921–1938, 2002.
- [28] H. Darcy. *Les fontaines publiques de la ville de Dijon: exposition et application*. Victor Dalmont, 1856.
- [29] E. Detournay and A. Cheng. Fundamentals of poroelasticity. *Analysis and Design Methods: Comprehensive Rock Engineering: Principles, Practice and Projects*, 2:113–171, 1993.
- [30] M. Discacciati, E. Miglio, and A. Quarteroni. Mathematical and numerical models for coupling surface and groundwater flows. *Applied Numerical Mathematics*, 43(1):57–74, 2002.
- [31] M. Discacciati and A. Quarteroni. Convergence analysis of a subdomain iterative method for the finite element approximation of the coupling of Stokes and Darcy equations. *Computing and Visualization in Science*, 6(2-3):93–103, 2004.

- [32] M. Discacciati and A. Quarteroni. Navier-Stokes/Darcy coupling: modeling, analysis, and numerical approximation. *Revista Matemática Complutense*, 22(2):315–426, 2009.
- [33] M. Discacciati, A. Quarteroni, and A. Valli. Robin-Robin domain decomposition methods for the Stokes-Darcy coupling. *SIAM Journal on Numerical Analysis*, 45(3):1246–1268, 2007.
- [34] L. Euler. General principles of the motion of fluids. *Physica. D: Nonlinear Phenomena*, 237:1825–1839, 2008.
- [35] R. Fedorenko. The speed of convergence of one iterative process. *USSR Computational Mathematics and Mathematical Physics*, 4(3):227–235, 1964.
- [36] F. Gaspar, J. Gracia, F. Lisbona, and C. Oosterlee. Distributive smoothers in multigrid for problems with dominating grad-div operators. *Numerical Linear Algebra with Applications*, 15(8):661–683, 2008.
- [37] F. Gaspar, F. Lisbona, P. Matus, and V. Tuyen. Numerical methods for a one-dimensional non-linear Biot’s model. *Journal of Computational and Applied Mathematics*, 2015.
- [38] F. Gaspar, F. Lisbona, and C. Oosterlee. A stabilized difference scheme for deformable porous media and its numerical resolution by multigrid methods. *Computing and Visualization in Science*, 11(2):67–76, 2008.
- [39] F. Gaspar, F. Lisbona, C. Oosterlee, and R. Wienands. A systematic comparison of coupled and distributive smoothing in multigrid for the poroelasticity system. *Numerical Linear Algebra with Applications*, 11(2-3):93–113, 2004.
- [40] F. Gaspar, F. Lisbona, and P. Vabishchevich. Staggered grid discretizations for the quasi-static Biot’s consolidation problem. *Applied Numerical Mathematics*, 56(6):888–898, 2006.
- [41] F. Gaspar, Y. Notay, C. Oosterlee, and C. Rodrigo. A simple and efficient segregated smoother for the discrete Stokes equations. *SIAM Journal on Scientific Computing*, 36(3):A1187–A1206, 2014.

- [42] W. Hackbusch. On the convergence of a multi-grid iteration applied to finite element equations. *Report, Universitat Koln*, pages 76–12, 1977.
- [43] W. Hackbusch. On the multi-grid method applied to difference equations. *Computing*, 20(4):291–306, 1978.
- [44] W. Hackbusch. Survey of convergence proofs for multi-grid iterations. *Special topics of applied mathematics, North-Holland, Amsterdam*, pages 151–164, 1980.
- [45] W. Hackbusch. On the convergence of multi-grid iterations. *Beiträge Numerical Mathematics*, 9:213–239, 1981.
- [46] W. Hackbusch. Multi-grid methods and applications. *Computational Mathematics*, 4, 1985.
- [47] W. Hackbusch. Parabolic multi-grid methods. In *Proc. of the sixth int’l. symposium on Computing methods in applied sciences and engineering, VI*, pages 189–197. North-Holland Publishing Co., 1985.
- [48] N. Hanspal, A. Waghode, V. Nassehi, and R. Wakeman. Development of a predictive mathematical model for coupled Stokes/Darcy flows in cross-flow membrane filtration. *Chemical Engineering Journal*, 149(1):132–142, 2009.
- [49] F. Harlow and J. Welch. Numerical calculation of time-dependent viscous incompressible flow of fluid with free surface. *Physics of Fluids*, 8(12):2182–2189, 1965.
- [50] V. Henson. Multigrid methods for nonlinear problems: an overview. In *Electronic Imaging 2003*, pages 36–48. International Society for Optics and Photonics, 2003.
- [51] M. Hoffmann. *The Navier–Stokes–Darcy problem*, Weierstrass Institute, Germany, 2013.
- [52] M. Hubbert. Darcy’s law and the field equations of the flow of underground fluids. *Hydrological Sciences Journal*, 2(1):23–59, 1957.
- [53] M. Hubbert and D. Willis. Mechanics of hydraulic fracturing. *Society of Petroleum Engineers*, 210:153–168, 1972.

- [54] V. John and L. Tobiska. Numerical performance of smoothers in coupled multigrid methods for the parallel solution of the incompressible Navier-Stokes equations. *International Journal for Numerical Methods in Fluids*, 33(4):453–473, 2000.
- [55] I. Jones. Low Reynolds number flow past a porous spherical shell. In *Mathematical Proceedings of the Cambridge Philosophical Society*, volume 73, pages 231–238. Cambridge University Press, 1973.
- [56] G. King. Thirty years of gas shale fracturing: what have we learned? In *SPE Annual Technical Conference and Exhibition*. Society of Petroleum Engineers, 2010.
- [57] P. Kumar, P. Luo, F. Gaspar, and C. Oosterlee. A multigrid multilevel Monte Carlo method for transport in Darcy-Stokes system. *Submitted for publication*, 2017.
- [58] P. Kumar, C. Oosterlee, and R. Dwight. A multigrid multilevel monte carlo method using high-order finite-volume scheme for lognormal diffusion problems. *International Journal for Uncertainty Quantification*, 7(1):57–81, 2017.
- [59] B. Lamichhane and B. Wohlmuth. Mortar finite elements for interface problems. *Computing*, 72(3):333–348, 2004.
- [60] M. Larin and A. Reusken. A comparative study of efficient iterative solvers for generalized Stokes equations. *Numerical Linear Algebra with Applications*, 15(1):13–34, 2008.
- [61] W. Layton, F. Schieweck, and I. Yotov. Coupling fluid flow with porous media flow. *SIAM Journal on Numerical Analysis*, 40(6):2195–2218, 2002.
- [62] T. Levy and E. Sanchez-Palencia. On boundary conditions for fluid flow in porous media. *International Journal of Engineering Science*, 13(11):923–940, 1975.
- [63] P. Luo, C. Rodrigo, F. Gaspar, and C. Oosterlee. Multigrid method for nonlinear poroelasticity equations. *Computing and Visualization in Science*, 17(5):255–265, 2015.

- [64] P. Luo, C. Rodrigo, F. Gaspar, and C. Oosterlee. On an Uzawa smoother in multigrid for poroelasticity equations. *Numerical Linear Algebra with Applications*, 24, e2074. doi:10.1002/nla.2074, 2016.
- [65] P. Luo, C. Rodrigo, F. Gaspar, and C. Oosterlee. Monolithic multigrid method for the coupled Stokes flow and deformable porous medium system. *Submitted for publication*, 2017.
- [66] P. Luo, C. Rodrigo, F. Gaspar, and C. Oosterlee. Uzawa smoother in multigrid for the coupled porous medium and Stokes flow system. *SIAM journal on Scientific Computing*, in press, 2017.
- [67] S. MacLachlan and C. Oosterlee. Local Fourier analysis for multigrid with overlapping smoothers applied to systems of PDEs. *Numerical Linear Algebra with Applications*, 18(4):751–774, 2011.
- [68] J. Maitre, F. Musy, and P. Nigon. A fast solver for the Stokes equations using multigrid with a Uzawa smoother. In *Advances in Multi-Grid Methods*, pages 77–83. Springer, 1985.
- [69] A. Márquez, S. Meddahi, and F.-J. Sayas. A decoupled preconditioning technique for a mixed Stokes–Darcy model. *Journal of Scientific Computing*, 57(1):174–192, 2013.
- [70] A. Mikelić and W. Jäger. On the interface boundary condition of Beavers, Joseph, and Saffman. *SIAM Journal on Applied Mathematics*, 60(4):1111–1127, 2000.
- [71] A. Mikelić, I. Yotov, R. Zakerzadeh, and P. Zunino. Partitioning strategies for the interaction of a fluid with a poroelastic material based on a Nitsche’s coupling approach. *Computer Methods in Applied Mechanics and Engineering*, 292:138–170, 2015.
- [72] S. Muntz. *Fluid structure interaction for fluid flow normal to deformable porous media*. PhD thesis, Department of Mathematics, Technical University of Kaiserslautern, Germany, 2008.
- [73] S. Murata, N. Satofuka, and T. Kushiya. Parabolic multi-grid method for incompressible viscous flows using a group explicit relaxation scheme. *Computers & Fluids*, 19(1):33–41, 1991.

- [74] C. Navier. Mémoire sur les lois du mouvement des fluides. *Mémoires de l'Académie (royale) des sciences de l'Institut (imperial) de France*, 6(1823):389–416, 1823.
- [75] C. Oosterlee and F. Gaspar. Multigrid relaxation methods for systems of saddle point type. *Applied Numerical Mathematics*, 58(12):1933–1950, 2008.
- [76] S. Patankar. *Numerical heat transfer and fluid flow*. CRC Press, 1980.
- [77] M. Perić, R. Kessler, and G. Scheuerer. Comparison of finite-volume numerical methods with staggered and collocated grids. *Computers & Fluids*, 16(4):389–403, 1988.
- [78] A. Quarteroni and A. Valli. *Domain decomposition methods for partial differential equations*. Number CMCS-BOOK-2009-019. Oxford University Press, 1999.
- [79] L. Richards. Capillary conduction of liquids through porous mediums. *Physics*, 1(5):318–333, 1931.
- [80] B. Rivière and I. Yotov. Locally conservative coupling of Stokes and Darcy flows. *SIAM Journal on Numerical Analysis*, 42(5):1959–1977, 2005.
- [81] I. Rybak, J. Magiera, R. Helmig, and C. Rohde. Multirate time integration for coupled saturated/unsaturated porous medium and free flow systems. *Computational Geosciences*, 19(2):299–309, 2015.
- [82] P. Saffman. On the boundary condition at the surface of a porous medium. *Studies in Applied Mathematics*, 50(2):93–101, 1971.
- [83] V. Schmidt. *Stochastic Geometry, Spatial Statistics and Random Fields*. Springer, 2015.
- [84] R. Showalter. Diffusion in poro-elastic media. *Journal of Mathematical Analysis and Applications*, 251(1):310–340, 2000.
- [85] R. Showalter. Poroelastic filtration coupled to Stokes flow. *Lecture Notes in Pure and Applied Mathematics*, 242:229–241, 2005.

- [86] B. Smith, P. Bjorstad, and W. Gropp. *Domain decomposition: parallel multilevel methods for elliptic partial differential equations*. Cambridge University Press, 2004.
- [87] J. South and A. Brandt. *Application of a multi-level grid method to transonic flow calculations*. Technical report, NASA Langley Research Center, Hampton, VA, United States, 1976.
- [88] H. D. Sterck, K. Miller, G. Sanders, and M. Winlaw. Recursively accelerated multilevel aggregation for markov chains. *SIAM Journal on Scientific Computing*, 32(3):1652–1671, 2010.
- [89] G. Stokes. *On the effect of the internal friction of fluids on the motion of pendulums*, volume 9. Pittsburgh Press, 1851.
- [90] K. Stüben and U. Trottenberg. *Multigrid methods: Fundamental algorithms, model problem analysis and applications*. Springer, 1982.
- [91] C. Tang. Numerical simulation of progressive rock failure and associated seismicity. *International Journal of Rock Mechanics and Mining Sciences*, 34(2):249–261, 1997.
- [92] R. Temam. *Navier-Stokes equations*, volume 2. North-Holland Amsterdam, 1984.
- [93] K. Terzaghi. *Theoretical soil mechanics*. Wiley, 2007.
- [94] U. Trottenberg, C. Oosterlee, and A. Schuller. *Multigrid*. Academic Press, 2000.
- [95] S. Vanka. Block-implicit multigrid solution of Navier-Stokes equations in primitive variables. *Journal of Computational Physics*, 65(1):138–158, 1986.
- [96] C. Venner. *Multilevel solution of the EHL line and point contact problems*. PhD thesis, University of Twente, 1991.
- [97] T. Washio and C. Oosterlee. Krylov subspace acceleration for nonlinear multigrid schemes. *Electronic Transactions on Numerical Analysis*, 6(271-290):3–1, 1997.

- [98] P. Wesseling. *An Introduction to Multigrid Methods*. John Wiley & Sons Ltd, 1992.
- [99] P. Wesseling and P. Sonneveld. Numerical experiments with a multiple grid and a preconditioned Lanczos type method. *Approximation methods for Navier-Stokes problems*, pages 543–562, 1980.
- [100] R. Wienands and W. Joppich. *Practical Fourier analysis for multigrid methods*. CRC Press, 2004.

Curriculum Vitae

Peiyao Luo

12-08-1990 Born in Xi'an, China

Education

2008-2012 Bachelor of Science in Applied Mathematics
Minor: Information and Computational Science
Northwestern Polytechnical University, Xi'an, China

2012-2015 Master of Science in Applied Mathematics
Minor: Computational Mathematics
Northwestern Polytechnical University, Xi'an, China

2013-2017 PhD in Applied Mathematics
Delft University of Technology, Delft, The Netherlands
Thesis: Multigrid Method for the Coupled Free Fluid Flow and Porous Media System
Promotor: Prof.dr.ir. C.W. Oosterlee

List of Publications

- **Publications in Refereed Journals**

1. P. Luo, C. Rodrigo, F.J. Gaspar and C.W. Oosterlee. **Mono-lithic multigrid method for the coupled Stokes flow and deformable porous medium system.** *Submitted for publication*, 2017.
2. P. Luo, C. Rodrigo, F.J. Gaspar and C.W. Oosterlee. **Uzawa smoother in multigrid for coupled porous medium and Stokes flow system.** *SIAM Journal of Scientific Computing*, *in press*, 2017.
3. P. Luo, C. Rodrigo, F.J. Gaspar and C.W. Oosterlee. **On an Uzawa smoother in multigrid for poroelasticity equations.** *Numerical Linear Algebra with Applications*, doi:10.1002/nla.2074, 24(1), 2016.
4. P. Luo, C. Rodrigo, F.J. Gaspar and C.W. Oosterlee. **Multigrid method for nonlinear poroelasticity equations.** *Computing and Visualization in Science*, 17(5): 255-265, 2015.
5. P. Kumar, P. Luo, F.J. Gaspar and C.W. Oosterlee. **A multigrid multilevel Monte Carlo method for transport in Darcy-Stokes system.** *Submitted for publication*, 2017.

- **Publications in Refereed Proceedings**

1. P. Luo, C. Rodrigo, F.J. Gaspar and C.W. Oosterlee. **On a multigrid method for the coupled Stokes and porous media flow problem.** *In AIP Conference Proceedings*, doi:10.1063/1.4992706, 2017.

Awards and Presentations

- **Awards:**

1. Winner of Student Paper Competition of the 18th Copper Mountain Conference On Multigrid Methods, Colorado, USA, March 2017.
2. Finalist in the 2017 BGCE student Prize at the SIAM Conference on Computational Science and Engineering, Atlanta, USA, February 2017.
3. NDNS+PhD travel grant, the Netherlands, June 2014.

- **Oral Presentations:**

1. Seminar in Department of Mathematics (invited), Tufts University, USA, April 2017.
2. 18th Copper Mountain Conference on Multigrid Methods, Colorado, USA, March 2017.
3. SIAM Conference on Computational Science and Engineering, Atlanta, USA, February 2017.
4. 14th International Conference of Numerical Analysis and Applied Mathematics, Rhodes, Greece, September 2016.
5. 14th Copper Mountain Conference on Iterative Methods, Colorado, USA, March 2016.
6. Workshop “Flow in Deformable Porous Media”, Zaragoza, Spain, November 2015.
7. The 8th International Congress on Industrial and Applied Mathematics, Beijing, China, August 2015.

8. Spring Meeting of the Werkgemeenschap Scientific Computing (invited), Antwerp University, Belgium, May 2015.
9. 2014 European Multigrid Conference, Leuven, Belgium, September 2014.
10. Workshop “Flow in Deformable Porous Media”, Zaragoza, Spain, August 2014.

• **Poster Presentations:**

1. Kick-off DCSE Event entitled Future Computing, Delft, The Netherlands, May 2017.
2. The 41th Woudschoten Conference, Zeist, The Netherlands, October 2016.
3. The 40th Woudschoten Conference, Zeist, The Netherlands, October 2015.
4. The 39th Woudschoten Conference, Zeist, The Netherlands, October 2014.